

Graphene based Nanostructures: towards Application with Carbon Nanofibers

Von der Naturwissenschaftlichen Fakultät der
Gottfried Wilhelm Leibniz Universität Hannover

zur Erlangung des Grades
Doktor der Naturwissenschaften (Dr. rer. nat.)

genehmigte Dissertation
von

Annas Bin Ali, M.Sc. (Saudi Arabien)

2021

Referent: Prof. Dr. techn. et rer. nat. habil. Franz Renz
Korreferent: Prof. Dr.-Ing. Ralf Franz Sindelar
Weiterer Korreferent: apl. Prof. Dr. rer. nat. habil. Bernhard Wilhelm Roth
Weiterer Korreferent: Assoc. Prof. Amir Al- Ahmed, Ph.D.

Tag der Promotion: 20.07.2021

“The first thing is to establish that something is possible, then the probability will occur”

- **Elon Musk**

Acknowledgments

I would like to acknowledge many people for their support, help and trust in me during my doctorate. I would like to thank Prof. Dr. Franz Renz for being my doctoral advisor and for constant support and motivation. He has kept me positive at different points and provided me with necessary technical insight that helped me in doctoral work. Prof. Dr. Sindelar serves a special mention and thanks for mentoring me throughout the doctoral work. The technical discussions and each milestone of doctoral work was done with his time-to-time guidance. Within the time of my studies and the work in his group, he became more and more my paragon and without his kind guidance I would not have achieved what I have achieved. I really appreciate his support, ideas and experience, the carte blanche for the research and project I was working on and trust in me and my skills. Thanks for all the encouragement. I would also like to thank my co-supervisor Prof. Dr. Christoph Tegenkamp, who was a constant help in technical matters, particularly related to the electrical transport characterization. I had discussed with him repeatedly on electrical transport in carbon nanofibers and he was a great help indeed. Besides, he was also extremely helpful in publishing and reviewing the publication work.

Moreover, I am thankful for the financial support of the Hannover School for Nanotechnology, as well as for the engagement of Fritz Schulze Wischeler who coordinated the planning within this interdisciplinary program. I would also like to thank Graduate Academy at Leibniz University Hannover for awarding me a doctoral completion grant.

I would like to thank my family; my parents Liaqat Ali and Naheed Ali, my brothers Hassaan and Hanzila. I am also thankful to my partner Ayesha for boosting and keep me going. Similarly, I would extend my gratitude to my mentors which were constant motivation. And not to be forgotten, I want to thank my colleagues from the AK-Renz and Prof. Sindelar's group. I was enjoying a lot of lab work and especially office work with a good friend Dietrich Müller, whom I shared my working place with. We supported and encouraged each other in good and bad times. Especially, the fun time at the office place and deep talks about nearly everything.

Finally, many thanks to the referees of this thesis: Prof. Dr. Franz Renz, Prof. Dr. Ralf Sindelar and Prof. Bernhard Roth.

Kurzzusammenfassung

Graphen-Nanostrukturen haben in den letzten zwei Jahrzehnten, aufgrund ihrer ausgezeichneten physikalischen, chemischen, optischen und elektronischen Eigenschaften, große Aufmerksamkeit bei den Forschern weltweit erregt. Das anhaltende Bestreben elektronische Geräte immer kleiner zu bauen hat den Bedarf an alternativen Materialien mit hohem Aspekt Verhältnis und verbesserten elektrischen Eigenschaften verstärkt. Im Vergleich zu Kohlenstofffasern dienen Kohlenstoff-Nanofasern mit Submikrometer-Durchmesser als Brückentechnologie, auf der die grundlegenden Graphen-Konzepte greifbar angewendet und gemessen werden können. Das Dissertationsprojekt basiert auf diesem Konzept. In diesem Zusammenhang konzentriert sich die vorliegende Forschungsarbeit auf die Realisierung von Graphen-Nanostrukturen durch Kohlenstoff-Nanofasern, graphische Struktur und elektrische Transporteigenschaften.

Die Arbeit diskutiert systematisch die grundlegenden Prozessparameter und deren Einfluss auf die graphitische Struktur vom Elektrosponning über die Stabilisierung bis hin zur Carbonisierung. Die graphitische Struktur ist von großer Bedeutung, da sie die elektrischen, mechanischen und chemischen Eigenschaften bestimmt. Insbesondere werden zwei verschiedene Ansätze zur Modifizierung der graphitischen Struktur von Kohlenstoff-Nanofasern verwendet, nämlich die Kriechspannungsinduzierte Graphitisierung und die Nanokohlenstoffschablonierte Graphitisierung. Sowohl die unabhängigen als auch die synergistischen Effekte dieser beiden Ansätze wurden erforscht. Zunächst auf die Polyacrylnitril-Graphitisierung und dann auf die elektrischen Transporteigenschaften. In der zweiten und dritten Phase der Arbeit werden diese beiden Ansätze separat im Detail untersucht. Es wird gezeigt, dass Kriechspannung während der Stabilisierung die Menge an zyklisiertem PAN bei niedrigeren Temperaturen erhöht. Es wird aufgezeigt, dass bei gleichem Zyklisierungsgrad die graphitische Ordnung der Kohlenstoff-Nanofasern nach der Carbonisierung deutliche Unterschiede aufweist. Die Anwendung von Kriechspannungen vermeidet die Krümmung der Graphenebenen, die durch die in-situ Hepta- und Penta-Ringbildung stattfindet. Darüber hinaus verbessert die auf Nanokohlenstoffeinschlüssen basierende Templat-Graphitisierung die graphitische Ordnung von PAN durch Senkung des I_D/I_G -Verhältnisses, Erhöhung der Kristallitgröße und Verbesserung der Orientierung der graphitischen Domänen. Die Verbesserung der graphitischen Ordnung wird auf die Verankerung der PAN-Ketten durch den Einschluss von Nanokohlenstoffen während der Stabilisierung zurückgeführt, die den Verlust der Ausrichtung der Polymerketten verhindert. Weiterhin wird der Nanokohlenstoff-Templating-Effekt für die Keimbildung und das Wachstum der Kohlenstoffkristalle beobachtet.

In der letzten Phase des Projekts werden vielmehr die synergetischen Effekte dieser beiden Ansätze auf den Graphitisierungsgrad und den elektrischen Transport von PAN untersucht. Der sp^2 -Anteil und die Anordnung der graphitischen Domänen wird durch Nanokohlenstoffeinschlüsse (CNTs) beeinflusst. Der kombinierte Effekt von CNTs und Kriechspannung erhöht zwar den sp^2 -Anteil, verschlechtert aber deren Ausrichtung. Durch die Untersuchung der kooperativen und individuellen Wirkung der oben genannten Ansätze konnte festgestellt werden, dass der elektrische Transport in Submikron-Kohlenstoff-Nanofasern hauptsächlich von der Ausrichtung der graphitischen Domänen (sp^2 -Cluster) abhängig ist. Der elektrische Transport könnte als kumulativer Effekt der bandbasierten Leitfähigkeit entlang der sp^2 -Einheiten und des Tunnelns zwischen sp^2 und sp^3 -Clustern verstanden werden. Diese Erkenntnisse könnten den Weg für die Herstellung von Kohlenstofffasern mit maßgeschneiderter graphitischer Struktur und elektrischer Leitfähigkeit für Anwendungen in Kabeln, Energiespeichern und Sensorelektroden ebnen.

Schlüsselwörter: Polyacrylnitril, Kohlenstoff, Nanofasern, Stabilisierung, Graphitisierung

Abstract

Graphene nanostructures have got great attention of the researchers worldwide in the last two decades owing to their excellent physical, chemical, optical, and electronic properties. The continuing efforts to miniaturize the electronic devices have stirred the need for searching alternate materials with high aspect ratio and improved electrical properties. Carbon nanofibers having sub-micron diameter serve as a bridge where the fundamental graphene concepts could be tangibly applied and measured compared to carbon fibers. The thesis project stems from this concept. In this context, the present research work is focused on the realization of graphene nanostructures through carbon nanofiber, its graphitic structure and electrical transport properties.

The thesis systematically discusses the basic process parameters and their impact on the graphitic structure from electrospinning to stabilization and carbonization. The graphitic structure is significant as it dictates the electrical, mechanical, and chemical properties. Particularly, two different approaches are used to modify the graphitic structure of carbon nanofibers, namely creep stress induced graphitization and nanocarbon templated graphitization. Both the independent and synergistic effects of these two approaches have been explored, first on the polyacrylonitrile graphitization and then on the electrical transport properties. We showed that creep stress during stabilization improves the degree of cyclization of PAN at lower temperatures. It was found that though the degree of cyclization may be the same, the graphitic order of carbon nanofibers after carbonization shows marked difference. The application of creep stress avoids the curving of graphene planes which takes places due to in-situ hepta- and penta-ring formation. Moreover, the nanocarbon inclusion based templated graphitization improves the PAN graphitic order by lowering of I_D/I_G ratio, increasing the crystallite size, and enhancing the orientation of graphitic domains. The improvement of graphitic order is attributed to the anchoring of PAN chains by nanocarbon inclusion during stabilization which prevents the loss of polymer chain alignment. Further, the nanocarbon templating effect for nucleation and growth of carbon crystal was observed.

The last phase of the project explores rather the synergistic effects of these both approaches on graphitization degree and electrical transport of PAN. The sp^2 fraction and ordering of graphitic domains is influenced by nanocarbon inclusion (CNTs). However, the combined effect of CNTs and creep stress does increase the sp^2 fraction but deteriorates their alignment. By investigating the mutual and individual effect of above approaches, we were able to conclude that the electrical transport in sub-micron carbon nanofiber is mainly dependent on the alignment of graphitic domains (sp^2 clusters). The electrical transport could be understood as the cumulative effect of band-based conductivity along sp^2 units and tunneling between sp^2 and sp^3 clusters. These findings will pave a way for fabrication of carbon fibers with tailored graphitic structure and electrical conductivity for applications in cables, energy storage and sensing electrodes.

Keywords: Polyacrylonitrile, carbon nanofibers, stabilization, graphitization

Table of Contents

Acknowledgement	I
Kurzzusammenfassung	II
Abstract	III
1 INTRODUCTION	1
1.1 Motivation and Description	1
1.2 Objectives:	2
1.3 Project Phases:	3
1.4 Organization of thesis:	5
2 THEORETICAL BACKGROUND	7
2.1 Carbon Nanostructures.....	7
2.2 Carbon Fibers – Fundamentals and structure.....	9
2.3 Carbon fiber – history	10
2.4 Polyacrylonitrile (PAN) – Structure	11
2.5 Carbon fiber – State of the art: Manufacturing processes and routes	12
2.5.1 Spinning of Polymer precursor fibers:	13
2.5.2 Stabilization process:	15
2.5.3 Carbonization and Graphitization process:	16
2.6 Carbon nanofibers (CNFs).....	18
2.6.1 CNF structure:.....	18
2.6.2 Synthesis of Carbon nanofibers – Fabrication routes	20
2.6.3 Electrospinning - the process:	21
2.7 Properties of Carbon nanofibers:	24
2.7.1 Mechanical properties	24

2.7.2	Thermal Properties.....	25
2.7.3	Electrical Properties.....	25
2.8	Applications of Carbon nanofibers.....	26
2.9	Recapping the Objective.....	28
3	METHODOLOGY AND TECHNIQUES.....	30
3.1	Materials.....	30
3.2	Fundamental Procedure – State of Art.....	30
3.3	Techniques and Analysis.....	32
3.3.1	Scanning Electron Microscope (SEM).....	32
3.3.2	FTIR and polarized FTIR spectroscopy.....	32
3.3.3	X-ray Diffraction.....	34
3.3.4	Transmission Electron Microscope.....	34
3.3.5	Raman Spectroscopy.....	35
3.3.6	X-ray Photoelectron Spectroscopy (XPS).....	36
3.3.7	4PP STM/SEM Setup.....	37
4	RESULTS.....	46
4.1	Development and Characterization of Carbon Nanofiber – Optimization and Structure (Phase 1) 47	
4.1.1	Preface.....	47
4.1.2	Optimization for electrospinning parameters:.....	47
4.1.3	Molecular structure for as spun, stabilized, and carbonized PAN nanofibers.....	50
4.1.4	Crystallography and structural analysis of carbonized PAN nanofibers:.....	52
4.2	Creep stress induced stabilization and graphitization in polyacrylonitrile carbon nanofibers....	54
4.2.1	Preface & Summary.....	54

4.3	Carbon nanofiber reinforced with graphene nanoplatelets – Nano-carbons templated graphitization and electrical transport.....	65
4.3.1	Preface and Summary	65
4.4	Synergistic effect of nanocarbon inclusion (CNTs) and creep assisted stabilization on 1) graphitization in PAN and 2) electrical transport in low dimensional carbon - Cumulative and independent effect of approach 1 and 2	83
4.4.1	Preface and Summary	83
5	Conclusion and Outlook.....	99
5.1	How does it serve – Future takeaway	102
6	Appendix.....	104
6.1	List of Publications	104
6.2	Curriculum Vitae	106

1 INTRODUCTION

This chapter presents the background and motivation for the thesis project. Based on this, the objectives are delineated which are pursued in the form of phases. The scope of the phases is described and lately the organization of the thesis is presented at the end of this chapter for better understanding of the reader.

1.1 Motivation and Description

Carbon fibers and their derived nanomaterials/composites have been extensively studied over nearly half decade. They have been used for potential application in the chemical industry, material science, reinforcement of composites, and energy storage due to their outstanding physical and chemical properties [1, 2]. In fact, among the carbon allotropes, 1D carbon fiber is the most widely explored candidate as far as its commercialization and application volume is concerned. The carbon fiber market is expected to reach ~ 3.7 billion \$ by 2025, which reflects the high expectations of applications [3, 4].

With the advent of ‘Nanotechnology’, a new perspective of preparing nano-scale materials with improved mechanical, electrical and related properties has generated the need to fabricate submicron materials. Especially after the discovery of Graphene in 2004, often termed as ‘wonder-material’, tremendous amounts of research and development is focused to replicate and realize its extraordinary properties [5, 6]. Graphene serves as the central building block of all graphitic materials as it offers the possibility of wrapping up graphene into 0D fullerene structures, rolling it into 1D carbon nanotubes (CNTs) and stacking them in the forms of sheet [7, 8]. However due to high cost and problems with transfer and scalability, the properties of graphene are realized through its derivatives. Furthermore, on one hand carbon fibers gathered huge application volume. Henceforth, inspired by exploration of graphene nanostructures and bridging the fundamental science of graphene and application of carbon fibers, we have come across this dissertation work. Carbon fibers which have been around for a couple of decades are made through spinning-

stabilization-carbonization, recognized as a conventional process for carbon fiber production. The size of these “Carbon fibers” is $\sim 6 - 7 \mu\text{m}$ after the carbonization process [9]. We tend to invoke nanotechnology in perspective of scalable and tangible carbon fibers with submicron diameters, termed as carbon nanofibers (CNFs). Carbon nanofiber is the focus material in this project work for exploring the graphene nanostructures. Due to reduced diameter $\sim 100 - 300 \text{ nm}$, the properties of carbon nanofibers are markedly different due to increased surface area and changing reaction kinetics during stabilization process which affects the end graphitic structure. The graphitic structure of carbon nanofibers; degree of graphitization, graphene edge to plane ratio, crystalline structure and arrangement/alignment of graphene planes dictate the physical and chemical properties, especially the electrical transport properties [10]. Carbon nanofibers are tangible and can be spun into yarns and assemblies of layer mats. The whole project revolves around exploration of graphene nanostructures in carbon nanofibers with characterization of each step in the carbon fiber traditional process. The structure-property relationships are studied from the perspective of further modifications/doping to carbon nanofibers and detailed investigations of electrical transport properties.

1.2 Objectives:

The doctoral research project is based on realization of ‘Graphene nanostructures’ through 1D carbon nanofibers. The aim is to explore the polyacrylonitrile (PAN) based carbon nanofiber’s basic structure and changes during the spinning-stabilization-carbonization process and investigate the graphitic structure and electrical transport properties. This theme is realized through following specific objectives:

- Structural integration and characterization of PAN structure in spinning-stabilization-carbonization process
- Investigate the physical/chemical process and stress induced chemical reactions in the stabilization stage.

- Study the effect of nanocarbon inclusions (carbon nanotubes and graphene nanoplatelets) on PAN graphitic structure
- Investigating the effect of CNTs doping and stress induced stabilization on graphenic structure and electrical transport properties along with their synergistic effects
- Studying and probing the electrical transport phenomena in these highly conductive 1D carbon nanofibers mats and exclusive measurements on single carbon nanofibers

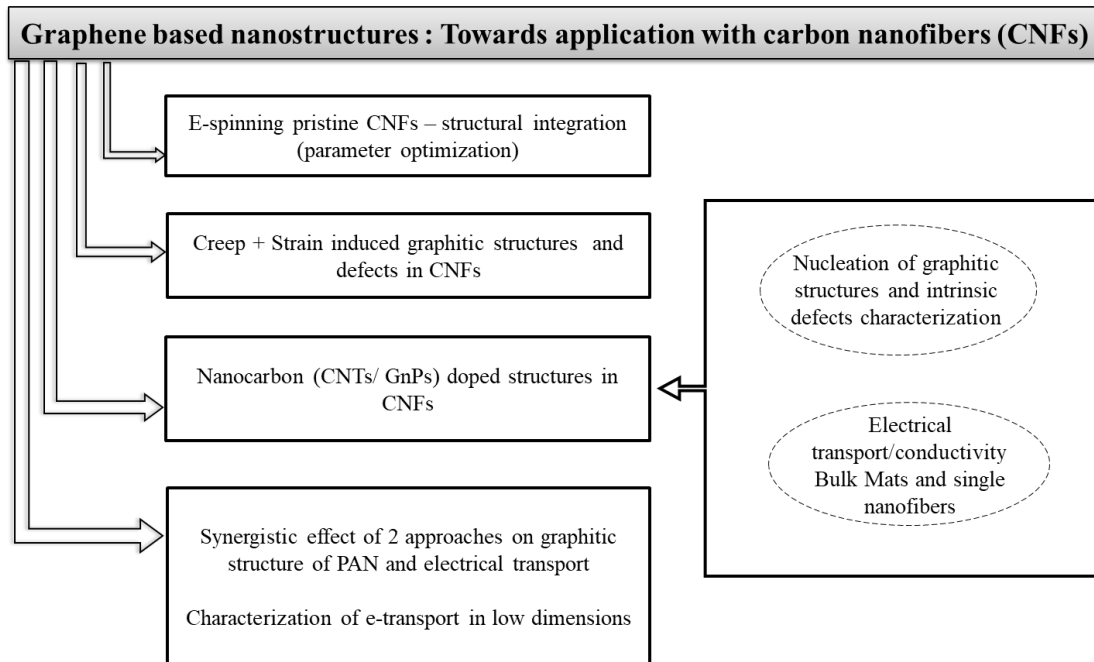


Figure 1- Schematic illustration of project focus and phases

1.3 Project Phases:

The initial part of project deals with the process window for the nanofiber fabrication, i.e., temperature for pyrolysis, electrospinning parameters, solvents, etc., to be systematically explored. Furthermore, different stages of carbon nanofiber development such as electrospinning, oxidative Stabilization and carbonization/graphitization are to be characterized in this stage. The overall process for carbon nanofiber development is a complex process and each stage has multiple parameters from spinning-voltages, flow-

rate of precursor solution, polymer concentration, spinning distance to the parameters for the stabilized and carbonized products as atmosphere, heating rate and temperature [11]. The patented state of the art carbon fiber production process will be optimized for production of carbon nanofibers. The fundamental objective of this phase is to optimize the process parameters for spinning, stabilization, and carbonization process to achieve homogeneity and ensure repeatability. The findings of this phase setup the basis for the investigation to be made in the next phases by keeping the process parameter constant.

The second stage is focused on creep stress induced graphitic structure with focus on stabilization and carbonization. The effect of mechanically driven chemical reactions during the oxidative stabilization stage are studied as they affect the end graphitic structure. The oxidative stabilization stage is the most crucial stage in CNFs fabrication, particularly because the ring scission and foundation of graphene like ribbon structures takes place during it [12, 13]. Stabilization is generally performed by 1) clamping the ends of fiber mats to cater the entropic shrinkage effects which otherwise would result in loss of nanofibers after carbonization and 2) application of tension/stress to PAN nanofibers. To observe the effect of stress induced stabilization, the stabilization is performed at various temperatures before complete cyclized structure is formed and the ring cyclization index of non-creep stress stabilized PAN nanofibers is compared with creep stress stabilized nanofibers. Moreover, the orientation factor for PAN in both cases of stabilization is analyzed. Later graphitic structure is compared for each case and conclusions are drawn for the role of creep stress in stabilization and graphitization.

Third stage deals with doping of nanocarbons to carbon nanofibers. Nano-carbons (NCs) such as graphene nano-platelets (GNPs), carbon nanotubes (CNTs) and graphene nano-ribbons doping result in change in the graphitic structure of carbon lattice which impact the electrical transport properties and electron transfer. Both the transport properties of electrons in carbon lattice and electron transfer mainly depend on the orientation of carbon lattice planes and ratio of edge to basal planes [6-8]. Hence, the addition of nanocarbons help to tailor the intrinsic defects produced during the electrospinning-stabilization-

carbonization process. Therefore, based on XRD, XPS, TEM and Raman of nanocarbon doped CNFs, the investigations of lattice structure (orientation, degree of graphitization, basal planes to edge plane ratio, crystallite size) are carried out in this phase. Graphene nanoplatelets are used as graphitic templates in this phase. Electrical transport properties of pristine PAN and GNPs reinforced PAN carbon nanofiber mats are characterized. Furthermore, electrical anisotropy for templated and pristine structures is also evaluated.

The fourth and last phase of the project is related to the findings of the phase 2 and phase 3, focusing on detailed analysis of the synergistic effects of creep induced stabilization and nanocarbon inclusion effects on the graphitic growth and electrical transport properties. Hence, the two-fundamental conclusions from phase 2 and phase 3, i.e., creep stress induced stabilization effects on graphitic structure of carbon nanofiber and nanocarbon templated graphitization, are brought together and cumulative effect of each case is investigated. Electrical transport properties for pristine carbon nanofiber mats/assemblies are measured and the anisotropy in electrical conductivity is evaluated. This phase of the thesis-work conclusively serves to summarize the concept of graphitization and electrical transport in carbon nanofibers. Electrical transport in sub-micron carbon nanofibers is relatively complex due to the presence of discontinuous domains unlike traditional carbon fibers. To investigate the dictating factor and in-general the phenomena for electrical transport, different cases are studied and compared in context of electrical transport properties of single filament of nanofibers (100 - 200 nm). Carbon nanotubes are used as nanocarbon inclusions for templated graphitization in this last phase. These nanostructures are smaller in dimensions and can be reinforced inside carbon nanofibers which effectively allows to systematically investigate the electrical transport in single nanofibers with nanoprobe.

1.4 Organization of thesis:

The thesis is divided into different chapters starting from chapter 1 which describes the motivation, objective, and the project phases of the whole research work. Chapter 2 deals with theoretical background

and overview of the topic of carbon nanofibers; structure, preparation methods and properties. This allows the novice readers to grasp the fundamental understanding of necessary concepts. Chapter 3 serves as materials and methods for the project work. It explains the basic method, materials, process parameters and techniques used in the investigation of each research phase. After this, chapter 4 is based on results and discussions. Within this chapter there are sub-chapter representing a project phase. Details of the first phase are included and for the rest of the three phases, respective three publications are included with a preface and summary. Subsequently, a conclusion is presented in chapter 5 which summarizes the findings of the thesis. Lastly, chapter 6 is the appendix and includes the information of publications and short vitae of candidate.

2 THEORETICAL BACKGROUND

This chapter presents the theoretical background of the theme of the thesis project. This chapter covers the fundamental literature on carbon nanomaterials, state of the art carbon fiber production process and its comparison to carbon nanofiber structure and its properties.

2.1 Carbon Nanostructures

Carbon is the sixth most common element in the universe. Based on the ability of carbon orbitals to hybridize in sp , sp^2 and sp^3 configurations, it exists in number of allotropic form naturally occurring (diamond, amorphous carbon and graphite) and additional allotropes such as graphene, carbon nanotubes, fullerenes, and nano-diamonds [14]. Various allotropic forms of carbon are shown in figure 2. Graphite consists of carbon atom connected in hexagonal structure. They are sp^2 orbital hybrids and the atoms form in planes with each bound to three nearest neighbors 120° apart. It is an excellent conductor of electricity due to the delocalization of π -electrons. The interest in carbon-based nanomaterials has increased exponentially in the past few decades (starting with the discovery of fullerenes in 1985), then with that of carbon nanotubes (CNTs) in 1991 and of graphene in 2004 [15, 16]. Fullerenes are assemblies of carbon atoms arranged in pentagonal and hexagonal rings forming a closed structure following the formula C_{20+m} , where m is an integer. Graphene is one-atom-thick planar sheets of sp^2 -bonded carbon atoms that are densely packed in a honeycomb crystal lattice. Carbon nanotubes (CNTs) are two assemblies of rolled graphene sheets of carbon atoms as single walled carbon nanotubes (SWCNTs) formed by a single sheet, double and multi-walled carbon nanotubes (MWCNTs) formed by two and more sheets of graphene. CNTs have a diameter in the range from few angstroms to tens of nanometers with a length of several micrometers up to centimeters having both ends of the tubes capped by fullerene like structures [7, 17-19].

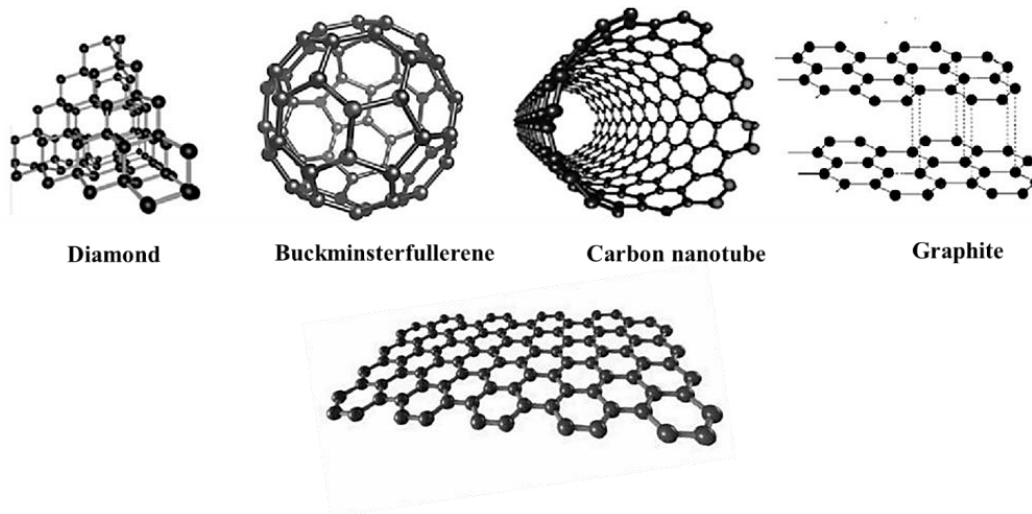


Figure 2 Allotropes of Carbon

Graphene serves as a building block for carbon materials with various dimensionalities (0D Buckyballs, 1D nanotubes, and 3D graphite). The properties of carbon nanomaterials make them widely used in many fields ranging from material science, energy production and storage, biology and medicine owing to exceptional tensile strength, electrical, optical and thermal properties [17]. Table 1 shows properties of various carbon nanomaterials.

Table 1- Properties of Various Carbon Nanomaterials

Carbon Material	Hybridization	Electrical conductivity (S/cm)	Young modulus (GPa)
Graphite (3D)	sp^2	10^4	–
Graphene (2D)	sp^2	10^6	856.4 ± 0.7 964.0 ± 0.68 (a)
SWCNTs (1D)	Mostly sp^2	10^5	1000
MWCNTs (1D)	Mostly sp^2	10^3 – 10^5	1000
Fullerene C60 (0D)	sp^2	10^{-5}	–
Diamond (0D)	sp^3	10^{-2} – 10^{-15}	–

2.2 Carbon Fibers – Fundamentals and structure

Among the carbon materials, carbon fiber (CF) is the most extensively researched material both in academia and industry. The basic units comprising CFs are hexagonal carbon crystalline planes, which resemble the structure of graphite (figure 3a). Each carbon is connected with four other carbons, three of them are sp^2 hybridizations (\sim bond length is 1.415 \AA), while the other forms the inter-lamellar stacking, inter-layer spacing is $\sim 3.35 \text{ \AA}$ [3]. The sp^2 carbon bonding possesses aromaticity, the electrons are highly delocalized and easy to transport between different hexagons. In perfect fibers, these layers are regular ABAB (graphitic) while in less perfect fibers the layers are random and turbulent. Figure 3b shows carbon crystallite in carbon fibers with $L_{a\parallel}$ (parallel to fiber axis), $L_{a\perp}$ (perpendicular to the fiber axis), L_c (depth of crystallite), and d_{002} (inter-layer/planar spacing) [1]. In disordered fibers, the graphene layers are twisted or bent and there are defects such as lattice gaps, imperfections, and dislocations. In general, the structure of carbon fibers is the stack of turbostratic layers. The proposed model for PAN based carbon fibers is shown in figure 4, illustrating typical core-shell structure [20, 21].

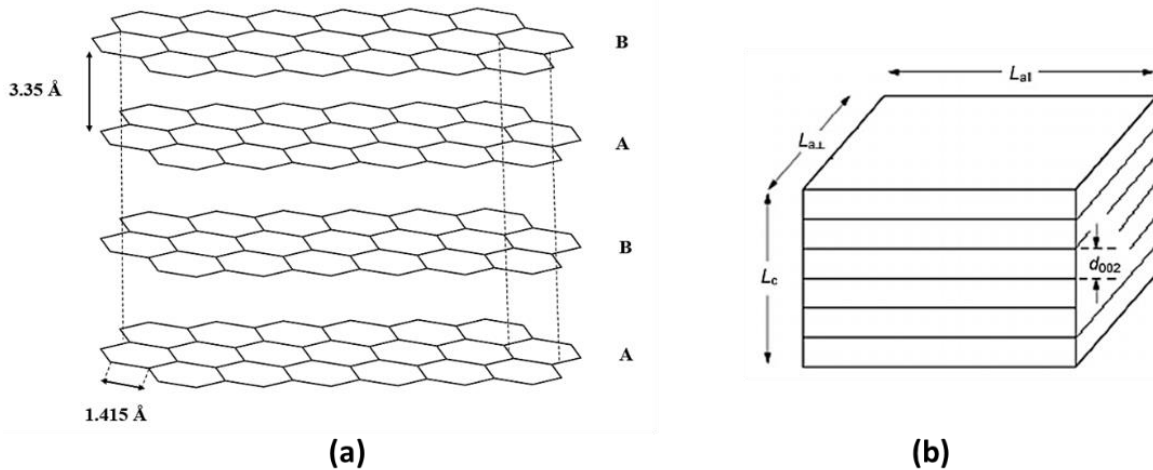


Figure 3- (a) Graphite crystallite structure with regular ABAB stacking, (b) Schematic illustration of carbon crystallite in carbon fiber showing different crystalline dimensions.

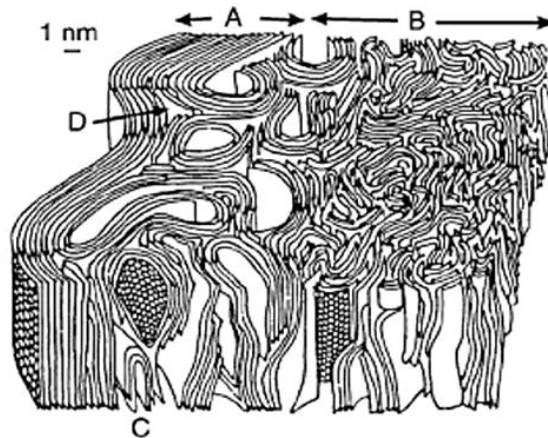


Figure 4- Proposed model for PAN derived carbon fiber, A and B represent the skin and core regions while C and D shows hairpin defect and wedge disclination

2.3 Carbon fiber – history

The first commercial carbon filament was produced in 1879. It was derived from the cellulose precursor and was used as an incandescent lamp filament. After this bamboo and cotton fibers were produced and pyrolyzed to produce carbon fiber. The first ever modern carbon fiber was produced from rayon precursor fibers [2, 21]. It was until 1940, when DuPont developed the Polyacrylonitrile (PAN) fiber, and its thermal stability was realized. The first extensive study of carbonization and graphitization of PAN fibers was done in 1961 by Shindo in Japan. Shindo recognized the importance of an oxidative heat treatment step prior to the carbonization and graphitization steps, resulting in marked increase in carbon yield [22-24]. The tensile modulus of 112 GPa was reported which was about three times that of produced from rayon precursor fibers. In the 1970s, petroleum pitch was used to make high modulus carbon fibers. However, processes to purify and spin pitch into fibers are expensive. Additionally, the compressive strength of the pitch-based carbon fibers is much lower than PAN-based carbon fibers. Now, more than 90 % of commercial carbon fibers are made from PAN precursors. PAN-based fibers are recognized as the most employed precursor to produce the high strength and conductive fibers carbon fibers [21].

2.4 Polyacrylonitrile (PAN) – Structure

The chemical and physical structure of the PAN molecule is shown in figure 5. The molecules tend to form a rod-like helical structure due to the presence of dipole repulsion between intra-nitrile groups. Physical structure from the wide-angle x-ray diffraction (WAXD) shows hexagonal or orthorhombic geometry as shown in figure 6. For hexagonal packing, a/b ratio is $3^{1/2}$ while for orthorhombic packaging, it is either larger or less than $3^{1/2}$. The two-phase theory used to describe the crystal structure of PAN shows that it consists of both the ordered regions (crystalline portion) and disordered regions (amorphous portion) with alternating sections [25, 26]. PAN molecules are stiffer, and it is difficult to form folded structures in PAN unlike other flexible thermoplastics such as polyethylene and polypropylene. Nevertheless, PAN dominates rayon and pitch precursors for developing high performance carbon fibers mainly due to:

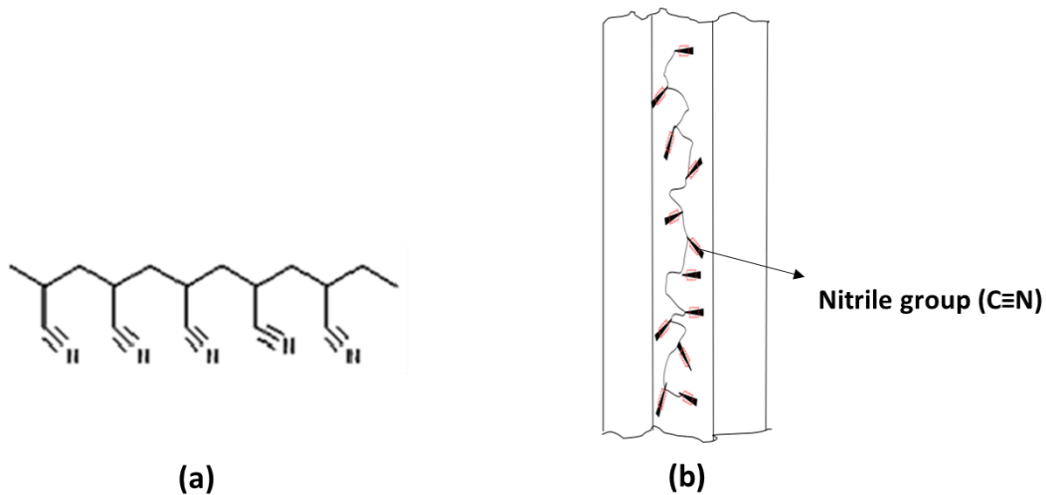


Figure 5 Schematic figure of PAN molecule. (a): chemical structure; (b): conformation – typical helical structure.

- PAN's structure allows higher production rate of pyrolysis maintaining its basic structure and preferred molecular orientation along the fiber axis.
- PAN decomposes before it melts

- PAN has a high degree of molecular orientation, which can be harnessed during spinning. It has been reported that it can be stretched up to nearly 1300%. Moreover, the polymer molecular orientation can be done during the oxidative stabilization process through various post spinning treatments [27].
- PAN has high carbon yield (50 - 55%) when pyrolyzed to 1000 °C and above compared to ryan and pitch.

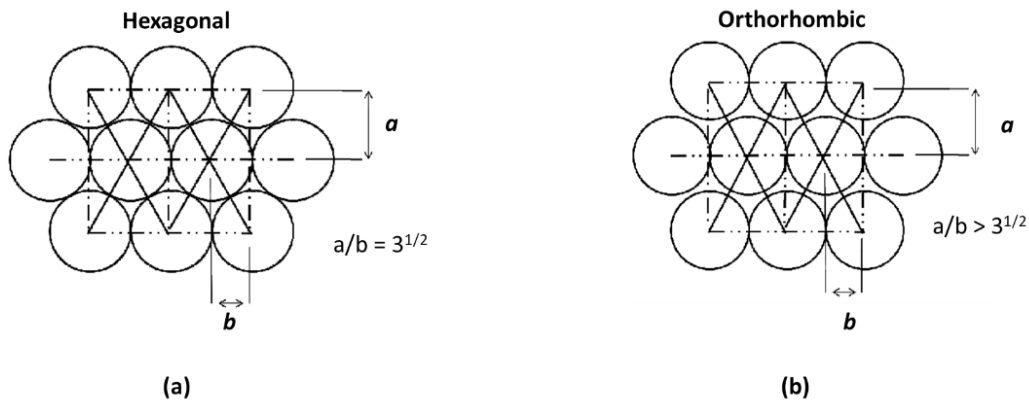


Figure 6 - Illustration of hexagonal and orthorhombic packing of PAN molecule

2.5 Carbon fiber – State of the art: Manufacturing processes and routes

Pyrolysis of polymer precursor fibers is the widely used process for carbon fiber development. The whole fabrication process involves following steps:

- Spinning/drawing of polymer precursor to obtain fibers
- Oxidation and stabilization at 200 - 300 °C in air under tension
- Carbonization at 1000 - 1500 °C in inert atmosphere
- Graphitization at 2500 - 3000 °C

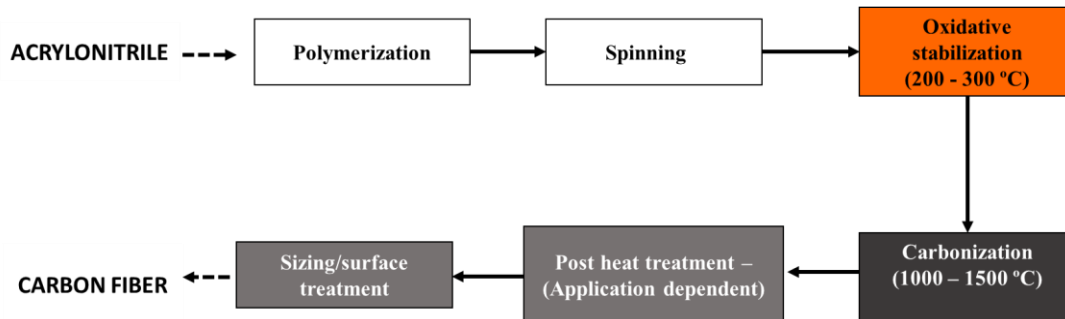


Figure 7- Carbon fiber production process

2.5.1 Spinning of Polymer precursor fibers:

The properties of carbon fibers are dictated by PAN precursor fibers. PAN undergoes cyclization reactions well before its melting point; hence it cannot be processed in melt-form with conventional spinning techniques. The melt spinning can be performed until aided by the various additives and plasticizers. The addition of such additives/plasticizers serve to diminish the nitrile-nitrile group interactions reducing the melting point range. Industrially, the most common precursor fiber spinning methods are wet spinning, dry spinning and melt spinning. However, it is now known that none of the processes reaches CF properties as obtained via wet spinning processes. Various techniques are available for spinning of acrylic fibers for carbon fiber manufacturing [28-30].

Melt spinning has comparatively higher spinning speeds. Since PAN degrades before melting, the process involves mixing the polymer with polyethylene glycol (PEG) and water. This results in decreasing the melting point of the precursor (plasticizing effect), thus preventing polymer degradation [31].

In **Dry spinning**, the fibers are extruded into an evaporation chamber with hot gas to evaporate them. The extruded fibers are further stretched in boiling water to obtain higher molecular orientation. The extrusion of spinning dope is performed into the air gap of ~ 100 - 300 mm where the filament undergoes stretching, producing a high degree of molecular orientation.

Wet spinning consists of spinning the fibers in liquid-gel state into a coagulation bath containing higher concentration of solvent. The spinneret is immersed in the coagulation bath where fibers are spun. The fibers are drawn during spinning and by optimizing the conditions of drawing and coagulation bath, the properties of fiber can be modified. The polymer solutions are spun through a spinneret with a variety of holes each having a diameter in the range of $\sim 50 - 100 \mu\text{m}$. The composition and conditions in the coagulant bath are crucial for optimizing the precursor fiber morphological structure. Specifically, the coagulation rate is chosen with care since it affects the formation of skin on the surface of precursor fibers and cross section of fibers [29].

Further processing steps of wet spinning include washing, drawing and application drying. To remove the excess solvent from the fibers, the coagulated fiber bundles are washed with hot water and/or water steam in conjunction with the fiber drawing process. Fibers are drawn at elevated temperature, typically in the range of $120^\circ\text{C} - 160^\circ\text{C}$, using ethylene or glycerol as a drawing medium. These processes are significant to improve the molecular structure with increased crystallite size and degree of crystallinity [32].

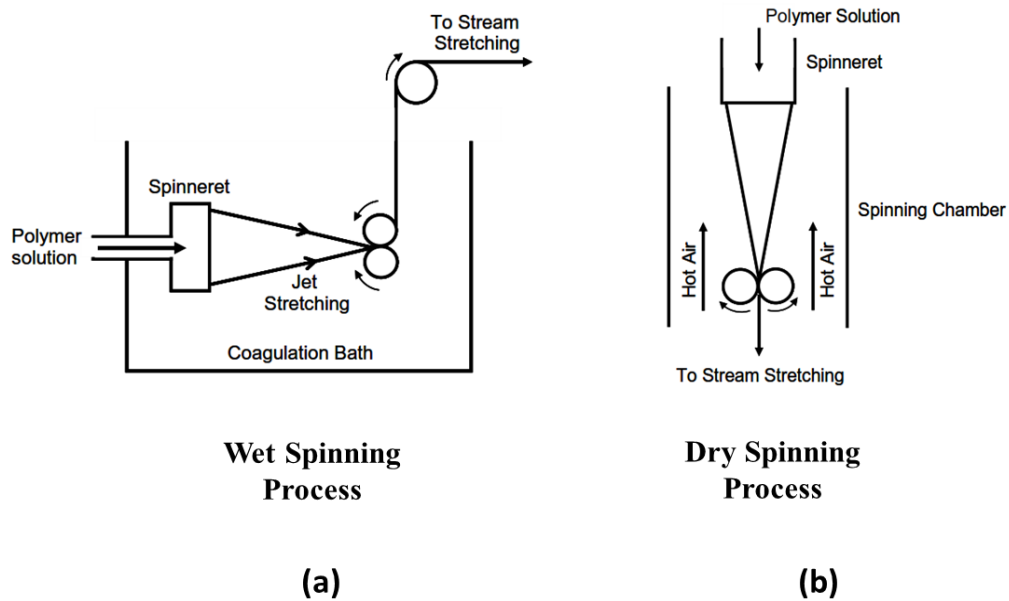


Figure 8- (a) Wet and (b) dry spinning process for PAN precursor fibers

2.5.2 Stabilization process:

The most significant step in carbon fiber production is the stabilization and it has been studied extensively over half a century. The process of stabilization is performed at 200 - 300 °C with a heating rate of 1-2 °C/min. The normal duration of stabilization varies from 30 min to 12 h depending on the requisite structure. During stabilization various reactions take place such as cyclization, oxidation, dehydration and intermolecular cross-linking [13, 33]. The high conversion temperature in the oxidation step coupled with highly exothermic reaction kinetics results in the evolution of heat, producing defects inside the fiber and on the surface of the filaments, This is predominant in larger fiber tows [34].

Cyclization is the most important reaction in stabilization, during cyclization, the nitrile groups in precursor fibers form a stable ladder polymer with adjacent groups. **Oxidation** has been reported to initiate the cyclization by diffusion of oxygen, first in the amorphous region of PAN. Moreover, the primary reaction caused by heating was cyclization and the cyclized ladder polymer serves as the foundation for oxidation reaction. Oxidation happens after cyclization, and afterwards dehydration takes place. However, it is impossible to separate the dehydration and oxidation reactions. **Dehydration** results in the formation of C=C double bonds which improve thermal stability and reduce chain scission. It is important to mention that the cyclization does not occur along the whole PAN chains and the typical cyclized segment length is around 3 ~ 5 nitrile groups. It has been proposed that the transfer reaction occurs leading to the propagation of further cross-linking [35, 36] .

All these reactions convert the linear PAN molecules into hexagonal ring structure containing carbon-nitrogen double bonds via generation of C=C bonds, hydroxyl (-OH) and carbonyl groups (-CO). The structure of stabilized PAN during different reactions in stabilization are shown in figure 9. The formation of ladder structure provides thermal stability and PAN can withstand the high temperature carbonization and graphitization process. Skipping the oxidative stabilization process results in fusion of precursor fibers and loss of material during carbonization. The stabilization process is performed via externally applied

tension which caters the loss of molecular orientation due to shrinkage. Two types of shrinkage processes take place during the oxidation process: physical shrinkage and chemical shrinkage. Physical shrinkage is due to the entropic relaxation and recoiling of polymer chains during the glass transition range whereas the chemical shrinkage is linked to the stabilization reactions, cyclization and chain-scission [37, 38]. During this stage, the density of PAN fiber increases from 1.18 to 1.36 g/cm³, the oxidized fibers then contain 62 - 70 wt. % carbon, 20 - 24 wt. % nitrogen, 5 - 10 wt. % oxygen, and ~ 4 wt. % hydrogen [12, 39].

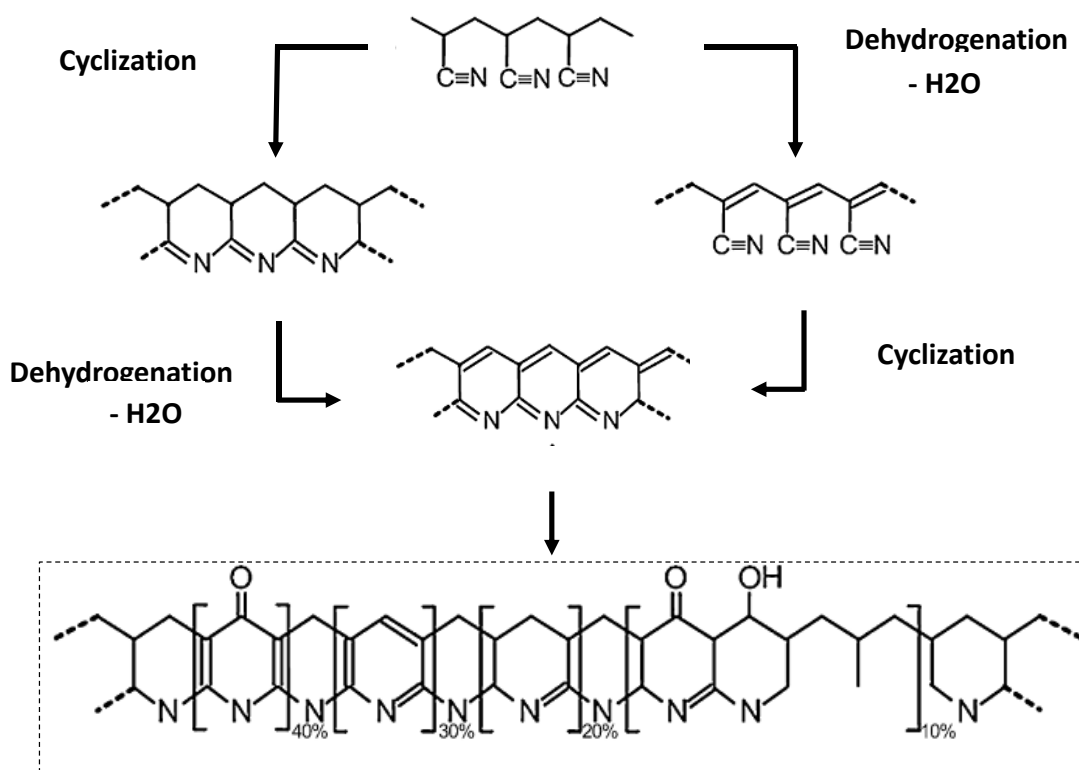


Figure 9- Cyclization, dehydrogenation, and chain scission reactions during stabilization

2.5.3 Carbonization and Graphitization process:

Stabilization precedes the carbonization process where the PAN fibers are heated at high temperatures usually till 1500 °C in an inert atmosphere (argon, nitrogen, or other non-oxidizing media). Heating rates of ~ 5 °C /min or 3 °C /min are used as further higher rates lead to enhanced pore formation causing surface in-homogeneities due to diffusion of gases. Typical carbonization process is divided into 2 stages, the first

stage involves heating up to 600 °C - 700 °C with a relatively lower heating rate and the second stage, up to 1500 °C where the higher heating rate doesn't damage the surface of fiber. The evolution of elements such as N₂, H₂ and HCN take place. Overall reduction in fiber diameter is observed and compared to the precursor PAN fibers the diameter is reduced to half. At this stage, these CFs contain > 98 wt. % carbon, 1-2 wt. % nitrogen, and 0.5 wt. % hydrogen [34, 40]. The ribbon-like polymer structure forms crosslinks in the low temperature regime, and subsequently additional condensation reactions follow up till 1600 °C, forming a turbostratic carbon phase. The proposed mechanism of carbonization by Watt et. al [35] is shown in figure 10. Nitrogen is removed as N₂ from the stabilized PAN structure as neighboring graphene sheets are linked to each other by substituting the N atoms located at graphene edge. The primary structure of CF is composed of crystallites of bent layers of preferably sp²-hybridized carbon atoms (turbostratic carbon). The carbon layers are disordered in stacking compared to a highly crystalline graphite.

During carbonization, there is formation of small crystallites and size of these crystallites increases and stacking of graphene planes take place. The heating of fibers above 1500 °C results in growth of crystallite size and long-range ordering of graphene planes occur. This process is termed as graphitization and is generally performed above 1500 °C till temperature as high as 3000 °C. By modifying the PAN precursor structure and optimization of stabilization and carbonization process parameters, control of graphitic structure can be achieved [27, 41]. For almost a century, optimization in these process parameters and spinning of precursor material had been worked on to produce high quality carbon fibers, high modulus carbon fiber and high strength carbon fibers with excellent electrical conductivities [28, 42].

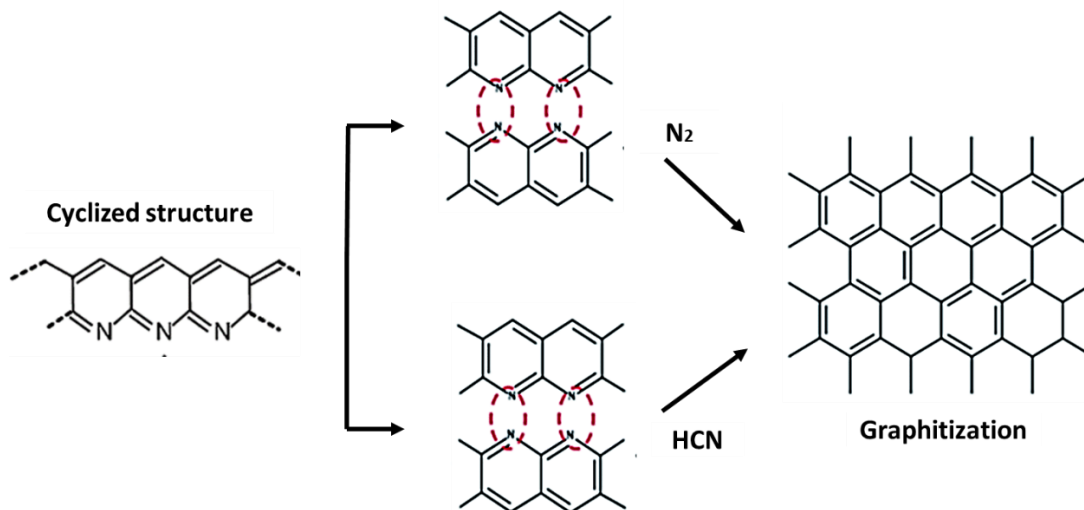


Figure 10- Mechanism of Carbonization process

2.6 Carbon nanofibers (CNFs)

2.6.1 CNF structure:

Presently, the carbon fiber production majorly relies on wet and solution spinning process to produce precursor fibers having size in order of tens of micron. The carbonized fibers after stabilization, carbonization, salinization, and sizing treatment have size of $\sim 7 \mu\text{m}$. With the advent of nanotechnology, materials with properties in sub-micron level are extensively explored. Reducing the fiber diameter results in not only enormous increase in the surface area but also diminishes the possibility of defect inclusion and typical skin-core fiber morphology. Basically, carbon nanofiber (CNF) is a quasi-one-dimensional carbon material between carbon nanotube and carbon fiber [3, 43]. Depending upon the methods, various structures of carbon nanofibers are possible with stacking manner of graphene layers such as tubular, platelets, herringbone and stacked cup as shown in figure 12. Carbon nanofibers (CNFs) prepared by electrospinning have orientation of graphene layers parallel to the fiber axis with a turbostratic structure. Increase in graphitization temperatures results in the improvement of holistic graphitic structure [10]. Figure 11 shows carbon fiber (produced by Teijin, $6 \mu\text{m}$) and carbon nanofibers produced in the present work (electrospinning-stabilization-carbonization process, 100 - 300 nm).

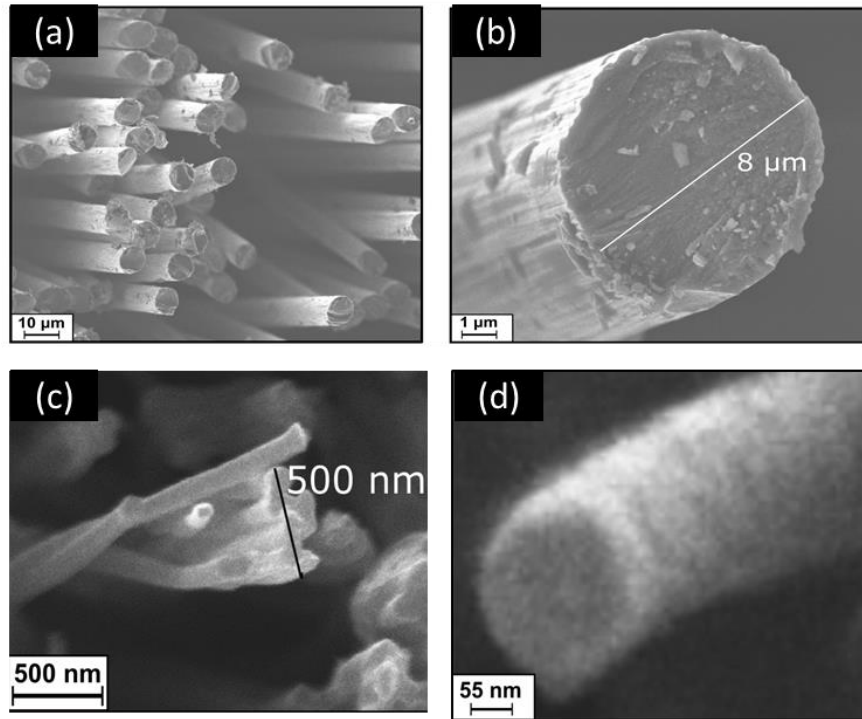


Figure 11 (a, b) Carbon Fibers and (c, d) Carbon Nanofibers

Carbon nanofibers and carbon nanotubes both have hexagonal crystalline planes, resembling the graphite structure. Both have sp^2 carbon bonding in hexagonal rings and possess aromaticity [44], the electrons are highly delocalized and easy to transport between different hexagons, this makes CNTs and CNFs good conductor for electricity. CNTs can be either single, double and multi-walled with diameter between 0.6 – 50 nm [45]. CNFs on the other hand have comparatively large diameter in the range of 50 - 300 nm. The properties of both are highly dependent on the structure and size. For CNTs, depending on the rolling direction of graphene cylinders/planes relative to tube axis. CNTs are classified as zigzag, armchair, and chiral respectively. CNFs have rolled graphene sheets which are majorly canted along fiber axis or have tubular or platelets arrangement with turbostratic structure. This gives CNFs more active open edges that can be chemically functionalized, enabling facile charge transfer. CNTs on the other hand are chemically inert and are chemically functionalized by destroying the end-caps. Intrinsically, CNFs possess more structural defects compared to CNTs, which reflects in their better physical properties [7, 46].

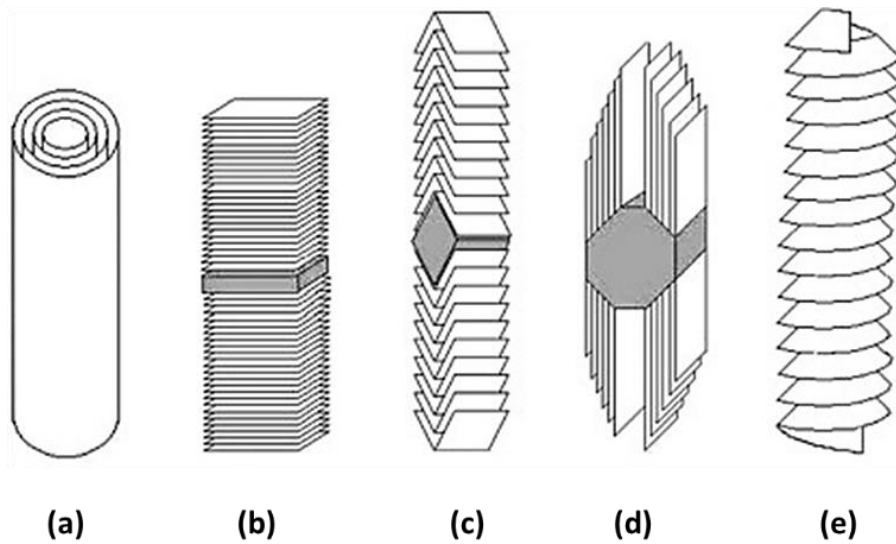


Figure 12 Structure of (a) multi-walled CNTs. Different types of structures of carbon nanofibers ;(b) graphene platelets, (c) graphene fishbones, (d) graphene ribbons and (e) stacked-cup [15, 47, 48]

2.6.2 Synthesis of Carbon nanofibers – Fabrication routes

The following section discusses different synthesis processes for carbon nanofibers such as chemical vapor deposition, templating method, drawing and phase separation. There are several techniques for producing nanofibers such as vapor evaporation method, template method and electrostatic spinning process [15, 44, 49, 50]. In chemical vapor deposition (CVD), carbon nanofibers (CNFs) are produced in a quartz tube with C_2H_2 as carbon source and metals such as iron, nickel, cobalt, and chromium to dissolve carbon to form metal carbide. The process involves heating the catalyst powder in a ceramic crucible inside the quartz tube to nearly $200\text{ }^\circ\text{C}$. Subsequently the carbon source is introduced and temperature is raised to $700\text{ }^\circ\text{C} - 800\text{ }^\circ\text{C}$ to produce CNFs [51, 52]. Later they are cooled and washed several times. The process is expensive, and rather produces short carbon nanofibers that are difficult to align, reinforce and assemble in composites for applications. Phase separation involves dissolution, gelation and extraction using different solvent freezing and drying methods which result in formation of porous foam [53]. Template based synthesis is used to make solid and hollow nanofibers [54, 55]. However the defects introduced by template and production of one-by-one continuous nanofiber are not feasible using this technique [50]. Among these

methods, electrospinning of polymer solution is a facile method for producing the fibers with submicron diameter. For all the thrust areas investigated in this thesis, electrospinning is used as a method to produce precursor nanofibers. These subsequently stabilized in air and carbonized in inert atmosphere to produce the carbon nanofibers. The stabilization and carbonization nearly follow the same process as done for fabrication of traditional carbon fibers in industry.

2.6.3 Electrospinning - the process:

Electrospinning technology is a widely used method to produce polymer fibers ranging from 2 nm to several micron from solutions of synthetic and natural polymers. The technique has gained much attention in the last decade due to its versatility in spinning a wide variety of polymers and its ability to consistently produce fibers in the submicron range which otherwise is hard to achieve, using standard mechanical fiber-spinning technologies [56, 57]. The electrospinning process involves employing a high electrical field to generate electrostatic forces inducing formation of a jet from a polymer solution. Higher voltage is applied to the polymer solution, an electric field is generated between the needle of syringe containing the spinning dope and the grounded collector. Fundamentally, the electrospinning system consists of three major parts: a high voltage power supply, a spinneret, and a grounded collector plate (usually a metal screen, plate, or rotating mandrel). The spinning solution drops from a needle forming a ‘Taylor cone’, named after Sir Geoffrey Taylor, who explained the effect of electric field on the liquid droplet [58, 59]. Polymer solution held by surface tension at the end of a capillary tube is subjected to an electric field and as the electric field reaches a critical value, the repulsive electrical forces overcome the surface tension. Eventually, a charged fiber jet erupts from the droplet which undergoes series of bending instability and ultra-stretching during this course. This all is accompanied by rapid evaporation of solvent and the nanofibers are deposited on the collector. A typical schematic of the electrospinning process is shown in figure 13. The first patent on electrospinning technology was issued in 1934, however it didn’t gain much intention until 1969 when Sir Geoffrey Taylor published his work on regarding “Electrically Driven Jets”, discussing the effect of electric field on the

geometry of the suspended liquid droplets [60]. In early 1970, Baumgarten reported spinning of acrylic resin in dimethyl formide (DMF) for various concentrations and viscosities to produce sub-micron fibers [58]. The findings showed that the solution viscosity is increased as the fiber diameter is increased. Following equation is used to predict the relation between the fiber diameter and solution viscosity by the following equation:

$$d = \eta^{0.5}$$

Where d is the diameter of the fiber and η is the viscosity of solution in poise. The electrospinning process can be adjusted to control the fiber morphology and diameters by varying, solution flow rate, electrospinning voltage, polymer solution concentration, solution conductivity and needle to collector distance.

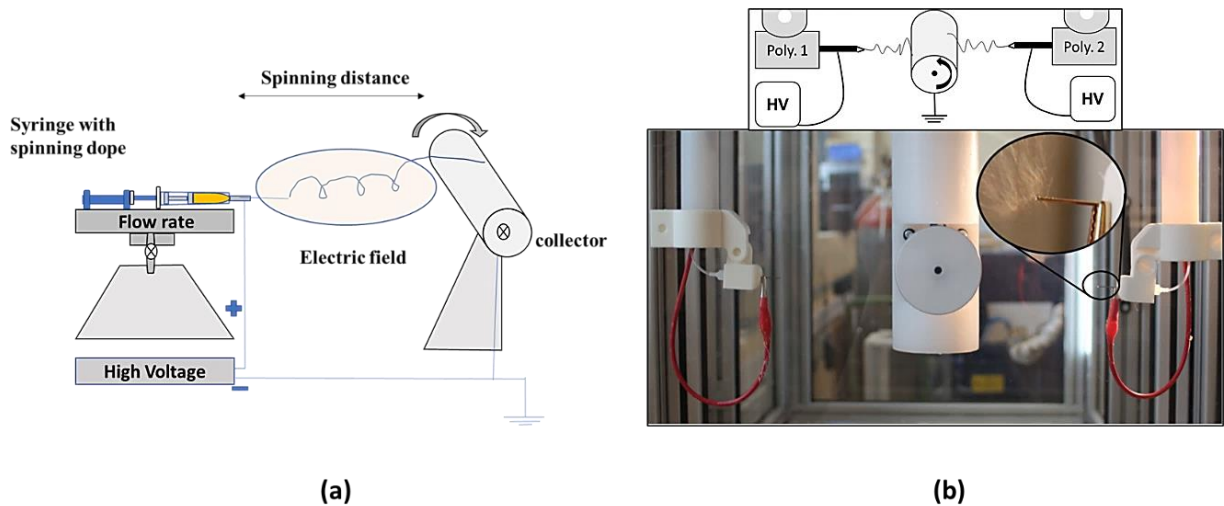


Figure 13- (a) Schematic illustration and (b) digital image of electrospinning process

Various studies have been conducted over the years to investigate different parameters that influence the nanofiber. Moreover, it is now established that the diameter of the fiber produced by electrospinning is influenced not only by the concentration of the polymer but also by its molecular conformation [56, 61]. A

dimensionless parameter, Berry number (Be), is used by numerous researchers as a working index for controlling the diameter of fibers.

$$Be = \eta C$$

The degree of polymer chains entanglements in a solution can be described by Be , where the η is the polymer intrinsic viscosity defined as the ratio of specific viscosity to the concentration at an infinite dilution and C is the concentration of the polymer solution [59]. Lot of studies discussing the Berry number, it is established to be an effective way to classify the spin ability of polymers. The intrinsic viscosity of a polymer is highly dependent on its molecular weight. The fibers diameter is influenced by the electrical voltage applied, higher electrical voltage results in increased stretching forces on Taylor cone and fiber jet is more stretched leading to decrease in fiber diameter. Similarly, conductivity of polymer solution has a great influence on formation of stable jets. The effect of distance between the capillary tip and the grounded target has also been studied by various groups. In general, the smaller the distance between the tip of needle and collector/target, the larger the diameter of fibers produced as there is insufficient time for the fiber-jet elongation. Nevertheless, all these factors affect the final morphology and diameter of produced nanofibers. The relations of each cannot be strictly exclusive since one parameter influences the other and the morphology of the nanofiber is highly objective for each influencing parameter and type of polymer solution used as a spinning dope. [56, 62]. The table 2 shows the main process parameters involved in the electrospinning process.

Presently, the electrospun nanofibers with smaller pores and higher surface area are successfully employed in various fields, such as nano-catalysis, tissue engineering scaffolds, protective clothing, filtration, biomedical, pharmaceutical, optical- electronics, biotechnology, defense, and security. Further this technology is now exclusively studied for layer-by-layer printing, near-field electro-printing, electro-writing and 3D printing techniques using various modifications to the electrospinning setups and parameters.

Table 2 Various parameters for electrospinning process

Operation Parameters	Solution Parameters	Physical Parameters
Voltage	Viscosity	Humidity
Flow rate	Dielectric constant	Temperature
Needle to collector distance	Polymer molecular weight	
	Conductivity of Polymer solution	
	Polymer concentration	

2.7 Properties of Carbon nanofibers:

2.7.1 Mechanical properties

Carbon fibers possess excellent mechanical, electrical and thermal properties. Mechanical properties such as modulus, tensile strength, toughness are dependent on the processing conditions, graphitic microstructure, and fiber diameter. The tensile strength of electrospun based carbon nanofibers is reported to be ~ 600 MPa with modulus of 60 GPa [63, 64]. Joseph et al. [65] reported that elastic modulus of CNFs ranged from 6 to 207 GPa using three-point bend test with carbon nanofiber mounted on copper grid and the AFM cantilever. It was concluded that tensile strength is dependent on the aligned graphite layers of the outer wall that were closest to the inner wall. Moreover, it was observed that the elastic modulus seemed to be independent of wall thickness for CNFs wall thickness of greater than 80 nm. It is worth mentioning here that the properties are highly dependent on the heat treatment temperature. Carbon nanofiber composites reinforced with carbon nanotubes (CNTs) have been reported to have increased mechanical properties in terms of tensile strength and elastic modulus by 38 % and 84 %. Similarly, reinforcing with graphene oxide and graphene platelets have shown marked increase in mechanical properties [66]. Compared to conventional carbon fibers, the mechanical properties of carbon nanofibers are difficult to evaluate. Most of the reported measurements are aided with assumptions and simplification due to complex

structural complexity of CNFs derived from variations in inner and outer wall thickness, cone angle, orientation of graphite planes the determination of their mechanical properties had posted considerable difficulties.

2.7.2 Thermal Properties

Thermal conductivity of carbon nanofibers is $\sim 2000 \text{ W mK}^{-1}$ (reported value for parent class of carbon nanofibers and vapor grown nanofibers). Compared to CNFs, the thermal conductivity of CNTs is estimated to be around $6000 \text{ W m}^{-1} \text{ K}^{-1}$, twice higher than diamond. The thermal conductivity (K) follows; $K = \sum C r v^2 \tau$, where C is the specific heat contribution from electron (C_{el}) and phonon (C_{ph}), v is the group velocity of phonons and τ is the phonon relaxation time. The findings from Benedict and Hone suggest that phonon excitations dictate the thermal properties of CNFs [67]. Most studies focused on thermal conductivity for CNFs are related to reinforcing them in polymer matrices, since the polymers have poor thermal conductivity. Due to their small size and high aspect ratio, they have extremely large surface area to volume ratio, which improves the interaction with the polymer matrix. Various studies have been made for CNFs reinforced in thermoplastic matrices such as poly-lactic acid, polyethylene (high density and low density) and polystyrene [68-70].

2.7.3 Electrical Properties

Electrical conductivity of CNFs is estimated to be $1 \times 10^4 - 1 \times 10^5 \text{ S/m}$. The electrical properties of CNFs are also highly dependent on graphitic structure and processing conditions. Very earlier studies by Endo et al. [71] reported conductivity of vapor grown carbon nanofibers to be around $1.8 \times 10^4 \text{ S/m}$. Typical electrical conductivity for commercially produced carbon fiber ranges from $1 \times 10^3 - 1 \times 10^4$ [72][73]. Carbon nanofibers possess higher electrical conductivity than micron sized carbon fibers, however the mechanical integrity and strength is inferior to that of carbon fibers. Very few production plants all around the globe exist focusing on sub-micron sized carbon fibers due to challenges with its higher cost. CNTs

comparatively have very high electrical conductivity of than CNFs ($\sim 1 \times 10^7$ S/m) [74]. Carbon nanotubes and carbon nanofibers are ballistic transporters for electron conduction when their structure is perfectly crystalline. The movement of electron is reduced due to defects in the crystalline structure that hinder the electron transport, leading to reduced mean path of electrons and lower electrical conductivity [75]. The interlayer interaction of CNFs also facilitates the electron transport. Resistance occurs only when electrons collide with defects in the crystalline structure. The amorphous structure and intrinsic defects impact the electron transport, reduce the mean free path of electrons, resulting in lower the electrical conductivity. In 3D conductors, electrons are free to scatter in any direction and each scattering event leads to electrical resistance; while in 1D conductors like CNFs, electrons can only travel back and forward along the fiber axis, where there is a significant reduction of scattering. Therefore, CNFs with high aspect ratio have high electrical conductivity. The study by Hermann et al. [76] showed that the electrical resistivity of CNFs graphitized at 2900 °C can reach up to 6.8×10^{-5} Ω .cm.

2.8 Applications of Carbon nanofibers

The light weight, high strength and stiffness accompanied with improved fatigue resistance, high thermal and electrical conductivity has enabled carbon fibers and derived composites to be used in a large number of structural application form aerospace, wind turbine blade, sports equipment, and transportation to pressure vessels and microelectronic device [77, 78]. The huge application volume of carbonized PAN fibers is increasing every year and the carbon fiber market is expected to reach ~ 4 billion \$ by 2025 [79]. Both in pristine form and as reinforcement in polymer matrices, carbon fiber has targeted nearly every field of our life today [22, 80].

PAN stabilized fiber mats are also used in many areas where heat resistance textiles and yarns are required. One of its kinds is PAN-OX produced by SGL Carbon group. It has been typically used as fire resistance textile in aircraft, train and cars seating, protective clothing for firefighter and racing drives. Similarly, the

oxidative stabilized PAN fiber produced by Zoltek is PYRON, which are used to replace asbestos in automotive brakes and clutches [81]. Carbon nanofibers are used as filler agents for different synthetic materials due to their excellent mechanical properties. In comparison with macroscopic fibers, a much lower quantity of nanofibers is required to achieve the same reinforcement. Additionally, their large specific surface area promotes relaxation processes in the matrix, resulting in improved interfacial strength [82].

In the medical sector, the application of carbon fiber includes Thermocomp-RC. Carbon fiber reinforced nylon 6/6 composite are used as the exoskeleton structure of a prosthetic arm and the Omni carbon-heart valve (a valve with a single hinge less pivoting disk). Carbon nanofibers offer promising potential to fabricate electrochemical sensors and biosensors [83, 84]. Vamvakaki et al. [85] reported CNFs for glucose sensing with high sensitivity, stability and reproducibility. CNFs based biosensors showed better response in comparison with SWCNTs and graphite powder. This is due to higher surface area and more active sites for adsorption of enzymes. Moreover, carbon fiber-reinforced fluoro-polymers and composites are used in pump wear rings, throat bushings, line shaft bearings, valve seats and washers. These parts require hot hardness, inherent strength, chemical resistance and dimensional stability; hence carbon fibers and derived composites serve the purpose [86]. Due to outstanding mechanical properties such as compressive strength with extremely light weight, carbon fibers are also used in pressure vessels for hydrogen and compressed natural gas storage tanks. PX35 tow by Zoltek, manufactured via filament winding of resin impregnated carbon fibers is used as key component in pressure vessel applications [87, 88].

The large surface area of a porous nanofibrous material is significant for energy conversion and storage. The automotive sector is working on employing carbon fibers not only as structural element but also as a storage electrode for next generation electric vehicle [89]. Carbon nanofibers with well interconnected pores offer good mechanical strength and electrochemical stability for porous separators [90]. They sustain a substantial uptake of electrolyte solution and enable high ion conduction. In catalysis, carbon nanofibers

loaded with metallic nanoparticles (Rh, Pt, Pd, etc.) are appropriate catalyst-carriers for hydrogenation reactions [91, 92].

In automotive sector, carbon fiber usage is increasing year by year to replace the traditional metal parts with light weight material with similar strength. Carbon fiber epoxy body panels are developed for Lamborghini Murcielago and hood pannel for Chervorlet Corvette Z06 [89, 93]. Replacing the body panels, truck chassis assemblies and space frames with carbon fibers reinforced composites reduce fuel cost. Very recently, AEVRO has launched first ever 3D printed all carbon fiber bike. Now a days, spring elements of car suspension system are being made by Polyether-ether ketone (PEEK) and polycarbonate (PC) based carbon fiber composites. The major parts of formula 1 racing car such as chassis, interior, and suspension components are made of CF-based epoxy composites. Starting from bicycle up to racing bikes, parts used in sports are also manufactured by CF-reinforced epoxy composites [94].

Aerospace sector has covered the most application volume as far as carbon fiber and carbon fiber composites are concerned. Both military and commercial-use helicopters have almost two-third part made of carbon fiber epoxy-based composites [95]. Generally, for aerospace, high-modulus carbon fiber (modulus 350 GPa) along with multifunctional epoxy resin is used. Pioneer in this sector, USA made a space shuttle having payload bay door, remote manipulator arm, and solid rocket motor cases from epoxy carbon fiber- composites. Carbon fibers are also used for EMI shielding, sensor, antistatic agent, and conductors. Exploiting excellent electrical conductivity of carbon fibers, they are also used in micro-electronic devices. Nevertheless, the demand for carbon fibers and their composites is increasing every day and it has already impacted the major and minor living applications [96].

2.9 Recapping the Objective

In summary, the application volume of carbon fibers and derived composites is at the rise. Due to the technological drive of e-mobility, energy harvesting and sustainability, the graphene based light weight

nanostructures with improved electrical properties is the fore-front of latest scientific research. As mentioned in chapter 1, the focus of the present work is encompassing the realization and investigation of graphene nanostructures using tangible carbon nanofibers for improved graphitic structure, targeting the electrical transport properties. Carbon nanofiber is relatively novel compared to carbon fiber and the details of its microstructure and structure-property relationship needs further exploration. The upcoming chapters sequentially describe different phases of the thesis.

3 METHODOLOGY AND TECHNIQUES

This chapter presents the properties of precursors and materials used, basic fabrication procedure adopted, and analytical/characterization tools employed in thesis work.

3.1 Materials

Polyacrylonitrile (PAN) was used as precursor material and mixed with Dimethyl formamide (DMF) to produce spinning dope (spinning solution). Carbon nanotubes (CNTs) and graphene nanoplatelets (GNPs) were used as nanocarbon inclusions to fabricate nanocarbon doped carbon nanofibers. These were the basic materials used for different investigations and for the project phases of the present research work. The table 3 shown below shows the list of chemicals used along with necessary details and their suppliers.

Table 3 Utilized chemicals, their details, and suppliers

Chemicals	Avg. Mw / Molar Mass (g/mol), density (ρ, g/cm³)	Supplier: Grade/Purity
Polyacrylonitrile (PAN)	Mw: 150,000	Sigma Aldrich
N, N-Dimethylformamide (DMF)	73.10 g/mol, 0.95 g/cm ³	Carl Roth, Germany 99.8 %
Multi-walled Carbon Nanotubes (MWCNTs)	12.01 g/mol, 1.800 g/ml	ABCR chemicals
Graphene Nanoplatelets (GNPs)	12.01 g/mol, 6-8 nm thick x 5 microns wide	ABCR chemicals

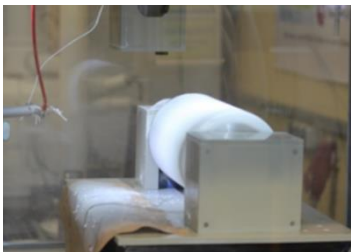


3.2 Fundamental Procedure – State of Art

As mentioned in section 1.3, there are different phases of the whole project based on which modifications are done to the basic fabrication process. The details of fabrication modification for each phase are

described in their respective chapters. The basic process which serves as state of art for fabrication of the ‘carbon nanofibers’ is described below and kept as a fundamental procedure for all investigations.

PAN spinning-dope was prepared by mixing required quantities in DMF solvent overnight for nearly a duration of 12 h at room temperature. The homogenous solution of PAN/DMF was electrospun using a tower electrospinning setup with needle and rotating collector. The spinning dope was loaded into the syringe and the solution was electrospun with accelerating voltage of 16 KV, distance of needle to collector of ~ 18 cm, collector speed of 8 m/s, solution flow rate of ~ 1 ml/h and the fiber mats were collected on rotating collector covered with aluminum foil. In the second stage, stabilization was performed in the air at 250 °C for a duration of 10 h at a heating rate of 1 °C /min. The stabilization is performed in different physical ways w.r.t to respective project phases. The stabilized nanofiber mats were carbonized subsequently with a heating rate of 5 °C /min with a various temperature from 800 °C to 1700 °C, with a dwell time (1, 5, 10 h) depending upon the desired microstructure. The parameters employed in the carbon nanofiber fundamental fabrication process are also described below in Table 4.

Table 4 Process parameters used in fundamental carbon nanofiber fabrication process

Electrospinning	Stabilization	Carbonization
Parameters	Parameters	Parameters
		
Voltage: 16 KV	Heating rate: 1 °C/min	Heating rate: 5 °C/min
Flow rate: 1.8 ml/h	Dwell time: 2 - 10 h	Dwell time: 1 - 10 h
Source to collector distance: 18 cm	Temperature: 230 - 250 °C	Temperature: 800 - 1700 °C

3.3 Techniques and Analysis

This section presents all the characterization tools and techniques used for the analysis and testing of the prepared samples. For each project phase different techniques were used to characterize the morphology, molecular structure, graphitic structure, and electrical transport properties.

3.3.1 Scanning Electron Microscope (SEM)

Morphology of spun nanofibers, stabilization and carbonized fibers were analyzed using morphology scanning electron microscope (SEM) (Zeiss Leo VP, 1455, Germany). The basic principle of the technique relies on the raster electron scanning in which electrons are either reflected from the very surface (back scattered electron) and the bulk (secondary electrons), carrying information about the samples analyzed. An electron beam is generated by a filament in a vacuum chamber and is focused by electromagnetic lenses to form a beam point. When the primary electron beam impinges on the specimen surface, secondary electrons are emitted and collected by a detector to generate an image [97, 98]. The non-conductive samples are coated (SC7620 Mini Sputter Coater, Quorum Technologies) before the analysis, since the high radiation density of the electron beam leads to static charges, which can affect the measurements due to electron accumulation at the measuring spot.

3.3.2 FTIR and polarized FTIR spectroscopy

For the analysis of the molecular structure of the as spun and the stabilized polyacrylonitrile mats, Fourier transform infrared spectroscopy (FTIR, Perkin Elmer 2) was used. The technique measures the infrared region of the electromagnetic radiation spectrum. Unlike the dispersive IR spectroscopy, FTIR spectroscopy irradiates a sample with many frequencies of IR light at once by means of an interferometer and post-processing of the transmitted light. In a typical procedure, beam source of various IR wavelength light is sent through a beam splitter. These two split beams are then reflected and recombined (with a path

difference between the beams) to construct an interference pattern, reflecting the constructive and destructive interference of the recombination. Subsequently, this interference pattern (interferogram) is sent to the sample, and the transmitted portion of the interferogram is sent to a detector. By comparing this with a reference sample beam spectrum in the detector, a Fourier transform is performed to obtain the full spectrum as a function of wavenumber [99].

The most prominent change occurring during the stabilization process in the PAN structure is the conversion of $C\equiv N$ groups to $C=N$ groups, which indicates cyclization process. The ring cyclization index (RCI) was calculated by measuring the integral intensity of absorbed IR, $C\equiv N$ (2240 cm^{-1}) and $C=N$ (1600 cm^{-1}) peaks, using the following equation:

$$RCI = \frac{I_{C=N}}{I_{C\equiv N} + I_{C=N}} \quad (1)$$

In addition, molecular orientation was evaluated using Hermann Orientation factor (f), which depends on the principle that the dichroic ratio of nitrile peak (2240 cm^{-1}) intensity is calculated when the plane of polarization was parallel (\parallel , A_0) and perpendicular (\perp , A_{90}) to the fiber axis. The orientation factor (f) is then given by the following expression:

$$f = \frac{2}{3} \frac{D-1}{2\cos^2\theta} \frac{D+2}{D+2} \quad \text{With } D = \frac{A_0}{A_{90}} \quad (2)$$

D is the dichroic ratio of polarized absorbance intensity of the nitrile peak (2240 cm^{-1}). θ is an angle between polymer chain backbone and nitrile group (this method makes use of this fixed angle (70°) between the backbone of polymer chain and the ($C\equiv N$) nitrile group. In a typical procedure, the potassium bromide (KBr) pellets were prepared. Afterwards, KBr and fiber mats were pressed, and direction of fiber alignment was marked.

3.3.3 X-ray Diffraction

X-ray diffraction technique (Bruker, D2 Phaser) was employed to have insight regarding interplanar spacing and crystallite size for as spun and specifically the carbonized polyacrylonitrile fiber mats. In this technique, X-rays are generated from an X-ray tube and a monochromator filter, so that it has a single wavelength frequency. The atoms in the crystal refract the X-rays and are elastically scattered onto a detector. Because they are elastically scattered, they have the same energy as the incident X-rays, generating a 2D diffraction pattern of the crystal. The scanning ranges from 10° - 80° with a step size of 0.03° using Cu- K_α ($\lambda = 1.5406 \text{ \AA}$) was employed to characterize the samples. The interlayer spacing, d (002) was evaluated using Bragg law ($d = (\lambda / 2 \sin\theta)$, where λ is the wavelength of the x-ray source and θ is the Bragg angle) while for calculating the crystallite size, Scherrer equation ($L_c = (K \lambda / \beta \cos\theta)$) was employed, where K is the shape factor (0.89 for L_c) and β is the full width at half maximum (FWHM) in radians) [100].

3.3.4 Transmission Electron Microscope

Transmission electron microscopy (TEM, FEI Tecnai G2 F20) was carried to characterize graphitic structure and alignment/orientation of carbon planes. Electrons are injected at the top of the column, accelerated down, passed through a combination of lenses and apertures to produce a focused beam of electrons. In TEM, the transmission of electron beam is highly dependent on the properties of material under examination. TEM uses transmitted electrons (electrons that are passing through the sample) to create an image compared to SEM. Henceforth, the details are finer with improved resolution to visualize atomic planes [101]. Imaging was carried out using field emission gun at accelerating voltage of 200 KV in bright field mode. Prior to that, sample preparation was done in facile way by ultrasonically small pieces of the fiber mats in 500 μl of ethanol for 15 min. Most of the solvent was removed in an air flow and ethanol solution containing the fibers was drop-casted onto a carbon coated copper grid (Quantifoil, 300 mesh) for

imaging to be performed. Based on the sample matrix, information regarding the orientation of graphene layers, curling and tortuosity in carbon planes was investigated.

3.3.5 Raman Spectroscopy

Raman spectroscopy (DXR2 Thermo Fisher Scientific) was employed extensively to characterize the graphitic structure, disorder and defects in carbon nanofiber end structure. The Raman-effect is based on scattering of light, which includes both elastic (Rayleigh) scattering at the same wavelength as the incident light, and inelastic (Raman) scattering at different wavelengths, due to molecular vibrations. Most of the scattered light is of the same wavelength as the laser source and there is no useful information – this is called Rayleigh scattering. However, a small amount of light ($\sim 0.0000001\%$) is scattered at different wavelengths, characteristic of the chemical structure of the analyte under study, this is termed Raman Scatter [102]. A Raman spectrum features several peaks with intensity and specific wavelength. For carbon-based nanomaterials, it is widely recognized to extract the information regarding the order/disorder in graphitic crystals, graphitization degree and graphene layer count to distinguish between single-, bi- and multi-layer graphene.

For all investigation in the present study, laser wavelength of 532 nm was used as an excitation source. Carbon nanofiber in the form of assemblies were directly placed on the glass slide and spectra were acquired in the range of $500 - 3500 \text{ cm}^{-1}$. Initially in the optimization phase, different laser powers were used, however, to avoid heating of the samples and false signals for all different phases studied in the present project, 1 mW of laser intensity was used. Mainly the confocal geometry $25 \mu\text{m}$ pinhole aperture geometry was employed. Nearly for all the measurements done, 10 exposures were made with exposure time of 3 seconds. The most significant D- and G-bands in carbon materials were deduced and evaluated. The R-value, i.e. the I_D/I_G intensity ratio, depends on the concentration of defects including grain boundaries and graphite edge planes, the alignment of the graphitic planes and the graphitization degree [103, 104]. The spectra were deconvoluted using Gaussian fitting after a baseline subtraction via Origin lab pro software

and I_D and I_G ratios (integral intensity of D- and G-band were evaluated. Moreover, the crystal size along the basal plane (L_a) was calculated (L_a (nm) = $(2.4 \times 10^{-10}) \lambda^{4\text{laser}} (I_D / I_G)^{-1}$). For the sample graphitized at 1500 °C or more, the high wavenumber 2D-band was observed which is active due to double resonance mechanism.

3.3.6 X-ray Photoelectron Spectroscopy (XPS)

X-ray Photoelectron spectroscopy (XPS, SPECS) was used to obtain the graphitic structure of the surface in-terms of sp^2 and sp^3 hybridized bonding in carbon structure. Al K_α emission source and recorded with Phoibos 100 spectrometer equipped with an MCD-5 detector at a pass energy of 20 eV. X-ray photoelectron spectroscopy is more surface sensitive compared to Raman spectroscopy, and the information depth is limited to ~ 10 nm. This makes it an interesting characterization tool as far as the structure and properties of surface and sub-surface of carbon nanofiber is concerned. The technique relies on the basic principle of Photoelectric effect to identify the elemental composition, chemical state, and electronic structure. Elemental composition as well as the bonding elemental composition, both can be determined using this technique. Material is irradiated with x-ray of known wavelength and the emitted electron kinetic energies are measured. A photoelectron spectrum is recorded by counting ejected electrons. Each element has a characteristic binding energy associated with its core electron levels [105, 106]. The measured kinetic energy of the ejected photoelectron is determined by the incoming energy of the incident X-ray photon, $h\nu$ (typically Al K_α radiation are used). The binding energy (BE) of the photoelectron is calculated by the relationship ($K.E = h\nu - B.E$). In the present study, XPS was performed to evaluate the sp^2 fraction and sp^2/sp^3 ratio via deconvolution of C1s spectra. The C1s-spectra were deconvoluted considering 3 major contributions, namely the shake-up emission at 290.7 eV, sp^2 hybridized carbon atoms at 284.4 eV and sp^3 hybridized carbon at 285.2 eV. The C1s spectra were fitted using symmetric Gaussian-Lorentzian functions including the Shirley background, under a limitation that the energy difference between the sp^2 - and the sp^3 -peak is ~ 0.8 eV [107].

3.3.7 4PP STM/SEM Setup

A four-point measurement technique was used to investigate the electrical transport properties of carbon nanofibers. As the name suggests, the current is passed via two measuring tips and the voltage drop is measured with the other two tips. The easiest approach to measure the resistance (R) of a conductor is to use the two-point probe (2PP) setup. In this geometry, both probes serve as current injectors as well as voltage probe simultaneously, henceforth the total resistance is the sum of resistance of the sample and the probes. In turn, the resistance of the probe consists of the actual contact resistance and the resistance of the lead. Hence, 2PP method depends on the value of probe resistance to evaluate the sample resistance. $R_{2PP} = R_s + R_p$, and $R_s = R_c + R_l$ (where R_s and R_p denote the resistance of the sample and the probes and R_c and R_l denotes contact resistance and the resistance of the leads. However, in the four-point probe (4PP) geometry, the current is injected through the outer probes while the voltage is measured between the inner probes, as shown in figure 14. Therefore, the probe resistance is negligible owing to the higher input impedance of the voltmeter.

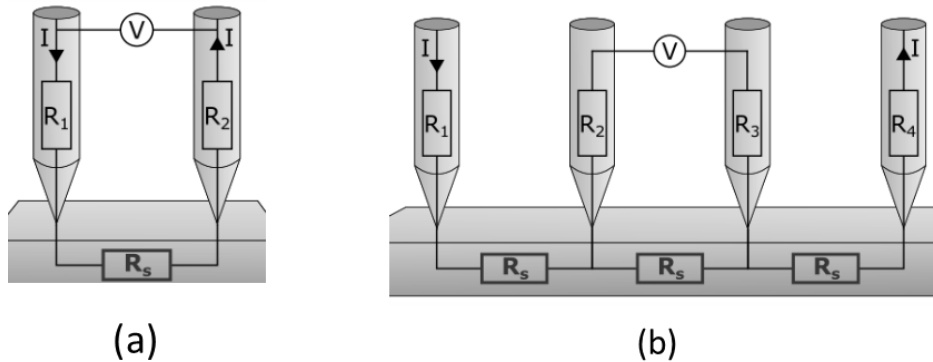


Figure 14- Two point and Four-point probe geometry

4PP-STM/SEM is a four-point probe arrangement technique, which is a combination of a four-point scanning tunneling microscope (STM) and a scanning electron microscope (SEM). All measurements of the electronic transport were carried out in an ultrahigh-vacuum chamber from Omicron Nanotechnology.

The setup consists of two sub-chambers, each with an arrangement for introducing samples into the vacuum system. These chambers are separated from each other by a valve. It has the advantage that both chambers can be equipped with samples independently of each other. The samples can be placed on the manipulator arm with a filament or with direct current or they can be heated on a cooling platform by using the cooling liquid nitrogen. A pyrometer for temperature control has a range between 300 °C and 2100 °C. The second area includes the 4PP-STM and the SEM [108]. A structure of the scanning unit of the four-point STM is shown in Figure 15a. There are four tip holders under the SEM. Three standard scanners and one high-resolution scanner, which allows an atomic resolution measurement on a surface. All scanners can be operated independently of each other by means of piezo motors controlling the spatial directions. In-situ rotational square measurements were performed on nanofiber mat to investigate the anisotropy in electrical conductivity based on nanofiber preferred orientation in the mat/bundle. Electrochemically etched tungsten tips with apex radii 20 - 70 nm were used to carry out the measurements (figure 15b). Carbonized bundles were placed on silicon substrate for measurements on fiber mats while to perform the measurements on single nanofibers, the mats were ultra-sonicated in acetone for a couple of minutes and then droplet-casted on Si substrate. This resulted in isolation of individual nanofibers from the fiber mat to carry out the measurements.

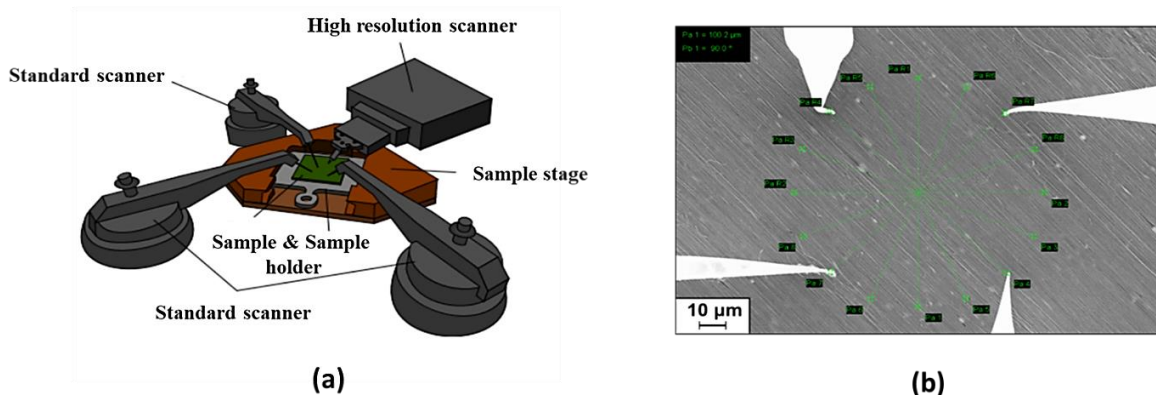


Figure 15 Schematic of 4pp STM scanning head with 4 probes, (b) Rotational sq. measurements in 4 tip arrangements on carbon nanofiber mat

References

- [1] S.-J. Park, Carbon fibers, (2015).
- [2] W. Ruland, Carbon fibers, *Advanced Materials* 2(11) (1990) 528-536.
- [3] E. Frank, F. Hermanutz, M.R. Buchmeiser, Carbon fibers: precursors, manufacturing, and properties, *Macromolecular materials and engineering* 297(6) (2012) 493-501.
- [4] P. Morgan, Carbon fibers and their composites, CRC press 2005.
- [5] K. Tanaka, S. Iijima, Carbon nanotubes and graphene, Newnes 2014.
- [6] R.B. Mathur, B.P. Singh, S. Pande, Carbon nanomaterials: synthesis, structure, properties and applications, CRC Press 2016.
- [7] P.J. Harris, Carbon nanotubes and related structures: new materials for the twenty-first century, American Association of Physics Teachers, 2004.
- [8] L. Dai, Carbon nanotechnology: recent developments in chemistry, physics, materials science and device applications, Elsevier 2006.
- [9] D.S. Bethune, R.B. Beyers, C.-h. Kiang, Carbon fibers and method for their production, Google Patents, 1995.
- [10] A. Ramos, I. Cameán, A.B. García, Graphitization thermal treatment of carbon nanofibers, *Carbon* 59 (2013) 2-32.
- [11] M. Inagaki, Y. Yang, F. Kang, Carbon nanofibers prepared via electrospinning, *Advanced Materials* 24(19) (2012) 2547-2566.
- [12] M.S.A. Rahaman, A.F. Ismail, A. Mustafa, A review of heat treatment on polyacrylonitrile fiber, *Polymer degradation and Stability* 92(8) (2007) 1421-1432.
- [13] S. Dalton, F. Heatley, P.M. Budd, Thermal stabilization of polyacrylonitrile fibres, *Polymer* 40(20) (1999) 5531-5543.
- [14] T.D. Burchell, Carbon materials for advanced technologies, Elsevier 1999.
- [15] S. Iijima, Helical microtubules of graphitic carbon, *nature* 354(6348) (1991) 56-58.
- [16] M.I. Katsnelson, Graphene: carbon in two dimensions, *Materials today* 10(1-2) (2007) 20-27.
- [17] D. Jariwala, V.K. Sangwan, L.J. Lauhon, T.J. Marks, M.C. Hersam, Carbon nanomaterials for electronics, optoelectronics, photovoltaics, and sensing, *Chemical Society Reviews* 42(7) (2013) 2824-2860.

- [18] R.H. Baughman, A.A. Zakhidov, W.A. De Heer, Carbon nanotubes--the route toward applications, *science* 297(5582) (2002) 787-792.
- [19] R.E. Smalley, Discovering the fullerenes, *Reviews of Modern Physics* 69(3) (1997) 723.
- [20] J.V. Larsen, T. Smith, Carbon Fiber Structure, NAVAL ORDNANCE LAB WHITE OAK MD, 1971.
- [21] J.-B. Donnet, R.C. Bansal, Carbon fibers, Crc Press 1998.
- [22] M.S. Dresselhaus, G. Dresselhaus, K. Sugihara, I.L. Spain, H.A. Goldberg, Graphite fibers and filaments, Springer Science & Business Media 2013.
- [23] S.-J. Park, History and structure of carbon fibers, *Carbon Fibers*, Springer 2018, pp. 1-30.
- [24] A. Shindo, Studies on graphite fiber, Gov. Ind, Res. Inst., Osaka, Rep 317(5) (1961).
- [25] B. Colvin, P. Storr, The crystal structure of polyacrylonitrile, *European Polymer Journal* 10(4) (1974) 337-340.
- [26] Z. Bashir, Co-crystallization of solvents with polymers: The x-ray diffraction behavior of solvent-containing and solvent-free polyacrylonitrile, *Journal of Polymer Science Part B: Polymer Physics* 32(6) (1994) 1115-1128.
- [27] E. Fitzer, Pan-based carbon fibers—present state and trend of the technology from the viewpoint of possibilities and limits to influence and to control the fiber properties by the process parameters, *Carbon* 27(5) (1989) 621-645.
- [28] W. Watt, Chemistry and physics of the conversion of polyacrylonitrile fibres into high-modulus carbon fibres, Elsevier Science Publishers B. V., *Handbook of Composites*. 1 (1985) 327-387.
- [29] M. Chen, C. Wang, Q. Gao, Y. Wang, M. Jing, W. Wang, Research on the multi-scale microstructure of polyacrylonitrile precursors prepared by a dry-jet wet spinning process, *High Performance Polymers* 31(6) (2019) 662-670.
- [30] B.S. Gupta, M. Afshari, Polyacrylonitrile fibers, *Handbook of Properties of Textile and Technical Fibres*, Elsevier 2018, pp. 545-593.
- [31] M. Yu, H. Rong, K. Han, Z. Wang, Y. Zhang, Y. Tian, Q. Dong, X. Zhao, H. Zhang, Process of melt-spinning polyacrylonitrile fiber, Google Patents, 2014.
- [32] N. Yusof, A. Ismail, Post spinning and pyrolysis processes of polyacrylonitrile (PAN)-based carbon fiber and activated carbon fiber: A review, *Journal of Analytical and Applied Pyrolysis* 93 (2012) 1-13.
- [33] M.K. Jain, A. Abhiraman, Conversion of acrylonitrile-based precursor fibres to carbon fibres, *Journal of materials science* 22(1) (1987) 278-300.
- [34] Z. Wangxi, L. Jie, W. Gang, Evolution of structure and properties of PAN precursors during their conversion to carbon fibers, *Carbon* 41(14) (2003) 2805-2812.

- [35] W. Watt, W. Johnson, Mechanism of oxidation of polyacrylonitrile fibres, *Nature* 257(5523) (1975) 210-212.
- [36] O. Bahl, L. Manocha, Characterization of oxidised pan fibres, *Carbon* 12(4) (1974) 417-423.
- [37] E.N. Sabet, P. Nourpanah, S. Arbab, Quantitative analysis of entropic stress effect on the structural rearrangement during pre-stabilization of PAN precursor fibers, *Polymer* 90 (2016) 138-146.
- [38] O.P. Bahl, L.M. Manocha, Shrinkage behaviour of polyacrylonitrile during thermal treatment, *Die Angewandte Makromolekulare Chemie: Applied Macromolecular Chemistry and Physics* 48(1) (1975) 145-159.
- [39] A. Gupta, I. Harrison, New aspects in the oxidative stabilization of PAN-based carbon fibers, *Carbon* 34(11) (1996) 1427-1445.
- [40] Y. Zhang, N. Tajaddod, K. Song, M.L. Minus, Low temperature graphitization of interphase polyacrylonitrile (PAN), *Carbon* 91 (2015) 479-493.
- [41] S. Lee, J. Kim, B.-C. Ku, J. Kim, H.-I. Joh, Structural evolution of polyacrylonitrile fibers in stabilization and carbonization, (2012).
- [42] B.A. Newcomb, Processing, structure, and properties of carbon fibers, *Composites Part A: Applied Science and Manufacturing* 91 (2016) 262-282.
- [43] M.F. De Volder, S.H. Tawfik, R.H. Baughman, A.J. Hart, Carbon nanotubes: present and future commercial applications, *science* 339(6119) (2013) 535-539.
- [44] Y.A. Kim, T. Hayashi, M. Endo, M.S. Dresselhaus, Carbon nanofibers, *Springer handbook of nanomaterials*, Springer2013, pp. 233-262.
- [45] T.W. Ebbesen, Carbon nanotubes: preparation and properties, CRC press1996.
- [46] T. Rath, Carbon Nanofibers: Synthesis, Properties and Applications, *Polymer Nanocomposites Based on Inorganic and Organic Nanomaterials* (2015) 63-88.
- [47] J. Vera-Agullo, H. Varela-Rizo, J.A. Conesa, C. Almansa, C. Merino, I. Martin-Gullon, Evidence for growth mechanism and helix-spiral cone structure of stacked-cup carbon nanofibers, *Carbon* 45(14) (2007) 2751-2758.
- [48] M. Endo, Y. Kim, T. Hayashi, Y. Fukai, K. Oshida, M. Terrones, T. Yanagisawa, S. Higaki, M. Dresselhaus, Structural characterization of cup-stacked-type nanofibers with an entirely hollow core, *Applied Physics Letters* 80(7) (2002) 1267-1269.
- [49] M. Endo, H. Kroto, Formation of carbon nanofibers, *The Journal of Physical Chemistry* 96(17) (1992) 6941-6944.
- [50] A.A. Almetwally, M. El-Sakhawy, M. Elshakankery, M. Kasem, Technology of nano-fibers: Production techniques and properties-Critical review, *J. Text. Assoc* 78(1) (2017) 5-14.

- [51] N. Hamada, S.-i. Sawada, A. Oshiyama, New one-dimensional conductors: Graphitic microtubules, *Physical review letters* 68(10) (1992) 1579.
- [52] N.M. Rodriguez, A. Chambers, R.T.K. Baker, Catalytic engineering of carbon nanostructures, *Langmuir* 11(10) (1995) 3862-3866.
- [53] T. Guo, P. Nikolaev, A.G. Rinzler, D. Tomanek, D.T. Colbert, R.E. Smalley, Self-assembly of tubular fullerenes, *The Journal of Physical Chemistry* 99(27) (1995) 10694-10697.
- [54] G. Che, B. Lakshmi, C. Martin, E. Fisher, R.S. Ruoff, Chemical vapor deposition based synthesis of carbon nanotubes and nanofibers using a template method, *Chemistry of Materials* 10(1) (1998) 260-267.
- [55] J. Hulteen, A general template-based method for the preparation of nanomaterials, *Journal of Materials Chemistry* 7(7) (1997) 1075-1087.
- [56] J. Doshi, D.H. Reneker, Electrospinning process and applications of electrospun fibers, *Journal of electrostatics* 35(2-3) (1995) 151-160.
- [57] T. Hongu, G.O. Phillips, *New fibers*, Elsevier 1997.
- [58] P.K. Baumgarten, Electrostatic spinning of acrylic microfibers, *Journal of colloid and interface science* 36(1) (1971) 71-79.
- [59] D.P. Smith, The electrohydrodynamic atomization of liquids, *IEEE transactions on industry applications* (3) (1986) 527-535.
- [60] G.I. Taylor, Electrically driven jets, *Proceedings of the Royal Society of London. A. Mathematical and Physical Sciences* 313(1515) (1969) 453-475.
- [61] L. Larrondo, R. St. John Manley, Electrostatic fiber spinning from polymer melts. I. Experimental observations on fiber formation and properties, *Journal of Polymer Science: Polymer Physics Edition* 19(6) (1981) 909-920.
- [62] J.M. Deitzel, J. Kleinmeyer, D. Harris, N.B. Tan, The effect of processing variables on the morphology of electrospun nanofibers and textiles, *Polymer* 42(1) (2001) 261-272.
- [63] Z. Zhou, C. Lai, L. Zhang, Y. Qian, H. Hou, D.H. Reneker, H. Fong, Development of carbon nanofibers from aligned electrospun polyacrylonitrile nanofiber bundles and characterization of their microstructural, electrical, and mechanical properties, *Polymer* 50(13) (2009) 2999-3006.
- [64] S.N. Arshad, M. Naraghi, I. Chasiotis, Strong carbon nanofibers from electrospun polyacrylonitrile, *Carbon* 49(5) (2011) 1710-1719.
- [65] J.G. Lawrence, L.M. Berhan, A. Nadarajah, Elastic properties and morphology of individual carbon nanofibers, *ACS nano* 2(6) (2008) 1230-1236.
- [66] X. Li, K. Li, H. Li, J. Wei, C. Wang, Microstructures and mechanical properties of carbon/carbon composites reinforced with carbon nanofibers/nanotubes produced in situ, *Carbon* 45(8) (2007) 1662-1668.

- [67] C.I. Contescu, K. Putyera, Dekker Encyclopedia of Nanoscience and Nanotechnology; -Six Volume Set, Taylor & Francis 2009.
- [68] S.M. Khan, N. Gull, M.A. Munawar, A. Islam, S. Zia, M. Shafiq, A. Sabir, S.M. Awais, M.A. Butt, M.T.Z. Butt, 2D carbon fiber reinforced high density polyethylene multi-layered laminated composite panels: structural, mechanical, thermal, and morphological profile, *Journal of Materials Science & Technology* 32(10) (2016) 1077-1082.
- [69] M.H. Gabr, W. Okumura, H. Ueda, W. Kuriyama, K. Uzawa, I. Kimpara, Mechanical and thermal properties of carbon fiber/polypropylene composite filled with nano-clay, *Composites Part B: Engineering* 69 (2015) 94-100.
- [70] S. Chen, J. Feng, Epoxy laminated composites reinforced with polyethyleneimine functionalized carbon fiber fabric: Mechanical and thermal properties, *Composites science and technology* 101 (2014) 145-151.
- [71] M. Endo, Y. Kim, T. Hayashi, K. Nishimura, T. Matusita, K. Miyashita, M. Dresselhaus, Vapor-grown carbon fibers (VGCFs): basic properties and their battery applications, *Carbon* 39(9) (2001) 1287-1297.
- [72] H. Matsumoto, S. Imaizumi, Y. Konosu, M. Ashizawa, M. Minagawa, A. Tanioka, W. Lu, J.M. Tour, Electrospun composite nanofiber yarns containing oriented graphene nanoribbons, *ACS applied materials & interfaces* 5(13) (2013) 6225-6231.
- [73] X. Zhang, S. Fujiwara, M. Fujii, Measurements of thermal conductivity and electrical conductivity of a single carbon fiber, *International Journal of Thermophysics* 21(4) (2000) 965-980.
- [74] T. Ebbesen, H. Lezec, H. Hiura, J. Bennett, H. Ghaemi, T. Thio, Electrical conductivity of individual carbon nanotubes, *Nature* 382(6586) (1996) 54-56.
- [75] B. Marinho, M. Ghislandi, E. Tkalya, C.E. Koning, G. de With, Electrical conductivity of compacts of graphene, multi-wall carbon nanotubes, carbon black, and graphite powder, *Powder Technology* 221 (2012) 351-358.
- [76] J. Heremans, Electrical conductivity of vapor-grown carbon fibers, *Carbon* 23(4) (1985) 431-436.
- [77] D. Church, A revolution in low-cost carbon fiber production, *Reinforced Plastics* 62(1) (2018) 35-37.
- [78] J.D. Buckley, D.D. Edie, *Carbon-carbon materials and composites*, William Andrew 1993.
- [79] A. Lefevre, S. Garnier, L. Jacquemin, B. Pillain, G. Sonnemann, Anticipating in-use stocks of carbon fiber reinforced polymers and related waste flows generated by the commercial aeronautical sector until 2050, *Resources, Conservation and Recycling* 125 (2017) 264-272.
- [80] L.H. Peebles, *Carbon fibers: formation, structure, and properties*, CRC Press 2018.
- [81] A. Handermann, Oxidized polyacrylonitrile fiber properties, products and applications, Zoltecorporation(<http://www.zoltek.com/white-paper-oxidized-polyacrylonitrile-fiberproperties-products-and-applications/>) (2017).

- [82] M. Kutz, Handbook of materials selection, John Wiley & Sons 2002.
- [83] T.E. McKnight, A.V. Melechko, D.K. Hensley, D.G. Mann, G.D. Griffin, M.L. Simpson, Tracking gene expression after DNA delivery using spatially indexed nanofiber arrays, *Nano Letters* 4(7) (2004) 1213-1219.
- [84] S.E. Baker, P.E. Colavita, K.-Y. Tse, R.J. Hamers, Functionalized vertically aligned carbon nanofibers as scaffolds for immobilization and electrochemical detection of redox-active proteins, *Chemistry of materials* 18(18) (2006) 4415-4422.
- [85] V. Vamvakaki, K. Tsagaraki, N. Chaniotakis, Carbon nanofiber-based glucose biosensor, *Analytical chemistry* 78(15) (2006) 5538-5542.
- [86] J. Fang, H. Niu, T. Lin, X. Wang, Applications of electrospun nanofibers, *Chinese science bulletin* 53(15) (2008) 2265-2286.
- [87] G.G. Tibbetts, G.P. Meisner, C.H. Olk, Hydrogen storage capacity of carbon nanotubes, filaments, and vapor-grown fibers, *Carbon* 39(15) (2001) 2291-2301.
- [88] V.V. Simonyan, J.K. Johnson, Hydrogen storage in carbon nanotubes and graphitic nanofibers, *Journal of alloys and compounds* 330 (2002) 659-665.
- [89] T. Rath, Carbon Nanofibers: Synthesis, Properties and Applications, Polymer Nanocomposites Based on Inorganic and Organic Nanomaterials; John Wiley & Sons: Hoboken, NJ, USA (2015) 63-88.
- [90] F. Rezaei, R. Yunus, N. Ibrahim, E.d.o.s.-c.-f.-r.p.c.f.c.b. Mahdi, Development of short-carbon-fiber-reinforced polypropylene composite for car bonnet, *Polymer-Plastics Technology and Engineering* 47(4) (2008) 351-357.
- [91] H. Zhang, W. Qiu, Y. Zhang, Y. Han, M. Yu, Z. Wang, X. Lu, Y. Tong, Surface engineering of carbon fiber paper for efficient capacitive energy storage, *Journal of Materials Chemistry A* 4(47) (2016) 18639-18645.
- [92] J. Wei, S. Geng, O. Pitkänen, T. Jarvinen, K. Kordas, K. Oksman, Green carbon nanofiber networks for advanced energy storage, *ACS Applied Energy Materials* 3(4) (2020) 3530-3540.
- [93] R.A. Sullivan, Automotive carbon fiber: Opportunities and challenges, *Jom* 58(11) (2006) 77-79.
- [94] S. Chand, Review carbon fibers for composites, *Journal of materials science* 35(6) (2000) 1303-1313.
- [95] Y. Yun-hua, P. Yue-xiu, F. Zhi-hai, S. Song, Evaluation of aerospace carbon fibers, *新型炭材料* 29(3) (2014) 161-168.
- [96] J. Lowe, Aerospace applications, Design and manufacture of textile composites, Elsevier 2005, pp. 405-423.
- [97] R.F. Egerton, Physical principles of electron microscopy, Springer 2005.

- [98] B. Inkson, Scanning electron microscopy (SEM) and transmission electron microscopy (TEM) for materials characterization, *Materials characterization using nondestructive evaluation (NDE) methods*, Elsevier 2016, pp. 17-43.
- [99] Z. Bacsik, J. Mink, G. Keresztury, FTIR spectroscopy of the atmosphere. I. Principles and methods, *Applied Spectroscopy Reviews* 39(3) (2004) 295-363.
- [100] B.E. Warren, *X-ray Diffraction*, Courier Corporation 1990.
- [101] J. Hren, *Introduction to analytical electron microscopy*, Springer Science & Business Media 2013.
- [102] D.A. Long, *Raman spectroscopy*, New York (1977) 1-12.
- [103] A.C. Ferrari, D.M. Basko, Raman spectroscopy as a versatile tool for studying the properties of graphene, *Nature nanotechnology* 8(4) (2013) 235.
- [104] A.C. Ferrari, Raman spectroscopy of graphene and graphite: disorder, electron–phonon coupling, doping and nonadiabatic effects, *Solid state communications* 143(1-2) (2007) 47-57.
- [105] J. Chastain, R.C. King Jr, *Handbook of X-ray photoelectron spectroscopy*, Perkin-Elmer Corporation 40 (1992) 221.
- [106] J.F. Watts, X-ray photoelectron spectroscopy, *Surface science techniques* 45 (1994) 5.
- [107] P. Merel, M. Tabbal, M. Chaker, S. Moisa, J. Margot, Direct evaluation of the sp³ content in diamond-like-carbon films by XPS, *Applied Surface Science* 136(1-2) (1998) 105-110.
- [108] I. Miccoli, F. Edler, H. Pfnür, C. Tegenkamp, The 100th anniversary of the four-point probe technique: the role of probe geometries in isotropic and anisotropic systems, *Journal of Physics: Condensed Matter* 27(22) (2015) 223201.

4 RESULTS

This chapter describes the results of all the research phases as mentioned in chapter 1. Each research phase is entitled to a sub-chapter in the following chapter. Specific study is published under each research phase. Preface and summary are included for each published study. For the first sub-chapter, the results are described in detail to develop the basic understanding; however, for the next sub-chapters, respective publication, preface, and summary is included.

4.1 Development and Characterization of Carbon Nanofiber – Optimization and Structure (Phase 1)

4.1.1 Preface

In the first phase of doctoral work, the carbon nanofiber fabrication process (electrospinning-stabilization-carbonization) is optimized, and the characterization of the basic as-spun, stabilized, and carbonized structure was performed. These process parameters were set as benchmark for all further studies. Similarly, stabilization and carbonization conditions are also explored. This deals with the investigation of structure and morphology of as-spun, stabilized, and carbonized of carbon nanofibers. SEM and FTIR are performed on spun and stabilized structure to observe fiber morphology, diameter, and molecular structure of PAN and stabilized PAN. Afterwards, carbonization was performed in an inert atmosphere (Ar/H₂) at various temperatures (800 °C, 1000 °C, 1200 °C, 1500 °C). The growth of graphitic structure and healing of intrinsic defects during carbonization at different temperatures is characterized by XRD and Raman. The study was presented at 23rd International Conference on Nanomaterials and Nanotechnology, March 15-16, 2018, as an invited talk and the later proceedings were published.

4.1.2 Optimization for electrospinning parameters:

The parameter optimization for the electrospinning process was carried out to produce uniform precursor nanofibers. Among the various process parameters in electrospinning, the polymer solution concentration has a primary effect on the bead formation and diameter of the fibers. PAN solutions were prepared from 8 - 20 wt.% (w.r.t PAN/DMF solution) with 3 wt. % concentration succession and diameter as-spun fibers were investigated. From figure 16a, it can be observed that as the concentration of the PAN in DMF solution is increased, the diameter of the fibers is also increased. Spinning below 7% resulted in nearly no stable fibers and rather an electrospaying of the PAN solution was observed. The beads were formed at lower polymer concentration, since at lower concentration of PAN there are higher numbers of solvent molecules

and fewer chain entanglements. This implies that the surface tension will have a dominating effect on the electrospinning process, resulting in bead formation. Contrary to this, at higher PAN concentration, there are higher numbers of chain entanglements in solution. The charges on the jet can stretch the solution with solvent molecules distributed among the PAN chains, resulting in bead-free fibers. At very higher concentration (above 20 wt.%) the solution was impossible to spin, due to increased viscosity and extensive chain entanglements resisting formation of the jet. Our findings showed that ~ 12 - 15 wt.% of PAN concentration is suitable for producing stable and bead-free nanofibers.

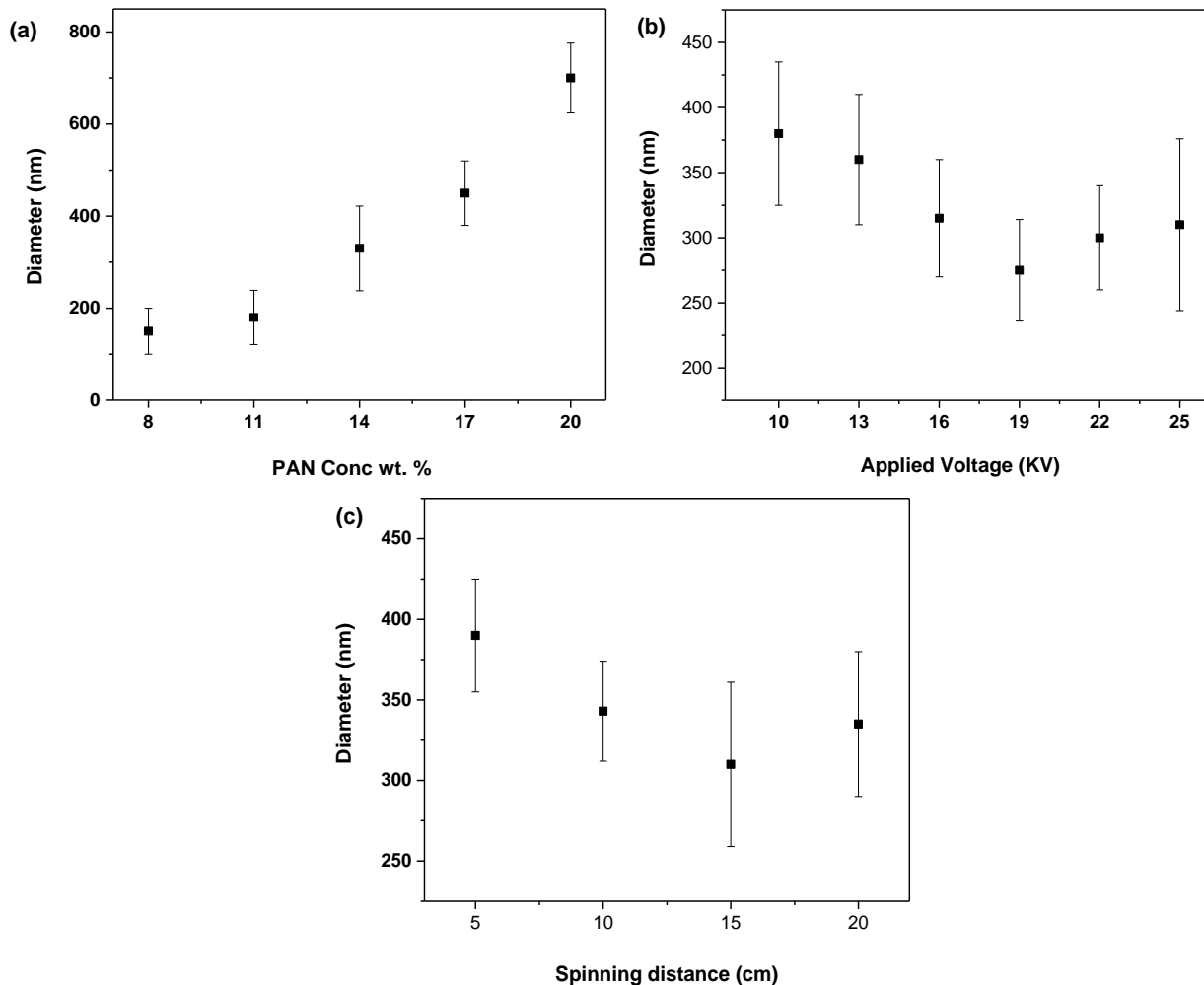


Figure 16 - Spinning process parameters: (a) effect of PAN concentration on fiber diameter (voltage: 16 KV, spinning distance: 15 cm), (b) effect of applied voltage on fiber diameter (PAN concentration wt. %: 14 wt. %, spinning distance: 15 cm), (c) effect of spinning distance on fiber diameter (PAN concentration wt. %: 14 wt. %, Voltage: 16 KV)

The effect of applied voltage on the fiber diameter is shown in figures 16b. The PAN concentration and spinning distance was kept constant to 14 wt.% and 15 cm. The voltage was varied from 10 KV to 25 KV with 3KV increment. The voltage of 10 KV resulted in disruption and discontinuous fiber jet with lot of solution dropping. Contrary to this, the applied voltage of 23 KV or more resulted in fibers flying off and haphazard fiber deposition. In-between this range, the fiber diameter was decreased as the applied voltage increases (figure 16b). Increase in voltage results in increased electric field strength and consequential greater stretching of PAN solution. This leads to reduction in fiber diameter. Some studies have reported an increase in fiber diameter with higher voltages. In principle, there are two factors which dictate the fiber diameter in this regard: 1) the strength of an electric field and 2) flight-time of the jet. Increase in voltage also resulted in increased jet acceleration, decreasing the flight time of fiber jet. This allows less time for fibers stretching before their deposition on collector, resulting in larger diameter of fibers. Therefore, these two factors were the reasons for different findings.

The spinning distance (needle to collector) also affects the electrospinning process and resulting fiber diameter. Variation of spinning distance affects the electric field strength and flight time. The PAN concentration of 14 wt.% and spinning voltage of 16KV was kept constant. The effect of spinning distance was examined every 5 cm, from 5 to 20 cm. With increasing distance, the reduction in diameter was observed till 15 cm after which a slight increase in diameter was observed (figure 16c). This could be attributed to the higher flight time of the fiber jet in the first phase till the fiber diameter is increased. A slight increase in fiber diameter for 20 cm indicates reduction in electric field strength due to increased distance. This causes less stretching of fiber jet which in turn results in increase in fiber diameter.

Based on this optimization, PAN solution concentration of 14 wt. %, spinning distance of 15 cm and 16-17 KV applied voltage was used as standard for investigations in further project phases. Figure 17 shows SEM micrographs for PAN based nanofibers at each of the three stage processes. The diameter for spun fibers was 330 ± 22 nm, with stabilized fibers around 314 ± 40 nm. Decrease in diameter was observed for

carbonized fibers (nanofiber carbonized at 1500 °C) with 188 ± 39 nm. The decrease in diameter is attributed to shrinkage accompanied by densification of CNF at elevated temperatures during stabilization and carbonization stages. The nanofibers observed are uniform and continuous with no apparent porosity.

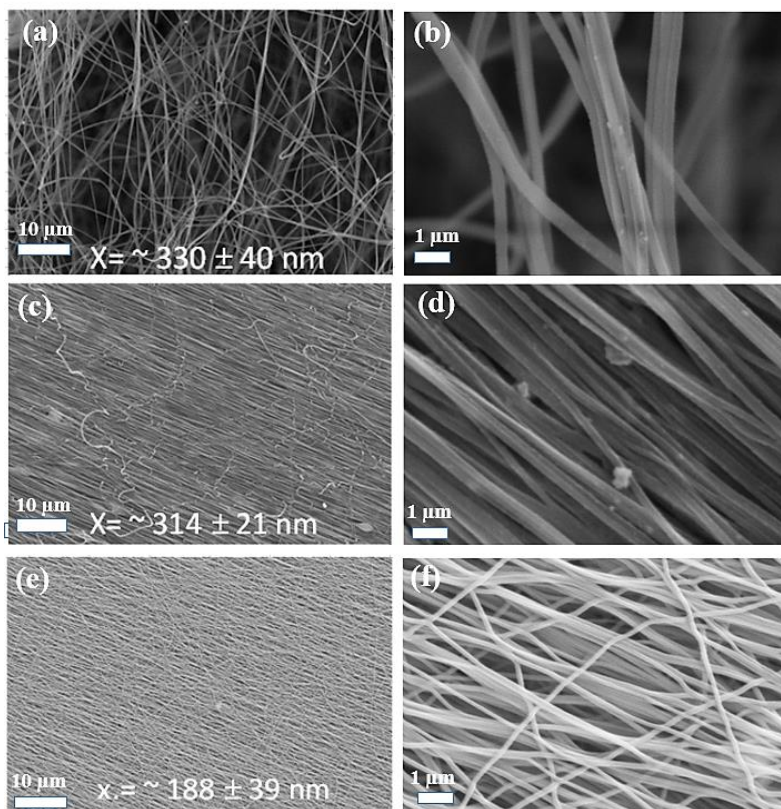


Figure 17 - SEM images: (a, b) as spun PAN, (c, d) stabilized PAN at 230 °C for 10h, (e, f) carbonized PAN at 1500 °C for 10 h

4.1.3 Molecular structure for as spun, stabilized, and carbonized PAN nanofibers

After the electrospinning process, stabilization of PAN nanofiber was performed by heating in air at 250 °C for 10 h using a low heating rate of 1°C/min under tension. Subsequently, PAN nanofibers were carbonized at heating rate of 5 °C/min with dwell time of 1h from 800 °C to 1500 °C. FTIR results (figure 18), for as-spun fibers shows sharp peaks at 2940 cm^{-1} , 2240 cm^{-1} and 1452 cm^{-1} , attributed to the C-H stretching, $\text{-C}\equiv\text{N}$ stretching and CH_2 bending. As the PAN nanofibers went through stabilization, an evolution of $\text{-C}=\text{N}$ peak is observed at 1600 cm^{-1} and the peak for $\text{-C}\equiv\text{N}$ disappears (figure 17).

Transformation of $-C\equiv N$ to $-C=N-$ in the PAN backbone is most crucial step in stabilization process leading to formation of ladder-like structure. The processes reported to take place during the stabilization process are oxidation, cross-linking, dehydrogenation (to eliminate hydrogen and form $-C=C-$ in PAN back bone) and cyclization (as shown in section 2.5.2). Cyclization is vital for fibers to last during the high temperature carbonization process. The process is an exothermic involving evolution of gaseous products and aids in holding the molecule together. FTIR results after the carbonization process (figure 18c) show absence of all above indicated peaks corresponding to $-C=N$ and C-H, pointing out that the elimination of non-carbon elements as nitrogen and hydrogen has taken place.

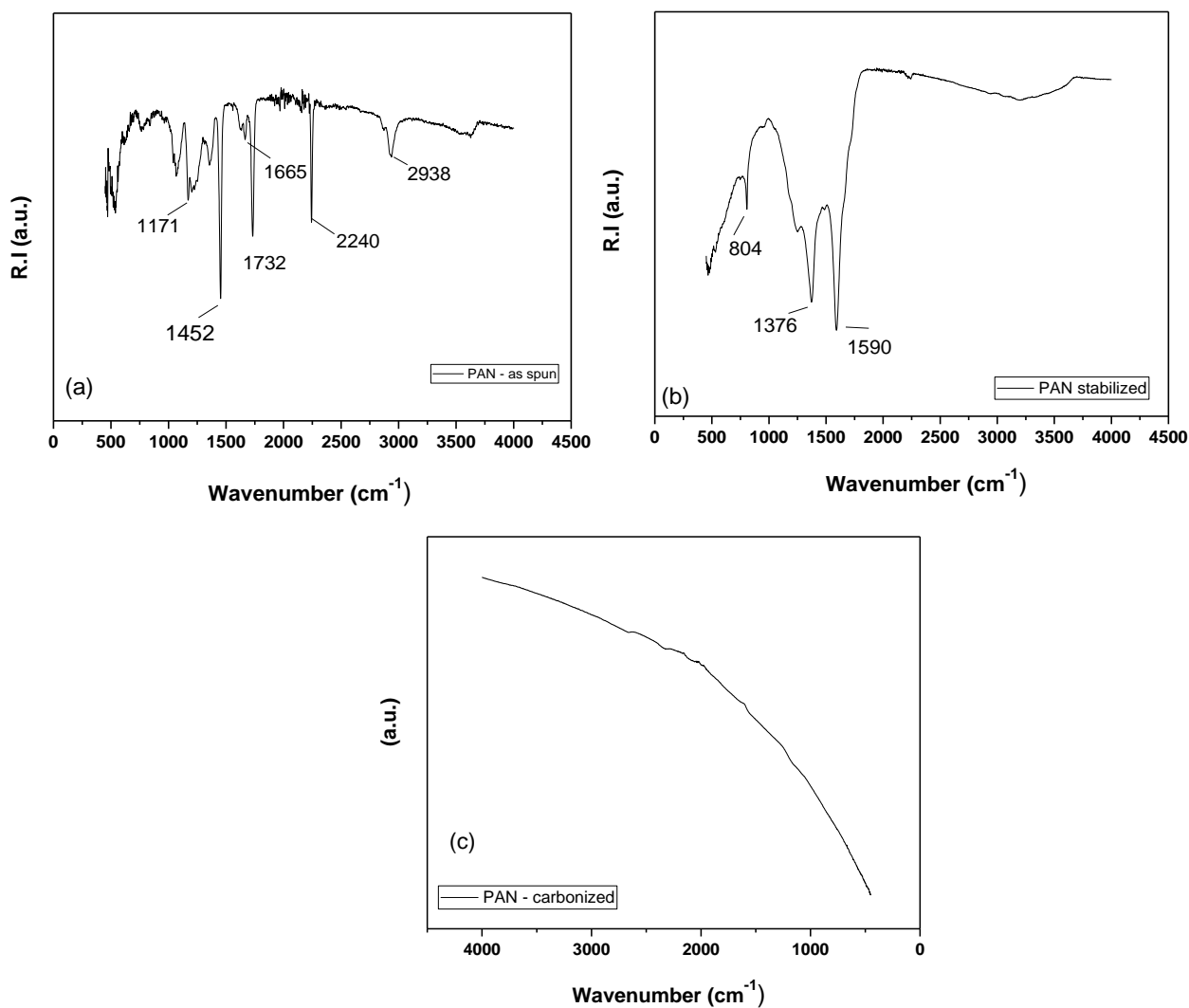


Figure 18- FTIR for (a) as spun, (b) stabilized and (c) carbonized PAN

4.1.4 Crystallography and structural analysis of carbonized PAN nanofibers:

The effect of heat treatment on the crystallite size of stabilized PAN nanofibers at different temperatures is shown in figure 19(a). The stabilized PAN nanofibers were carbonized at various temperatures for a duration of 1h. With increase in carbonization temperature from 800 °C to 1500 °C, an increase in crystallite size (L_c , basal plane) was observed from 10.71 Å to 13.20 Å.

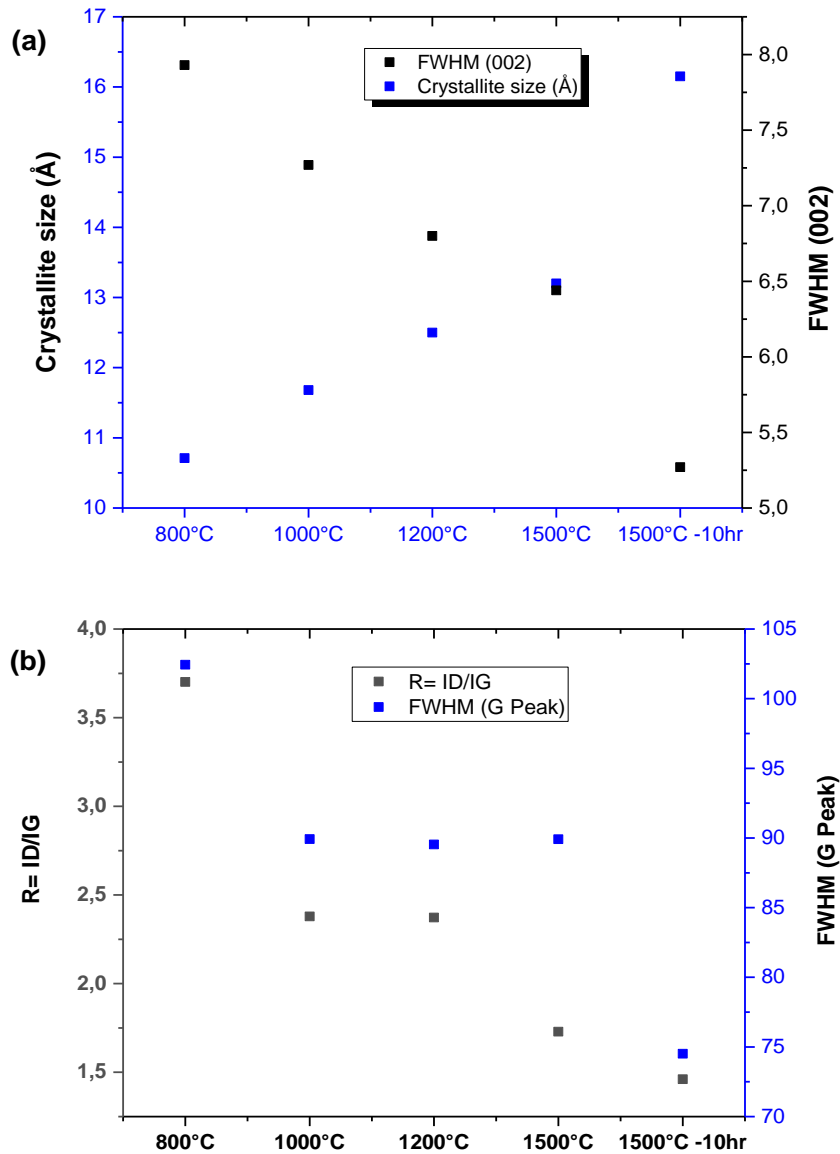


Figure 19- (a) Crystallite size L_c and FWHM for (002) peak as function of carbonization temperature, (b) I_D/I_G and FWHM for G-band peak as function of carbonization temperature

Along with an increase in crystallite size, a decrease in the FWHM was observed for the (002) signature peak. FWHM decreased with increase in heat treatment temperature indicating that amorphous carbon was transformed into ordered carbon and the degree of crystallinity has increased. A decrease in the interlayer spacing (table 2) from 3.61 Å to 3.49 Å was observed. Structural characterization was further explored using Raman spectroscopic analysis. Typical Raman spectra for carbon materials show D- and G-bands at 1332 cm⁻¹ to 1360 cm⁻¹ and 1500 to 1630 cm⁻¹ approximately, ascribed to defects in the graphitic structure and ordered graphitic structure. The R ratio is the measure of defects in graphite/graphene systems, defined as the integral intensity ratio of D- and G-band ($R=I_D/I_G$). Figure 19(b) shows a decrease in R ratio as the carbonization temperature was increased. R decreases from 3.72 to 1.46 as temperature was increased from 800 °C to 1500 °C. Increased annealing temperature for CNFs lead to ordering of graphene domains and reduction in graphitic defects.

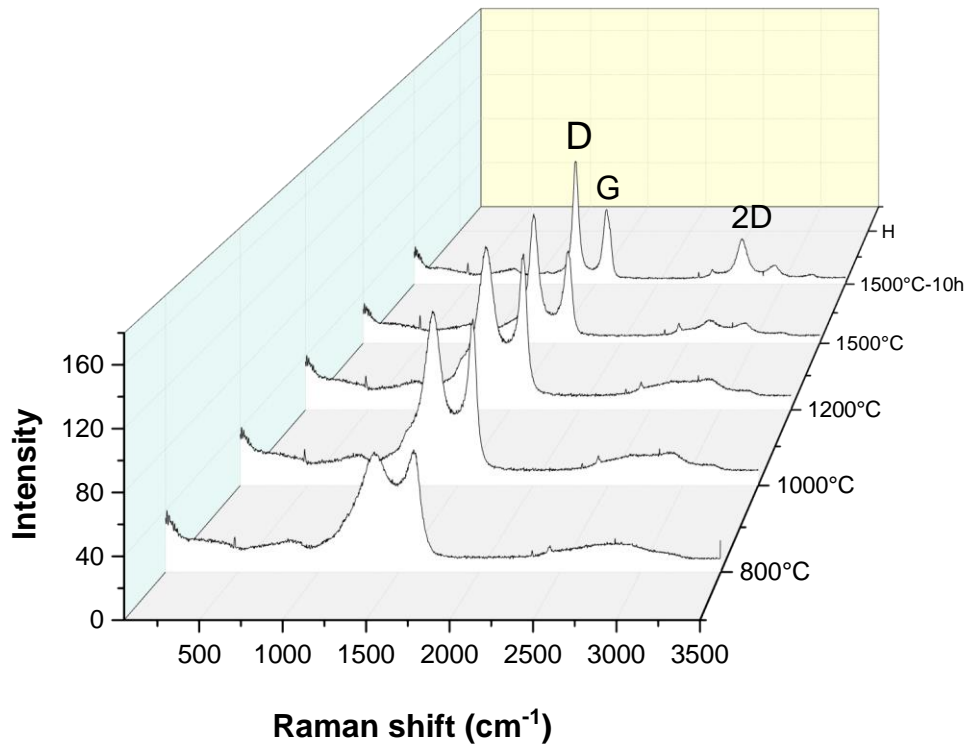


Figure 20 - Typical Raman spectra for PAN carbonized at different temperatures

Table 5- Interlayer spacing, FWHM (002) peak, crystallite size of PAN nanofibers carbonized at various temperatures

SAMPLE	2 θ (002)	d-spacing (002)/ (Å)	Crystallite size / (Å)	FWHM (002)
CF-800 °C-1hr	24.61	3.6159	10.71	7.93
CF-1000 °C-1hr	24.525	3.6282	11.68	7.27
CF-1200 °C-1hr	24.734	3.598	12.5	6.8
CF-1500 °C-1hr	24.856	3.5793	13.2	6.44
CF-1500 °C-10hr	25.433	3.4993	16.15	5.27

The author performed, investigated, and wrote all the work. This was later reviewed and analyzed by DR. FRANZ RENZ, DR. CHRISTOPH TEGENKAMP AND DR. RALF SINDELAR. The basic work was planned and executed at University of Applied Sciences Hannover together with reviews and discussions with involved partners (Institute of Inorganic Chemistry and Institute of Solid-state Physics, Leibniz University Hannover).

4.2 Creep stress induced stabilization and graphitization in polyacrylonitrile carbon nanofibers

4.2.1 Preface & Summary

After optimization and characterization of carbon nanofibers production process, the next stage dealt with a focus on the stabilization process, to understand the formation of graphene like ribbon structures from PAN. These ribbon-like structures are crucial for high temperature carbonization hence the stabilization was the focus of this phase. Any changes during the stabilization fundamentally impact the end graphitic structure after carbonization. Improvement in graphitic structure serves as fundamental for dictating the properties of carbon nanofibers. The mechanical, thermal, and electrical properties are dependent on the nucleation and growth of graphene layers, orientation, and long-range order. Owing to this, investigations were made on how the application of creep stress influences the chemical reactions during stabilization

which in turn impacts the graphitization of PAN. The work has been published in *Journal of Materials Science and Engineering* (DOI: <https://doi.org/10.4172/2169-0022.1000493>).

In general, the stabilization process is assisted by tension to cater the loss of molecular orientation due to the shrinkage and to further enhance the molecular orientation of PAN. Hence to study the impact of mechanically assisted chemical reactions, the stabilization was performed in two ways; 1) creep load applied to PAN nanofibers (PAN - T) and 2) clamping of PAN nanofibers (PAN - S). In the latter case, there was no external stress rather only innate shrinkage stress present due to entropic changes. Ring cyclization index (RCI) was calculated to evaluate the amount of the cyclized structure. The polarized FTIR spectroscopy was used to calculate the Herman orientation factor to determine the molecular orientation of PAN. The ring cyclization index (RCI) was evaluated for PAN - T and PAN - S stabilized samples at different temperatures 180 °C, 210 °C, 230 °C. RCI for PAN - T fibers and PAN - S showed different values at lower temperatures (190 °C and 210 °C) however at higher temperatures, both the PAN - T and PAN - S samples showed similar RCI values. This showed that creep stress influences the chain conformations and brings the PAN chains in suitable positions to form conjugated nitrile groups, resulting in higher degree of cyclization. However, at high temperatures (230 °C), the internal energy for PAN - S is high enough and dipole-dipole repulsions between the C≡N are reduced, therefore the difference of RCI between PAN - T and PAN - S nanofibers were reduced. Both PAN - S and PAN - T were also stabilized at 230 °C for 10 h and RCI showed RCI values reaching ~ 95 %. Interestingly, even though the RCI was the same for the nanofibers cyclized at 230 °C - 10 h with and without application of creep stress, a difference in the degree of graphitization was observed. Increased graphitization was observed for PAN nanofibers stabilized with creep stress as evidenced from reduced I_D/I_G and FWHM for G-band peak, increased L_c and L_a as evaluated from XRD and Raman analysis. The difference in degree of graphitization was attributed to the formation of relatively more curved and fullerene structures which resulted in reduced degree of graphitization for the pyrolysis of PAN - S precursor, whereas PAN - T nanofibers with high molecular orientation formed more ordered carbon planes. Even though the amount of cyclized material was the same, the application of creep

stress resulted in more sp^2 hybridized carbon. Creep stress during the stabilization assisted in sp^3 to sp^2 transformation which was reflected in a higher degree of graphitization.

The author conducted and investigated all the work from development to characterization and analysis. The results are reviewed and analyzed by DR. FRANZ RENZ, DR. CHRISTOPH TEGENKAMP AND DR. RALF SINDELAR.

The author wrote the manuscript on his own and it was edited and reviewed by the respective names above.

Electrospun Polyacrylonitrile Based Carbon Nanofibers: The Role of Creep Stress towards Cyclization and Graphitization

Annas Bin Ali^{1,2,3*}, Dreyer B^{1,2,3}, Renz F^{2,3}, Tegenkamp C^{3,4,5} and Sindelar R^{1,2,3}

¹University of Applied Sciences and Arts, Faculty II, Hochschule Hannover, Ricklinger Stadtweg 120, 30459 Hannover, Germany

²Institut für Anorganische Chemie, Leibniz Universität Hannover, Callinstr. 7, 30167 Hannover, Germany

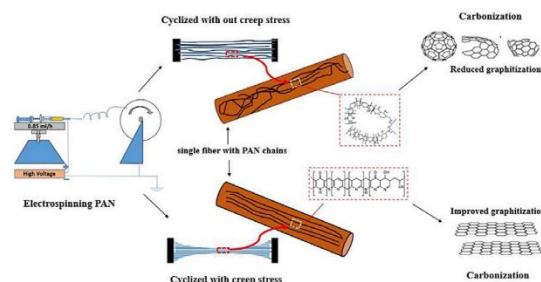
³Hannover School for Nanotechnology, Laboratorium für Nano und Quantenengineering (LNQE), Leibniz Universität Hannover, Schneiderberg 39, 30167 Hannover, Germany

⁴Institut für Festkörperphysik, Leibniz Universität Hannover, Appelstraße 2, 30167 Hannover, Germany

⁵Institut für Physik, Technische Universität Chemnitz, Reichenhainer Str. 70, 09107 Chemnitz, Germany

Abstract

The properties of these carbon nanostructures are determined by the structure and orientation of the graphitic domains during pyrolysis of carbon precursors. In this work, we investigated systematically the impact of creep stress during the stabilization process on the cyclization and molecular orientation of polyacrylonitrile as well as the graphitized structure after high temperature carbonization. Therefore, polyacrylonitrile (PAN) is electrospun and then stabilized with and without application of creep stress at different temperatures. The effect of creep stress on cyclization was monitored via Fourier transform IR spectroscopy (FTIR) and it was found that the degree of cyclization varies with the application of creep stress during the initial stages of cyclization at low temperatures (190°C and 210°C) in contrast to cyclization done at higher temperature (230°C). Herman molecular orientation factor was evaluated by polarized FTIR for PAN nanofibers cyclized with and without creep stress at 230°C-10 h. Subsequently, carbonization was performed at 1000°C and 1200°C for nanofibers cyclized at 230°C-10 h. Our results from XRD and Raman spectroscopy shows that the degree of graphitization and ordering of graphitic domains was enhanced for PAN nanofibers that were creep stressed during the cyclization process, even though both PAN nanofibers cyclized with creep stress and without creep stress showed the same amount of cyclized material. This increased degree of graphitization can be tracked to application of creep stress during the stabilization process which obviously favors the formation of sp^2 -hybridized carbon planes in the carbonization process. This finding highlights the impact of mechanical stress linking the cyclization of PAN nanofibers to graphitization. Our results will pave the way for a deeper understanding of mechano-chemical processes to fabricate well-aligned graphitic domains which improves the mechanical and electrical properties of CNFs.



Keywords: Carbon nanofibers; Polyacrylonitrile; Cyclization; Graphitization

Abbreviations: PAN: Polyacrylonitrile; CNF: Carbon Nanofibers; FTIR: Fourier Transform Infra-red Spectroscopy; XRD: X-ray Diffraction; SEM: Scanning Electron Microscopy; RCI: Ring Cyclization Index; FWHM: Full Width at Half Maxima

Introduction

Carbon nanostructured materials have gained a widespread attention during the recent past decades due to their extraordinary physical, mechanical and chemical properties [1,2]. Among the carbon nanostructured materials, carbon nanofibers (CNFs) with a typical dimensions of 100-300 nm have been extensively explored for different industrial applications due to their high surface area to volume ratio,

*Corresponding author: Annas Bin Ali, Hannover School for Nanotechnology, Laboratorium für Nano und Quanten engineering (LNQE), Leibniz Universität Hannover, Schneiderberg 39, 30167 Hannover, Germany, Tel: +49 511 9296-1320; E-mail: annas.bin.ali@acd.uni-hannover.de

Received October 16, 2018; Accepted October 26, 2018; Published October 30, 2018

Citation: Ali AB, Dreyer B, Renz F, Tegenkamp C, Sindelar R (2018) Electrospun Polyacrylonitrile Based Carbon Nanofibers: The Role of Creep Stress towards Cyclization and Graphitization. J Material Sci Eng 7: 493. doi: 10.4172/2169-0022.1000493

Copyright: © 2018 Ali AB, et al. This is an open-access article distributed under the terms of the Creative Commons Attribution License, which permits unrestricted use, distribution, and reproduction in any medium, provided the original author and source are credited.

good thermal and electrical conductivity as well as ease of fabrication [3-7]. Pitch, cellulose and polyacrylonitrile (PAN) are generally used as precursor materials for carbon fibers and carbon nanofibers (CNFs), however, PAN is the leading precursor for production of carbon fiber with a market share over 90% [8-10].

Among the traditional methods for producing CNFs such as vapor growth, spraying or catalyst supported growth; electrospinning is a comparably uncomplicated and cost effective method [11]. In a typical electrospinning process, an electrical potential is applied between the droplet of a polymer solution contained in syringe and grounded collector. When Coulombs forces acting on the droplet can overcome the surface tension of the droplet, a Taylor cone forms and the ejection of a fiber jet takes place. The collected nanofibers are then stabilized and finally carbonized to obtain CNFs [9].

Stabilization of PAN fibers in the temperature range of 200-250°C is the most critical step in the CNFs fabrication. The typical phenomena occurring in this process is the formation of ladder structures which lead to ring formation and eventually graphite like structure after high temperature carbonization [11,12]. During the stabilization process, polymeric chains relax and loose preferred orientation due to shrinkage. Hence, tension is applied to prevent physical shrinkage and increase the orientation [13,14]. Various studies have reported an increased degree of orientation and eventually improved the physical and mechanical properties by the application of stress during the stabilization step [14-16]. Gu et al. [17] found that a better molecular orientation can be achieved by optimizing the electrospinning parameters, which in turn results in an initiation of cyclization, i.e. ring formation, at lower temperatures for the PAN fibers as compared to casted PAN films. Wu et al. [18] reported that an increase of the tension during the initial stages of cyclization had a favorable effect on the degree of cyclization while in the latter stages, when cyclization proceeds in crystalline regions, the increase in tension had a depressing effect on initiation of cyclization. Another study reported, that tension affects the cyclized structure of PAN fibers and transforms the chain conformations which results in decreased energy barrier for cyclization between temperatures 175°C – 218°C [19].

Therefore, the bottom line is to have a high degree of chain orientation without reducing the amount of cyclized material, since this ring formation initiates the basis for graphite like ribbon structure after high temperature carbonization. Though some of the studies have reported on the effect of tension regarding the stabilization and degree of cyclization, almost no work was dedicated so far in investigating the effect of mechanical stress on cyclization and linking it to the graphitization process.

In this paper, we have investigated the effect of mechanical stress on the cyclization degree of PAN nanofibers at different temperatures (170°C, 190°C, 210°C, 230°C each for 2 h and at 230°C for 10 h) and related the effect creep stress during stabilization stage to the final graphitic structure. The PAN fibers cyclized with creep stress are denoted with a suffix 'T' as PAN-T indicating tension while the samples with only innate shrinkage stress are denoted suffix 'S' as PAN-S, having no application of creep stress. The findings suggest that the degree of cyclization is affected at lower temperatures and times, however at higher temperature (230°C-10 h) both samples cyclized with creep stress (PAN-T) and no creep stress (PAN-S) showed no differences in ring cyclization index (RCI). Nevertheless, the samples with creep stress showed a higher graphitization after carbonization. This implies that the molecular orientation achieved by creep stress plays an important role during graphitization.

Materials and Methods

Materials

Polyacrylonitrile (PAN) in powder form with molecular weight 150,000 Mw, purchased from Sigma Aldrich, was used as precursor for the fabrication of carbon nanofibers (CNFs). Dimethylformamide (DMF) was used as solvent for dissolving PAN as supplied by Carl Roth. For carbonization process, a mixture of 2% H₂/98% Ar was supplied by Westfalen AG.

Preparation of nanofibers

The complete process for fabricating of CNFs comprise three stages in total. First, PAN was dissolved in DMF by 16 wt% and then stirred over night for period of 12 h to obtain a homogenous solution. This mixture (PAN/DMF) was electrospun at 17 kV, 1 ml/h and 10 m/s collector speed while the fibers were collected on an aluminum foil.

In the second stage, the as-spun fibers were dried in air before they were stabilized at different temperatures (190°C, 210°C, 230°C for 2 h and 230°C for 10 h) either with creep stress and without creep stress. Details of the temperature profiles are summarized in Figure 1a. In the present work, two different cases were considered. (PAN-T) refers to PAN cyclized with externally applied creep stress while the (PAN-S) refers to PAN cyclized without creep stress and the only strain is due to the shrinkage/retardation stress which is congenital during the stabilization stage. For the PAN-T samples, one end of the fiber mats were clamped and the creep stress was applied while for PAN-S sample the ends were just loosely clamped by fixtures but no external strain was applied. There is also a third case for stabilization, where fiber ends are neither fixed and no load is applied, which leads to loss of material after high temperature carbonization process. Finally, the stabilized nanofibers were carbonized in a reduced atmosphere of 2% H₂/98% Ar at 1000°C or 1200°C. The time-temperature profile for carbonization is presented in Figure 1b.

Characterizations

X-ray diffraction was used for the structural characterization of CNFs samples. Diffraction patterns were recorded using a Bruker D2 Phaser. Samples were scanned from 10°-80° with a step size of 0.03° using Cu-K α ($\lambda=1.5406$ Å). The interlayer spacing, d (002) was calculated using Bragg law, $d=(\lambda/2 \sin\theta)$, where λ is the wavelength of the x-ray source and θ is the Bragg angle. The crystallite sizes were estimated using the Scherrer equation, $L_c=(K \lambda/\beta \cos\theta)$, where K is the shape factor (0.89 for L_c). β is the full width at half maximum (FWHM) expressed in radians.

Furthermore, Raman spectroscopy was used to obtain information about the structure and, in particular, disorder and defects in the CNF samples. Raman spectra were recorded using a DXR2 Thermo Fisher Scientific system with a laser wavelength of 532 nm as an excitation source. The spectra were acquired in the range of 1000-3000 cm⁻¹. The D and G bands in the spectra were deconvoluted using Gaussian fitting after a base line subtraction via Origin lab pro software. Moreover, the crystal sizes L_a (apparent crystallite size along the basal plane) of carbon nanostructures were calculated via L_a (nm) = $(2.4 \times 10^{-10}) \lambda^4 (ID/IG)^{-1}$ [20]. ID and IG are integral ratios of respective D and G band and λ is the laser wavelength (532 nm). Five spectra were recorded on different samples. The incident laser power of 1 mW was used for all measurements in order to minimize heating effects.

Fourier transform infrared spectroscopy (FTIR) was used to monitor the structural changes in PAN fibers during stabilization stage

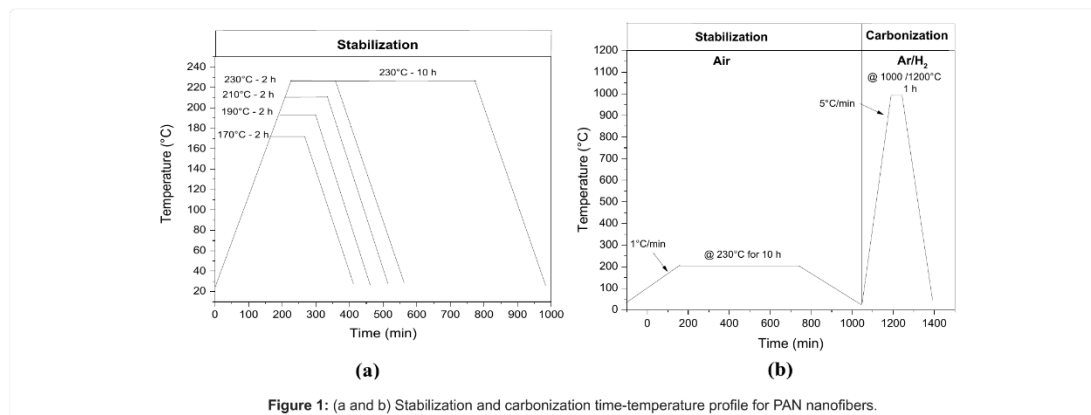


Figure 1: (a and b) Stabilization and carbonization time-temperature profile for PAN nanofibers.

via a Perkin Spectrum Two spectrometer operating in the wavenumber regime of 400–4000 cm^{-1} . The most prominent changes occurring during the stabilization process in the PAN structure is the conversion of $\text{C}\equiv\text{N}$ groups to $\text{C}=\text{N}$ groups, which indicates that cyclization has taken place. Hence, the ring cyclization index (RCI) was calculated in order to estimate the amount of the crosslink ladder polymer conversion by measuring the integral intensity of absorbed IR, $\text{C}\equiv\text{N}$ (2240 cm^{-1}) and $\text{C}=\text{N}$ (1600 cm^{-1}) peaks, using the following equation:

$$\text{RCI} = \frac{I_{\text{C}=\text{N}}}{I_{\text{C}=\text{N}} + I_{\text{C}\equiv\text{N}}} \quad (1)$$

Furthermore, the molecular orientation was studied by polarized FTIR using a Tl-bromiodide (KRS-5) holographic wire grid polarizer ($\varnothing 25\text{ mm}$). The degree of orientation is described by the Herman orientation factor (f). Thereby, the nanofiber bundles were irradiated with polarized IR and the spectrum was obtained with the plane of polarization parallel (\parallel, A_0) and perpendicular (\perp, A_{90}) to the fiber axis. The orientation factor (f) is then given by the following expression:

$$f = \frac{2}{32 \cos^2 \theta D + 2} \text{ With } D = \frac{A_{\parallel}}{A_{\perp}} \quad (2)$$

D is the dichroic ratio of polarized absorbance intensity of the nitrile peak (2240 cm^{-1}). The values of the Herman factor ranges from 0 to 1, where 0 indicates a random orientation of fibers while a value of 1 indicates perfectly aligned fibers. θ is an angle between polymer chain backbone and nitrile group, which in the present case is 70° . This method makes use of this fixed angle (70°) between the backbone of polymer chain and the ($\text{C}\equiv\text{N}$) nitrile group [21]. For polarization measurements, the potassium bromide (KBr) powder was used to prepare KBr pellets. KBr powder was placed overnight at 50°C to avoid moisture contaminations and the nanofiber samples were compacted in a KBr pellet. The direction of fiber axis was marked before irradiating the sample with polarized IR and spectra were recorded.

Results and Discussions

Effect of creep stress on cyclization

Typical IR spectra for PAN nanofibers, stabilized at different temperatures with creep stress are shown in Figure 2. As spun PAN nanofibers show IR spectra with signature peak at 2240 cm^{-1} indicating nitrile group ($\text{C}\equiv\text{N}$). In general, it can be observed that as the

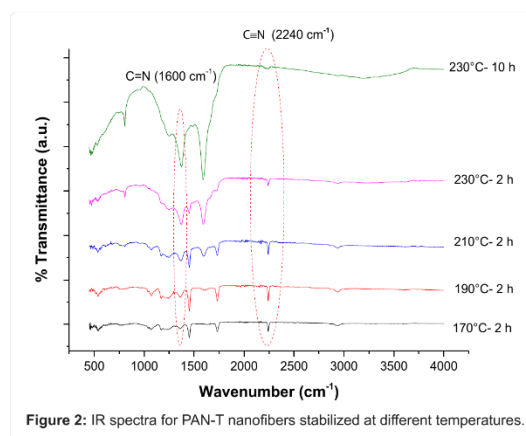


Figure 2: IR spectra for PAN-T nanofibers stabilized at different temperatures.

temperature is increased the intensity for $\text{C}\equiv\text{N}$ (2240 cm^{-1}) gradually decreases and an evolution of a $\text{C}=\text{N}$ (1600 cm^{-1}) peak is detected. As mentioned earlier, cyclization is the most critical process in the stabilization process where the conjugated $\text{C}=\text{N}$ bond formation takes place. At 230°C -2 h, the $\text{C}=\text{N}$ line becomes prominent indicating that cyclization has fairly occurred and a minute amount of uncyclized PAN is present as $\text{C}\equiv\text{N}$ with a weak intensity line [6].

The progress of the cyclization reaction is well visualized by plotting the ring cyclization index (RCI, Figure 3). Apparently, the RCI increases with increasing temperature for both PAN-T and PAN-S nanofibers. It is known that the cyclization of the nitrile group is initiated thermally by free radical mechanism and the Arrhenius equation suggests, the higher the temperature the higher the cyclization rate will be [22]. At 170°C , both the PAN-T and PAN-S sample showed nearly no cyclization, since no peak was observed at the position of the $\text{C}=\text{N}$ edge (Figure 2), in agreement with previous results claiming a formation temperature of around $\sim 180^\circ\text{C}$ [12,23]. The samples stabilized at 190°C show a difference in the cyclization index for PAN-T and PAN-S samples. The RCI at 190°C for PAN-T is around 23% whereas for PAN-S is 12%. As the temperature is increased to 210°C the same trend is observed, however, the difference in RCI

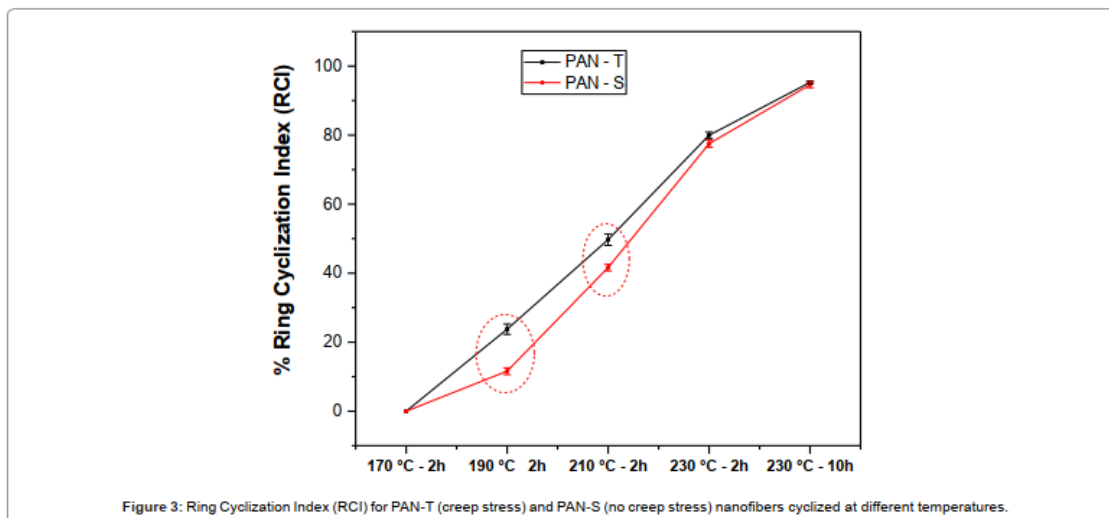


Figure 3: Ring Cyclization Index (RCI) for PAN-T (creep stress) and PAN-S (no creep stress) nanofibers cyclized at different temperatures.

for PAN-T and PAN-S sample is decreased as compared to the one observed at 190°C. Further, at 230°C-2 h the cyclization index nearly shows the same value for both samples.

The obvious difference in the RCI for PAN-T and PAN-S at 190°C and 210°C can be attributed to the fact that at lower temperatures the mobility of PAN chains is limited. The increased cyclization for the PAN-T samples at 190°C indicates that applied tension prevents a chain entanglements and helps in overcoming the dipole interactions between the adjacent nitrile groups to bring them in suitable positions for cyclization. It has been reported, that the ability to form conjugated C=N bonds depends on the isotacticity of polymers and the conformational energy changes, as the angle between the C≡N group and C-C backbone changes [24]. Hence, the likely impact of tension here is that it makes the C=N to rotate around the PAN backbone and increases the internal energy which results in overcoming the C=N repulsions and making new possible interactions to form a ladder structure (cyclization) [19]. However, at 230°C-2 h, the RCI shows nearly the same value for both samples. At 230°C, the temperature is high enough for the chain mobility to participate in cyclization reaction and the energy barrier for conformations is relatively decreased to form conjugated bonds, therefore the impact of tension is not fairly observed. Lastly, it can be observed that as the duration of cyclization is increased from 2 h to 10 h at 230°C, the RCI reaches up to ~95%. Indeed, the strong dependence on time shows, that kinetics is limiting the cyclization process.

The difference of RCI for PAN-T and PAN-S nanofibers is observed at lower temperatures, when the cyclization has just commenced. The cyclization initiates first in the amorphous regions and then extends to crystalline regions. So the impact of tension is visible in this regime, as the temperature is increased the cyclization extends to crystalline regions and mobility of chains is high enough to overcome the barrier for C=N dipole interactions [18,25]. However, it has been reported that increasing tension in the temperature regimes above 220-230°C delays the initiation of cyclization as it increases the spatial distance between the adjacent groups to get involved into the cyclization reaction [18]. The molecular orientation of the fibers was measured via polarized

FTIR. Polarized FTIR spectra of both PAN-T and PAN-S nanofibers at 230°C-10 h are shown in Figure 4a. The dotted and solid line correspond to polarized spectra when IR incident beam is parallel and perpendicular with respect to nanofiber stretching direction. The PAN-T fiber mat revealed an elongation of nearly 150%. The relative area under the peaks of cyclization sensitive C≡N nitrile group is used to calculate the Herman orientation factor (*f*). Figure 4b shows the orientation factor for samples stabilized at 230°C. 5 mm² of specimen piece was cut from the very central part of the PAN-T nanofiber mat as shown by the inset in Figure 4a inset. The fibers stabilized accompanied by creep stress show orientation factor value of 0.47 while the fibers which were only clamped with fixtures (only shrinkage stress) shows lower value of 0.02. The application of creep stress, along with the macroscopic alignment of PAN fibers (as shown by the SEM image Figure 5) during the hot drawing process in fact results in the molecular orientation of PAN chains which is evidenced by crystallization sensitive C≡N band in polarized IR spectra.

Effect of creep stress assisted stabilization on carbonization of PAN nanofibers

As observed, in presence of tension the degree of cyclization and the amount of cyclized material is increased for PAN stabilized at temperatures of 190°C and 210°C, while at higher temperatures for longer times (230°C-10 h) the amount of material is the same (RCI: 95%) for PAN-T and PAN-S nanofibers. Subsequently, to observe the influence of this creep stress during stabilization on the graphitic structure after carbonization process, both types of samples, stabilized at 230°C-10 h (PAN-T and PAN-S) were pyrolyzed at 1000°C and 1200°C. The graphitic structures and crystallite sizes were investigated afterwards by XRD and Raman spectroscopy. Thereby, more than 5 Raman spectra were collected for each sample. Typical averaged Raman spectra for samples both PAN-T and PAN-S samples pyrolyzed at 1000°C are shown in Figure 6a.

Typically, G- and D-peaks are the characteristic bands observed in carbon allotropes. The G peak is centered in the range of 1560-1600 cm⁻¹ arises from vibrations of carbon atoms in *sp*²-hybridized planes of

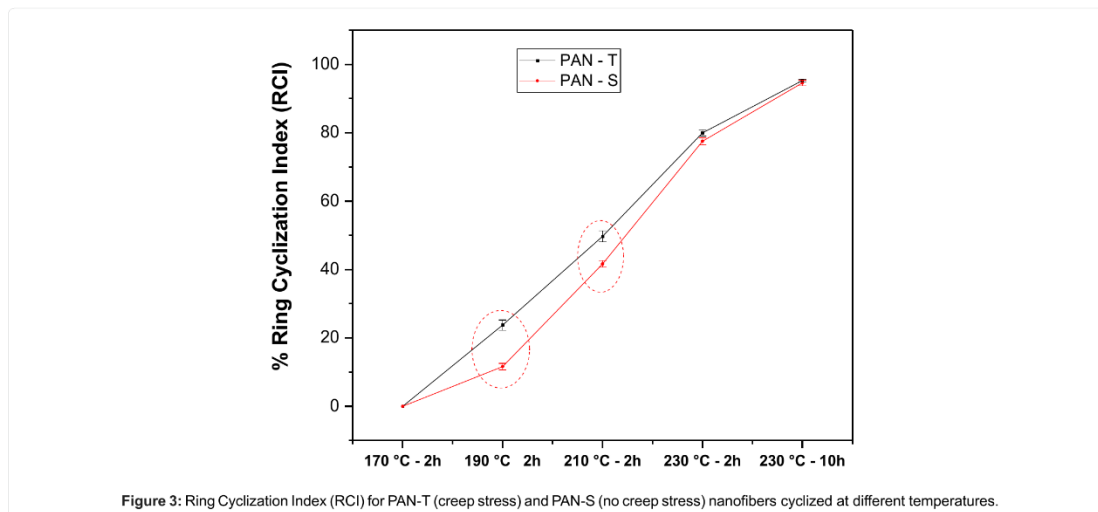


Figure 3: Ring Cyclization Index (RCI) for PAN-T (creep stress) and PAN-S (no creep stress) nanofibers cyclized at different temperatures.

for PAN-T and PAN-S sample is decreased as compared to the one observed at 190°C. Further, at 230°C-2 h the cyclization index nearly shows the same value for both samples.

The obvious difference in the RCI for PAN-T and PAN-S at 190°C and 210°C can be attributed to the fact that at lower temperatures the mobility of PAN chains is limited. The increased cyclization for the PAN-T samples at 190°C indicates that applied tension prevents a chain entanglements and helps in overcoming the dipole interactions between the adjacent nitrile groups to bring them in suitable positions for cyclization. It has been reported, that the ability to form conjugated C=N bonds depends on the isotacticity of polymers and the conformational energy changes, as the angle between the C≡N group and C-C back bone changes [24]. Hence, the likely impact of tension here is that it makes the C=N to rotate around the PAN backbone and increases the internal energy which results in overcoming the C=N repulsions and making new possible interactions to form a ladder structure (cyclization) [19]. However, at 230°C-2 h, the RCI shows nearly the same value for both samples. At 230°C, the temperature is high enough for the chain mobility to participate in cyclization reaction and the energy barrier for conformations is relatively decreased to form conjugated bonds, therefore the impact of tension is not fairly observed. Lastly, it can be observed that as the duration of cyclization is increased from 2 h to 10 h at 230°C, the RCI reaches up to ~95%. Indeed, the strong dependence on time shows, that kinetics is limiting the cyclization process.

The difference of RCI for PAN-T and PAN-S nanofibers is observed at lower temperatures, when the cyclization has just commenced. The cyclization initiates first in the amorphous regions and then extends to crystalline regions. So the impact of tension is visible in this regime, as the temperature is increased the cyclization extends to crystalline regions and mobility of chains is high enough to overcome the barrier for C=N dipole interactions [18,25]. However, it has been reported that increasing tension in the temperature regimes above 220-230°C delays the initiation of cyclization as it increases the spatial distance between the adjacent groups to get involved into the cyclization reaction [18]. The molecular orientation of the fibers was measured via polarized

FTIR. Polarized FTIR spectra of both PAN-T and PAN-S nanofibers at 230°C-10 h are shown in Figure 4a. The dotted and solid line correspond to polarized spectra when IR incident beam is parallel and perpendicular with respect to nanofiber stretching direction. The PAN-T fiber mat revealed an elongation of nearly 150%. The relative area under the peaks of cyclization sensitive C≡N nitrile group is used to calculate the Herman orientation factor (f). Figure 4b shows the orientation factor for samples stabilized at 230°C. 5 mm² of specimen piece was cut from the very central part of the PAN-T nanofiber mat as shown by the inset in Figure 4a inset. The fibers stabilized accompanied by creep stress show orientation factor value of 0.47 while the fibers which were only clamped with fixtures (only shrinkage stress) shows lower value of 0.02. The application of creep stress, along with the macroscopic alignment of PAN fibers (as shown by the SEM image Figure 5) during the hot drawing process in fact results in the molecular orientation of PAN chains which is evidenced by crystallization sensitive C≡N band in polarized IR spectra.

Effect of creep stress assisted stabilization on carbonization of PAN nanofibers

As observed, in presence of tension the degree of cyclization and the amount of cyclized material is increased for PAN stabilized at temperatures of 190°C and 210°C, while at higher temperatures for longer times (230°C-10 h) the amount of material is the same (RCI: 95%) for PAN-T and PAN-S nanofibers. Subsequently, to observe the influence of this creep stress during stabilization on the graphitic structure after carbonization process, both types of samples, stabilized at 230°C-10 h (PAN-T and PAN-S) were pyrolyzed at 1000°C and 1200°C. The graphitic structures and crystallite sizes were investigated afterwards by XRD and Raman spectroscopy. Thereby, more than 5 Raman spectra were collected for each sample. Typical averaged Raman spectra for samples both PAN-T and PAN-S samples pyrolyzed at 1000°C are shown in Figure 6a.

Typically, G- and D-peaks are the characteristic bands observed in carbon allotropes. The G peak is centered in the range of 1560-1600 cm⁻¹ arises from vibrations of carbon atoms in sp²-hybridized planes of

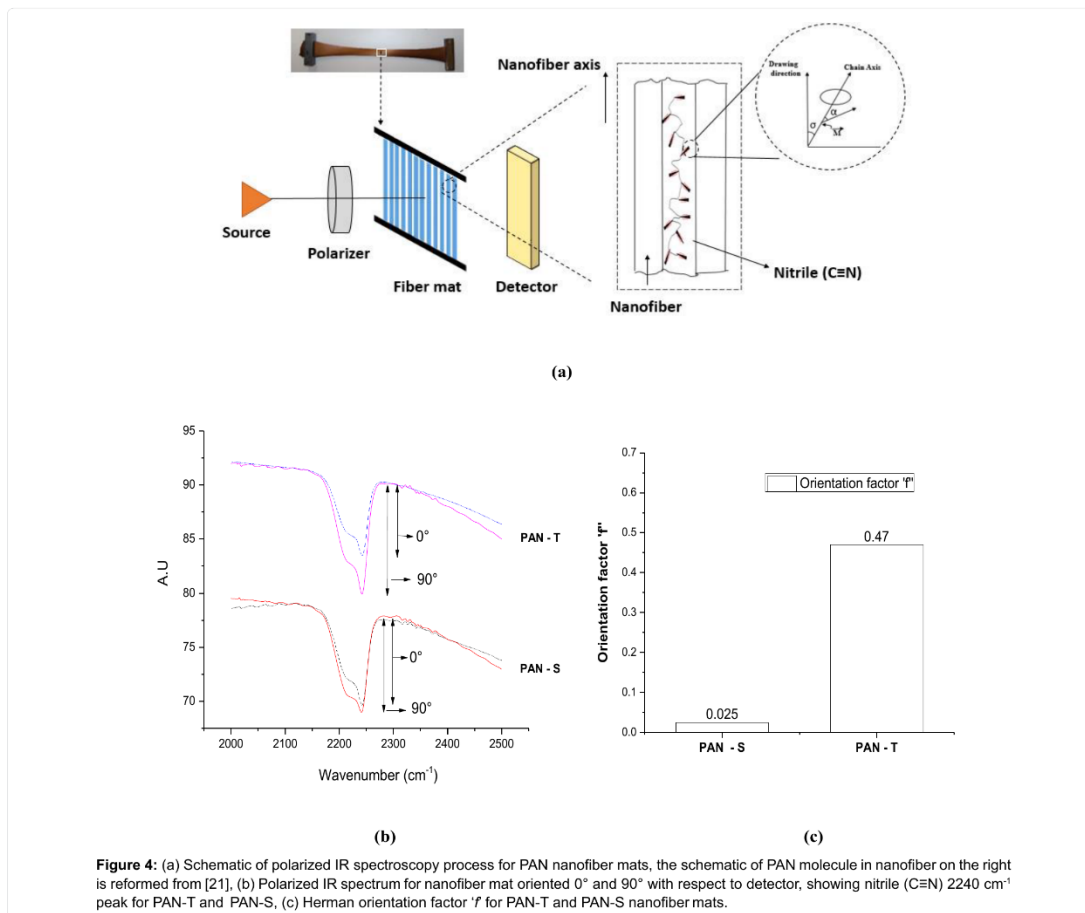


Figure 4: (a) Schematic of polarized IR spectroscopy process for PAN nanofiber mats, the schematic of PAN molecule in nanofiber on the right is reformer from [21], (b) Polarized IR spectrum for nanofiber mat oriented 0° and 90° with respect to detector, showing nitrile (C≡N) 2240 cm⁻¹ peak for PAN-T and PAN-S, (c) Herman orientation factor 'f' for PAN-T and PAN-S nanofiber mats.

carbon while D peak in the range of 1300-1400 cm⁻¹ is a defect induced band [26]. The sharpness and height of the G band peak is a qualitative representation for the presence of ordered/graphitic carbons [27]. The ratio of the integral intensity of these bands (*I*_D/*I*_G) is used to probe the disorder in the graphitic carbon. This ratio decreases for the samples which were cyclized with tension (Figure 6b). *R* value decreased by 12% and 17% for PAN-T samples pyrolyzed at 1000°C and 1200°C. Correspondingly, *L*_a (crystallite size along the basal plane) as evaluated from Raman spectra increased for the samples creep stressed during the whole stabilization process. The decreased value of *R* hints towards the formation of large *sp*²-hybridized clusters, indicating an increased graphitization [20]. Moreover, it was observed from the Raman spectrum of PAN 1000°C-T (Figure 6a) that the FWHM of the G peak decreases which is indicative for a better ordering of the domains. Furthermore, the crystallite size and graphitization was examined also by XRD. A typical XRD curve for PAN-1000°C-S and PAN-1000°C-T is shown in Figure 7a. The evolution of the (002) Bragg peak for carbon is clearly observed for PAN-1000°C-T, which is sharper and intense as compared to PAN-1000°C-S. The FWHM of the (002) peak is reduced

for PAN-T nanofibers (Figure 7b). The crystallite size *L*_c increases from 10.83 nm to 11.82 nm for samples carbonized at 1000°C samples. A similar increase in crystallite size is observed for the PAN nanofibers pyrolyzed at 1200°C.

The results from the diffraction pattern supports the Raman spectroscopy findings that the degree of graphitization increases. Both PAN-T and PAN-S samples (230°C for 10 h), before being carbonized had the same degree of cyclized material. The RCI showed a value of 95% for PAN-T and PAN-S samples, however the subsequent carbonization of these sample lead to a different degree of graphitization as observed from Raman and XRD analysis. The only difference is the degree of molecular orientation between the PAN-T and PAN-S samples as depicted in Figure 4. Hence a higher degree of molecular orientation for PAN chains is achieved during stabilization stages, assisted by the mechanical stretching has resulted in more ordered graphitic domains and relatively a higher degree of graphitization as compared the PAN stabilized without mechanical stretching.

During the oxidative stabilization process the formation of six

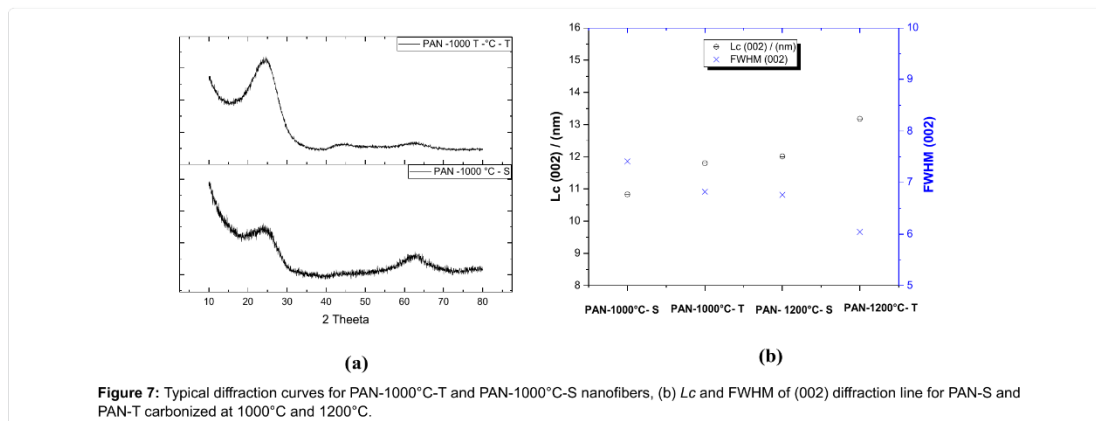
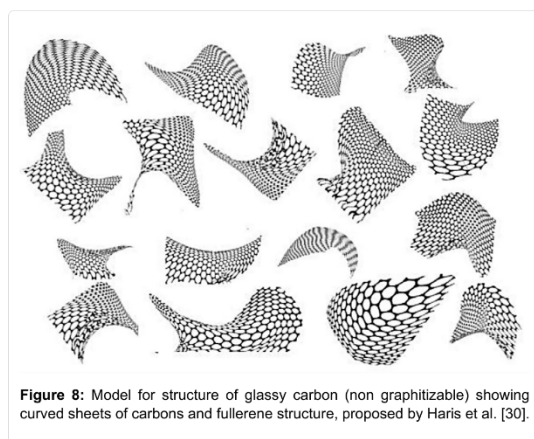


Figure 7: Typical diffraction curves for PAN-1000°C-T and PAN-1000°C-S nanofibers, (b) Lc and FWHM of (002) diffraction line for PAN-S and PAN-T carbonized at 1000°C and 1200°C.



carbon (hard carbons) by the nanotexture of crystallites. The highly oriented nanotexture results in formation of highly graphitized carbon while the latter have lower degree of graphitization [32]. The presence of curved planes formed during the pyrolysis of polymer precursor in stabilization process eventually hinders the sp^3 to sp^2 conversion [33]. A higher degree of graphitization for mechanically stretched PAN fibers can be attributed to the fact that application of mechanical stressed actually avoids the formation of such curved surfaces, which translates into more sp^2 hybridized carbon planes. D and G band from Raman spectra also hints that the sp^3/sp^2 ratio decreases for the PAN-T samples and more of sp^2 clustering takes place. Hence, even though the degree of cyclization is same for the PAN nanofibers after the stabilization stage but the application of mechanically applied creep stress during the stabilization stages results in increased molecular orientation which actually plays its role in inducing increased graphitization and sp^2 carbon planes, however the complete understanding of thermodynamics of this sp^3 to sp^2 conversion due to mechanical stress is still under research and is yet to be investigated further.

Conclusions

In this study, the effect of creep stress during the stabilization

process for polyacrylonitrile (PAN) nanofibers has been investigated and correlated with the carbonization process where graphitized structures are obtained. Two different cases were considered for stabilization, one set of PAN nanofiber mat was clamped with fixtures and was externally strained (PAN-T) while the second set of PAN nanofibers were clamped only with no external strain applied and the only strain was the one existing due to shrinkage (PAN-S) during the stabilization. The cyclization index was evaluated at different temperatures for PAN-T and PAN-S nanofiber mats. The chain alignment and orientation due to strain was also studied. Subsequently, the carbonization was performed for both PAN-T and PAN-S nanofibers. We conclude the following:

1- Our findings showed that RCI increases with increasing temperature. RCI for PAN-T fibers and PAN-S showed different values at lower temperatures (190°C and 210°C) however at higher temperatures both PAN-T and PAN-S samples showed similar RCI values. This suggests that stretching influences the chain conformations and adjusts the chains in suitable positions to form conjugated nitrile groups which results in an enhanced rate of cyclization. However, at high temperatures (230°C), the internal energy for PAN-S fibers is high enough and dipole-dipole repulsions between the $C\equiv N$ are reduced, therefore the difference of RCI between PAN-T and PAN-S nanofibers dissipates.

2- Moreover, the same values for RCI for PAN-T and PAN-S nanofibers (230°C-10 h) demonstrated difference in degree of graphitization. A higher degree of graphitization and less disorder was observed for PAN nanofibers stretched during stabilization stage. The difference in degree of graphitization was attributed to a potential formation of relatively more curved and fullerene structures which results in reduced degree of graphitization for the pyrolysis of PAN-S precursor, whereas PAN-T nanofibers with high molecular orientation leads to form more of the graphitic carbon planes. The application of creep stress results in higher sp^2 hybridized carbon planes. Creep stress during the stabilization assists in sp^3 to sp^2 transformation which reflects in higher degree of graphitization.

Overall, our study emphasizes the effect of strain during the stabilization process on cyclization which lays foundation for carbonized structure. This investigation can provide further insight into inducing higher graphitization of organic precursors by modifying the mechanical stress in addition to chemical changes by the thermal energy.

Acknowledgement

The authors are grateful to Hannover School for Nanotechnology (HSN) and Deutsche Forschungsgemeinschaft (DFG) for their financial support.

References

- Jariwala D, Sangwan VK, Lauhon LJ, Marks TJ, Hersam MC (2013) Carbon nanomaterials for electronics, optoelectronics, photovoltaics, and sensing. *Chem Soc Rev* 42: 2824-2860.
- Candelaria SL, Shao Y, Zhou W, Li X, Xiao J, et al. (2012) Nanostructured carbon for energy storage and conversion. *Nano Energy* 1: 195-220.
- Aprojanz J, Dreyer B, Wehr M, Wiegand J, Baringhaus J, et al. (2017) Highly anisotropic electric conductivity in pan-based carbon nanofibers. *J Phys-Condens Mat* 29: 494002-8.
- Ismagilov ZR, Shalagina AE, Podyacheva OY, Ischenko AV, Kibis LS, et al. (2009) Structure and electrical conductivity of nitrogen-doped carbon nanofibers. *Carbon* 47: 1922-1929.
- Peng S, Li L, Lee JKY, Tian L, Srinivasan M, et al. (2016) Electrospun carbon nanofibers and their hybrid composites as advanced materials for energy conversion and storage. *Nano Energy* 22: 361-395.
- Thavasi V, Singh G, Ramakrishna S (2008) Electrospun nanofibers in energy and environmental applications. *Energ Environ Sci* 1: 205-221.
- Kou L, Liu Y, Zhang C, Shao L, Tian Z, et al. (2017) A mini review on nanocarbon-based 1d macroscopic fibers: Assembly strategies and mechanical properties. *Nano-Micro Lett* 9: 9-51 (2017).
- Arshad SN, Naraghi M, Chasiotis I (2011) Strong carbon nanofibers from electrospun polyacrylonitrile. *Carbon* 49: 1710-1719.
- Inagaki M, Yang Y, Kang F (2012) Carbon nanofibers prepared via electrospinning. *Adv. Mater.* 24: 2547-2566.
- Zhang L, Aboagye A, Kelkar A, Lai C, Fong H (2014) A review: Carbon nanofibers from electrospun polyacrylonitrile and their applications. *J Mater Sci* 49: 463-480.
- Liu CK, Lai K, Liu W, Yao M, Sun RJ (2009) Preparation of carbon nanofibres through electrospinning and thermal treatment. *Polym Int* 58: 1341-1349.
- Rahaman MSA, Ismail AF, Mustafa A (2007) A review of heat treatment on polyacrylonitrile fiber. *Polym Degrad Stab* 92: 1421-1432.
- Eddie D (1998) The effect of processing on the structure and properties of carbon fibers. *Carbon* 36: 345-362.
- Yusof N, Ismail A (2012) Post spinning and pyrolysis processes of polyacrylonitrile (pan)-based carbon fiber and activated carbon fiber: A review. *J Anal Appl Pyrol* 93: 1-13.
- Li X, Qin A, Zhao X, Liu D, Wang H (2015) Drawing dependent structures, mechanical properties and cyclization behaviors of polyacrylonitrile and polyacrylonitrile/carbon nanotube composite fibers prepared by plasticized spinning. *Phys Chem Chem Phys* 17: 21856-21865.
- Wang PH (1998) Aspects on prestretching of PAN precursor: Shrinkage and thermal behavior. *J Appl Polym Sci* 67: 1185-1190.
- Gu S, Ren J, Wu Q (2005) Preparation and structures of electrospun pan nanofibers as a precursor of carbon nanofibers. *Synthetic Met* 155: 157-161.
- Wu G, Lu C, Ling L, Hao A, He F (2005) Influence of tension on the oxidative stabilization process of polyacrylonitrile fibers. *J Appl Polym Sci* 96: 1029-1034.
- Liu C, Hu L, Lu Y, Zhao W (2015) Evolution of the crystalline structure and cyclization with changing tension during the stabilization of polyacrylonitrile fibers. *J Appl Polym Sci* 132: 42182-42192.
- Ferrari AC, Meyer J, Scardaci V, Casiraghi C, Lazzeri M, et al. (2006) Raman spectrum of graphene and graphene layers. *Phys Rev Lett* 97: 187401-187405.
- Bashir Z, Tipping AR, Church SP (1994) Orientation studies in polyacrylonitrile films uniaxially drawn in the solid state. *Polym Int* 33: 9-17.
- Xiao S, Cao W, Wang B, Xu L, Chen B (2013) Mechanism and kinetics of oxidation during the thermal stabilization of polyacrylonitrile fibers. *J Appl Polym Sci* 127: 3198-3203.
- Liu Y, Chae HG, Kumar S (2011) Gel-spun carbon nanotubes/polyacrylonitrile composite fibers. Part iii: Effect of stabilization conditions on carbon fiber properties. *Carbon* 49: 4487-4496.
- Rizzo P, Auriemma F, Guerra G, Petraccone V, Corradini P (1996) Conformational disorder in the pseudo-hexagonal form of atactic polyacrylonitrile. *Macromolecules* 29: 8852-8861.
- Gupta A, Harrison (1997) New aspects in the oxidative stabilization of pan-based carbon fibers: II. *Carbon* 35: 809-818.
- Pimenta M, Dresselhaus G, Dresselhaus MS, Cancado L, Jorio A, et al. Studying disorder in graphite-based systems by raman spectroscopy. *Phys Chem Chem Phys* 9: 1276-1290.
- Ferrari AC, Robertson J (2004) Raman spectroscopy of amorphous, nanostructured, diamond-like carbon, and nanodiamond. *Phil. Trans. R. Soc. Lond. A: Mathematical, Physical and Engineering Sciences.* 362: 2477-2512.
- Harris P (2004) Fullerene-related structure of commercial glassy carbons. *Philos Mag* 84: 3159-3167.
- Harris PJ (2005) New perspectives on the structure of graphitic carbons. *Crit Rev Solid State Mater Sci* 30: 235-253.
- Harris PJ, Tsang SC (1997) High-resolution electron microscopy studies of non-graphitizing carbons. *Philos Mag A* 76: 667-677.
- Burket CL, Rajagopalan R, Foley HC (2008) Overcoming the barrier to graphitization in a polymer-derived nanoporous carbon. *Carbon* 46: 501-510.
- Inagaki M, Kang F (2014). *Materials science and engineering of carbon: Fundamentals.* (2nd edn). Butterworth-Heinemann (Elsevier), Oxford, UK.
- Franklin RE (1951) Crystallite growth in graphitizing and non-graphitizing carbons. *Proc R Soc Lond A.* 209: 196-218.

4.3 Carbon nanofiber reinforced with graphene nanoplatelets – Nano-carbons templated graphitization and electrical transport

4.3.1 Preface and Summary

The conclusions from Phase 2 showed that application of creep stress results in improving the graphitic structure of carbon nanofibers. Another approach to improve the graphitic structure of carbon nanofibers is rather by introduction of nanocarbons inclusions (nanotubes, graphene platelets, nanoparticles) to the carbon films and fibers. These nanocarbons have been used as reinforcements in various polymer matrices resulting in improving the polymer crystallinity. In the third stage of the project, this approach was explored, and graphene nano-platelets (GNPs) were used as nanocarbon inclusion. GNPs were introduced into the PAN precursor solution and electrospun-stabilized-carbonized to obtain carbon nanofibers doped with GNPs. Similar routes were followed to perform stabilization (fixation based, creep stress based) and subsequent carbonization. Graphitic structure was investigated and along with that electrical conductivity of nanofiber mats was also evaluated. This work has been published in *Nanomaterials – MDPI* (DOI: <https://doi.org/10.3390/nano10020351>).

The findings showed that addition of GNPs to PAN improves the crystallinity of carbonized PAN nanofibers. Raman spectroscopy shows reduction in the I_D/I_G ratio and FWHM of G-band peak for PAN/GNPs composite nanofibers compared to pristine PAN nanofibers. For both cases of stabilization, the PAN/GNPs showed increased degree of graphitization as evaluated from XRD and Raman for samples carbonized at various temperatures. Both the crystallite size along the basal plane (L_c) and lateral plane was increased (L_a). This indicated that stacking of graphene layers is taking place and transformation of amorphous carbon to ordered crystallite takes place. The results showed that GNPs is instrumental in supporting bi-fold functions: 1) They serve as nucleation agents for growth of graphene crystallite by templating effect of nanocarbons due to its highly crystalline structure, 2) They act as in-situ micro fixations in PAN matrix, anchoring the PAN chains resulting in evading the loss of alignment during stabilization.



The electrical conductivity measurements on nanofiber mats (3D) revealed highly anisotropic behavior, which was expected due the fact that nanofibers are aligned in one direction and there are fewer current paths for electron flow across the fiber direction. However, in comparison to pristine PAN, the anisotropy in electrical conductivity was reduced. We found out that GNPs engraved in the nanofiber mats act as a bridge for nanofibers to orient across the fiber alignment direction, which is facilitated due to the 2D geometry of graphene nano-platelets. This forms a conductive network across nanofiber alignment direction offering current paths across the conductive fiber as well. In general, the electrical conductivity along the nanofiber preferred orientation direction was increased due to improved graphitization.

The author performed all the synthesis, XRD, Raman, FTIR and SEM analysis was also conducted by the author himself. XPS experiments were conducted by JULIAN KOCHÉ from solid state physics department, LUH. The analysis and results were analyzed by author together with DR. FRANZ RENZ, DR. CHRISTOPH TEGENKAMP and DR. RALF SINDELAR.

The author wrote the manuscript on his own and it was edited and reviewed by the DR. FRANZ RENZ, DR. CHRISTOPH TEGENKAMP and DR. RALF SINDELAR.

Article

Graphene Nanoplatelet (GNPs) Doped Carbon Nanofiber (CNF) System: Effect of GNPs on the Graphitic Structure of Creep Stress and Non-Creep Stress Stabilized Polyacrylonitrile (PAN)

Annas Bin Ali ^{1,2,3,*}, Franz Renz ^{1,2}, Julian Koch ⁴, Christoph Tegenkamp ^{2,4,5}
and Ralf Sindelar ^{2,3}

- ¹ Institut für Anorganische Chemie, Leibniz Universität Hannover, Callinstr. 7, 30167 Hannover, Germany; franz.renz@acd.uni-hannover.de
 - ² Hannover School for Nanotechnology, Laboratorium für Nano und Quantenengineering (LNQE), Leibniz Universität Hannover, Schneiderberg 39, 30167 Hannover, Germany; christoph.tegenkamp@physik.tu-chemnitz.de (C.T.); ralf.sindelar@hs-hannover.de (R.S.)
 - ³ Faculty II, Hochschule Hannover, University of Applied Sciences and Arts, Ricklinger Stadtweg 120, 30459 Hannover, Germany
 - ⁴ Institut für Festkörperphysik, Leibniz Universität Hannover, Appelstraße 2, 30167 Hannover, Germany; koch@fkp.uni-hannover.de
 - ⁵ Institut für Physik, Technische Universität Chemnitz, Reichenhainer Str. 70, 09107 Chemnitz, Germany
- * Correspondence: annas.bin.ali@acd.uni-hannover.de

Received: 5 January 2020; Accepted: 13 February 2020; Published: 18 February 2020



Abstract: Improving the graphitic structure in carbon nanofibers (CNFs) is important for exploiting their potential in mechanical, electrical and electrochemical applications. Typically, the synthesis of carbon fibers with a highly graphitized structure demands a high temperature of almost 2500 °C. Furthermore, to achieve an improved graphitic structure, the stabilization of a precursor fiber has to be assisted by the presence of tension in order to enhance the molecular orientation. Keeping this in view, herein we report on the fabrication of graphene nanoplatelets (GNPs) doped carbon nanofibers using electrospinning followed by oxidative stabilization and carbonization. The effect of doping GNPs on the graphitic structure was investigated by carbonizing them at various temperatures (1000 °C, 1200 °C, 1500 °C and 1700 °C). Additionally, a stabilization was achieved with and without constant creep stress (only shrinkage stress) for both pristine and doped precursor nanofibers, which were eventually carbonized at 1700 °C. Our findings reveal that the GNPs doping results in improving the graphitic structure of polyacrylonitrile (PAN). Further, in addition to the templating effect during the nucleation and growth of graphitic crystals, the GNPs encapsulated in the PAN nanofiber matrix act in-situ as micro clamp units performing the anchoring function by preventing the loss of molecular orientation during the stabilization stage, when no external tension is applied to nanofiber mats. The templating effect of the entire graphitization process is reflected by an increased electrical conductivity along the fibers. Simultaneously, the electrical anisotropy is reduced, i.e., the GNPs provide effective pathways with improved conductivity acting like bridges between the nanofibers resulting in an improved conductivity across the fiber direction compared to the pristine PAN system.

Keywords: polyacrylonitrile; graphene nanoplatelets; stabilization; carbonization; shrinkage stress; creep stress; graphitization; electrical anisotropy

1. Introduction

Carbon fibers are by far the most prominent commercialized product in carbon and carbon reinforced materials. After nearly four decades of development, their properties regarding mechanical strength and electrical conductivity appear to have reached the saturation stage [1–3]. However, since the last decade, efforts are being made to employ nano-carbons as a reinforcement or property agent for an improved structure that would replicate into better mechanical, electrical and electrochemical properties. Especially the use of carbon nanofibers with average diameters of 100–300 nm as compared to carbon fibers (~7 µm diameter) are finding their ways into a variety of nano technological applications due to their high aspect ratio, increase of the surface area, high strength to weight ratio, improved charge transfer and greater possibility to modify the carbon chemistry [4–6].

Carbon nanofibers are typically fabricated via a top down approach by means of electrospinning followed by further steps for stabilization and carbonization or by a bottom up approach, using vapor growth processes. Electrospinning of polymer followed by stabilization in air and subsequent carbonization in a reduced atmosphere is not only a comparatively inexpensive and easy fabrication process, but it also offers a wide range of doping and chemical modifications to the made to polymer precursor in order to realize different functional properties [1,7,8]. Among various precursors known, polyacrylonitrile (PAN) is the most employed one for the production of carbon fibers [2,9]. In this top down approach, the cyclization process in the carbon nanofiber production is of extreme importance as during this step the formation of graphene-like ribbon structures take place. Without this process, a so-called ladder structure is avoided and PAN cannot withstand the carbonization process. The formation of the ladder like structure during the cyclization process prevents the fusion and loss of material at high temperature [8,10]. In general, the microstructure after carbonization is not highly graphitic and in order to increase the size and alignment of the graphitic domains, the fibers need to be graphitized at higher temperatures (2500 °C or more), which in turn increases the costs and energy consumption. Hence forth, the ability to improve the graphitic structure at lower temperatures is highly desirable with regards to economic and application perspective.

One of the approaches to improve the graphitic structure is to enhance the chain orientation inside the polymer precursor fiber during the stabilization process. During this process, tension is applied to the nanofibers to encounter the shrinkage of fibers, which otherwise reduces the polymer chain alignment. Recent studies have shown that the preservation and improvement of chain alignment is instrumental in producing highly graphitic aligned domains during the carbonization process, which in turn results in improved mechanical and electrical properties [11–13]. It is known further that the addition of various carbon allotropes (nanotubes, nanoparticles and graphene sheets) helps in improving the graphitization of carbon based films and nanofibers [5,14]. For example, single wall carbon nanotubes (SWCNTs) and multi walled carbon nanotubes (MWCNTs) have been incorporated in electrospun carbon nanofibers that results in improving the graphitization and crystallinity of PAN. Similarly, graphene nanoplatelets and graphene nano ribbons affect the crystallinity and graphitization of the polymer precursor [15–18]. Graphene nano platelets (GNPs), typically consisting of single to few layer sheets of sp²-hybridized carbon atoms forming two-dimensional layers with thickness in the nanometer scale, possess attractive characteristics such as high electrical conductivity, high modulus, high charge transfer capacity and high specific surface area [19,20]. As compared to chemical vapor deposition (CVD) grown carbon nanotubes (CNTs), the graphene platelets are comparatively cheaper. Additionally, dispersion of CNTs is tricky in a sense that it often gets curved inside the polymer matrix causing the grown graphitic layers to follow the curvature which results in a reduced graphitization [3]. GNPs used as dopants in carbon nanofibers can not only help in achieving high graphitic content at low temperatures, but also serve as anchors for polymer chains, thereby possibly relieving the use of external tension applied to nanofibers during the stabilization process. Only a very limited number of studies are available where the effect of GNPs on the graphitic structure of PAN has been investigated. One of the recent study done using PAN nanofibers doped GNPs revealed an increased degree of graphitization and an improved electrical conductivity developed by pressurized gyration followed by

spark plasma sintering [21]. However, no complete study is available for electrospun carbon nanofibers doped with graphene platelets, especially regarding the templating effect of GNPs on PAN graphitic structure in presence and absence of externally applied creeps stress during the stabilization. In order to explore this, we have investigated how GNPs impact the graphitization degree in the absence and presence of externally applied creep stress during the complete cyclization process and investigated if the absence of creep stress be mediate the by presence of GNPs only.

In principal, the following routes can be followed for stabilizing PAN nanofibers: (1) application of an externally applied creep load, (2) mechanical fixing of nanofiber mats, where only the inherent shrinkage stress due to entropic relaxation is present, and (3) neither externally applied stress nor any mechanical fixing. The first two cases, imposing dimensional constraints and stretching along the fiber axis, is known to avoid entropic relaxation or any physical shrinkage. For the third case, since the PAN fibers are not constrained, the process results in loss of material during the carbonization step. For the present study, the first two cases are considered. We report on the development of PAN and GNPs doped PAN nanofibers via electrospinning, followed by stabilization in air and carbonization in an inert atmosphere. The effect of adding GNPs to the stabilized and graphitized PAN structure was investigated by Infrared Spectroscopy (IR), Scanning Electron Microscopy (SEM), Raman, X-ray diffraction (XRD) and X-ray photoelectron spectroscopy (XPS). To realize the effect of applying creep stress during stabilization, pristine and doped nanofiber mats were also stabilized with creep stress and carbonized at 1700 °C. The conductivity of fiber mats was subsequently measured for carbonized samples for both cases (creep stress stabilized and non-creep stress stabilized system). The presence of GNPs acts as templates and nucleating agents for an improved graphitic structure. GNPs engraved in nanofiber matrix performs as micro-anchors, preserving the polymer chain alignment and reducing the effect of shrinkage in absence of external stress during the stabilization.

2. Material & Methods

2.1. Materials

Polyacrylonitrile (PAN: average molecular weight 150,000 M_w , Sigma Aldrich, St. Louis, MO, USA), dissolved in dimethylformamide (DMF, Carl Roth, Karlsruhe, Germany), was used as a precursor for carbon nanofiber production. Graphene nano platelets (GNPs) 6–8 nm thick and nearly 25 μm in width (ABCR GmbH, Karlsruhe, Germany) were added as nano dopant. A mixture of 2% H_2 /98% Ar (Westfalen AG, Hannover, Germany) was used as medium for high temperature carbonization process.

2.2. Synthesis of Carbon Nanofibers and Graphene Nanoplatelets (GNPs) Doped Carbon Nanofiber System

Typically, the precursor solution for the spinning process was prepared by dissolving polyacrylonitrile (PAN) in DMF (13 wt%). The mixture was dissolved at room temperature overnight for duration of 12 h. For PAN doped GNPs system, GNPs (1 wt% by PAN) were repeatedly ultrasonicated for 1 h in DMF for 15 min, followed by a 15 min break to avoid agglomeration due to heating. Afterwards, PAN was added to it and dissolved similarly for 12 h. Both spinning solutions (pristine PAN and PAN/GNPs) were electrospun at 17 kV, 1 mL/h and 10 m/s collector speed, while the fibers were collected on an aluminum foil. Electrospinning was followed by stabilization and high temperature carbonization. Stabilization is performed at 250 °C for duration of 10 h in air for as spun PAN mats and PAN/GNPs in two different ways. For one set of the samples, the nanofiber mats were stabilized with gripping both ends of the whole mats to reduce the entropic shrinkage, while for the other set of samples, an additional creep stress of ~16 MPa was applied for the entire duration of the cyclization process. The latter samples are denoted with suffix 'T'. PAN and PAN/GNPs were then carbonized under a mixture of 2% H_2 /98% Ar for duration of 1 h at four different temperatures (1000 °C, 1200 °C, 1500 °C and 1700 °C). Eventually, to observe the impact of creep stress, both PAN-T and PAN/GNPs-T were also carbonized at 1700 °C. The graphical abstract in Figure 1e sketches the complete fabrication process.

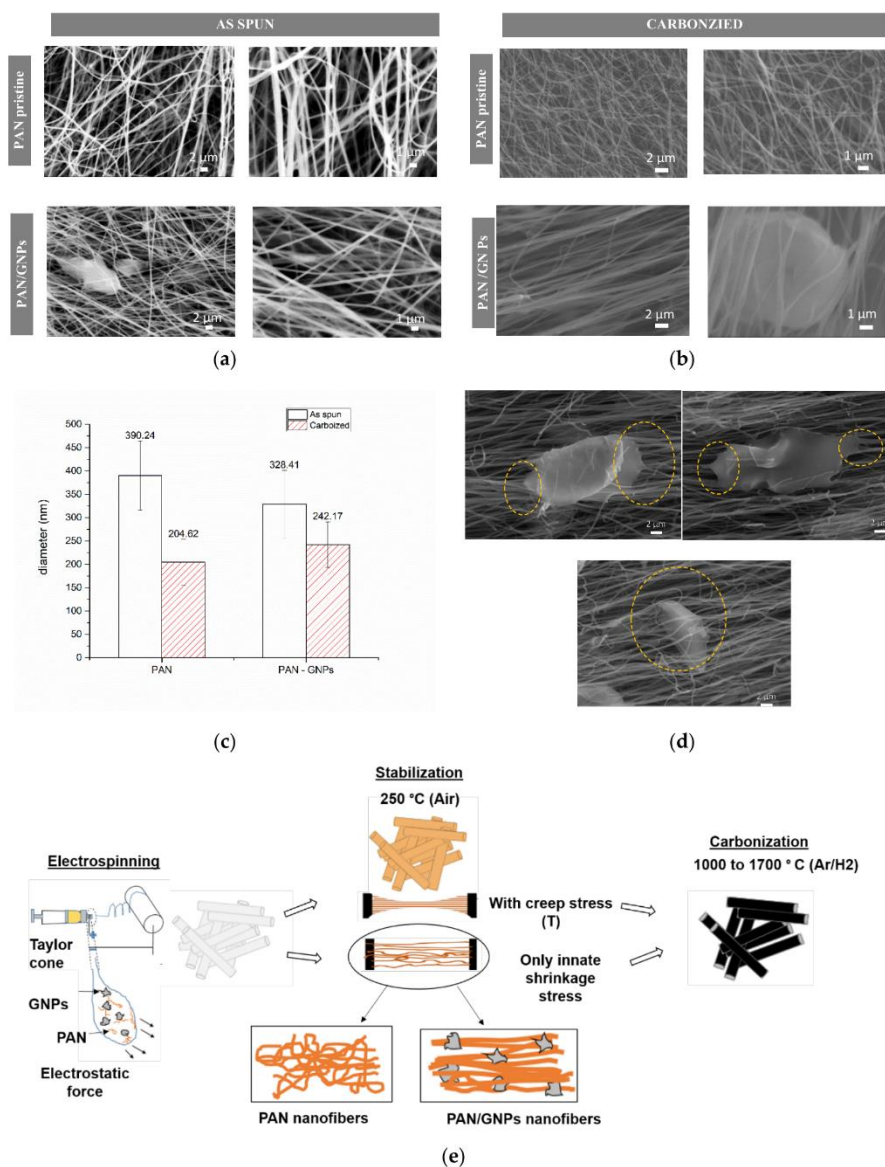


Figure 1. (a,b) Scanning Electron Microscopy (SEM) images for as-spun and carbonized pristine polyacrylonitrile (PAN) and PAN/graphene nanoplatelets (GNPs) doped nanofibers; (c) average diameter for as-spun and carbonized (1700 °C) PAN and PAN/GNPs nanofibers; (d) SEM images for carbonized PAN/GNPs nanofiber at 1700 °C showing graphene nanoplatelets (GNPs) engraved in nanofiber mats; (e) graphical abstract of polyacrylonitrile (PAN) and PAN/GNPs doped carbon nanofiber (CNF) showing fabrication process and two different ways in which stabilization is performed. GNPs helps in preserving the polymer chain alignment by acting as anchors and stretching the nanofibers.

2.3. Characterizations

The morphology of as-spun and carbonized PAN and PAN/GNPs mats were analyzed using Scanning Electron Microscopy (SEM, Carl Zeiss LEO 1455VP, Oberkochen, Germany). For measuring

the diameters of as-spun and carbonized PAN and PAN/GNPs, Image J was used. Fifty readings were taken from, in total, 10 different SEM images. Molecular structure of as-spun and stabilized mats was studied using Fourier Transform Infrared Spectroscopy (FTIR, Perkin Spectrum Two, Waltham, MA, USA). The ring cyclization index (RCI) was calculated in order to evaluate the amount of the cross-linked ladder polymer conversion by measuring the integral intensity of the C≡N (2240 cm⁻¹) and C=N (1600 cm⁻¹) peaks, ($RCI = \frac{I_{C=N}}{I_{C=N} + I_{C≡N}}$). Structural properties were analyzed using X-ray diffraction (XRD, Bruker D Phaser, Billerica, MA, USA). Diffraction patterns were recorded from 10° to 80° with a step size of 0.03° using Cu-K_α (λ = 1.5406). The interlayer spacing, *d* (002) was calculated using Bragg law, $d = (\lambda/2 \cdot \sin\theta)$, where λ is the wavelength of the X-ray source and θ is the Bragg angle. The crystallite size was estimated using the Scherrer equation, $L_c = (K \cdot \lambda / \beta \cdot \cos\theta)$, where *K* is the shape factor (0.89 for *L_c*). β is the full width at half maximum (FWHM) expressed in radians. The relative crystallinity for as spun PAN and PAN/GNPs nanofiber was finally calculated by the ratio of the area belonging to the crystalline PAN peak (~17°) and the total area, including the amorphous and crystalline portion. The graphitic structure and disorder within the nanofiber mats were characterized further using Raman spectroscopy (DXR2, Thermo Fisher, Waltham, MA, USA). Five spectra were recorded with a laser wavelength of 532 nm as an excitation source in the range of 1000–3000 cm⁻¹ with a low incident laser power of 1 mW to avoid heating effects. The D- and G-bands in the spectra were deconvoluted using Lorentz fitting of the *I_D* and *I_G* integral ratios. Moreover, the crystal sizes *L_a* (apparent crystallite size along the basal plane) of carbon nanostructures were estimated via $L_a \text{ (nm)} = (2.4 \times 10^{-10}) \cdot \lambda_{laser}^4 \cdot (I_D/I_G)^{-1}$ [22]. The degree of hybridization was calculated from sp² and sp³ fraction of the C1s photoemission spectrum taken with XPS using an Al-K_α emission. The kinetic energies were measured using a hemispherical analyzer with a pass energy of 20 eV. Including the Shirley background, the C1s spectra were fitted using symmetric Gaussian-Lorentzian sum functions under the constraint that the energy difference between the sp²- and the sp³-peak is 0.8 eV [23].

The electrical conductivity of the carbon nanofiber mats was measured by a 4-point probe method under ultra-high vacuum using a 4-tip STM/SEM system. The samples were cut into approximately 1.5 cm × 1.5 cm mats and were fixed to the sample holder using silver paste. Direction orthogonal and perpendicular to nanofiber axis was marked before for evaluating conductivity across and in fiber direction. The conductivity was calculated from the resistance *R* including the dimensions of the samples via $\sigma \text{ (S/cm)} = L/A_{true} \cdot R$, where *L* is the distance between the both ends. The effective area *A_{true}* was calculated by dividing the liner density of fiber mats by the density of CNF. Thereby the CNF density is assumed to be ~1.7 g/cm³, similar to density of commercial PAN based carbon fiber. The average values were calculated from five different samples for each type of sample.

3. Results and Discussions

3.1. Morphology and Molecular Structure of As-Spun and Stabilized Polyacrylonitrile (PAN) and PAN/GNPs

Figure 1a,b shows SEM images of as-spun and carbonized nanofiber mats (non-creep stress stabilization). Both pristine PAN and PAN, doped with GNPs, showed a uniform and fibrous morphology. However, for PAN/GNPs, the formation of beads in some regions is observed due to changes of the viscosity and conductivity of the solution. Apparently, graphene sheets are beaded in both as-spun and carbonized PAN nanofiber mats. Furthermore, the average diameter for as spun PAN/GNPs has also decreased (Figure 1c), which can be attributed to the high conductivity of GNPs. This induces large charge accumulation in the solution jet which results in strong electrostatic repulsion among jet sprays. After carbonization at 1700 °C, the PAN and PAN/GNPs show a reduction in their diameters due to evolution of volatile species during the stabilization and carbonization reactions. Additionally, the entropic shrinkage during the cyclization also results in reduction of the diameter [8,9]. Interestingly, the average diameter reduction for PAN is 47% compared to 26% for PAN/GNPs nanofibers. This indicates that the addition of GNPs improves the thermal stability of PAN and reduces the shrinkage with comparatively less loss of material during the stabilization and carbonization

processes. The effect of GNPs on PAN crystallinity was studied using XRD. The diffractograms for pristine PAN, GNPs and PAN/GNPs nanofiber mat are also shown in Figure 2a. PAN is a semi crystalline polymer showing a crystalline peak at $\sim 17^\circ$ corresponding to (100) crystallographic planes while a broad amorphous hallow at $\sim 29^\circ$ corresponds to (110), typical for semi-crystalline PAN. GNPs show a strong diffraction peak at $\sim 26^\circ$ corresponding to an interlayer spacing of 0.335 nm, which is close to that of graphite. The presence of a sharp peak indicates that not all GNPs are completely exfoliated. For the PAN/GNP composite both GNPs and PAN related peaks were found, i.e., the two phases coexist in as-spun PAN/GNPs nanofibers. Upon doping with GNPs, the amorphous portion is reduced and crystallinity of PAN increases. This high aspect ratio GNPs interact with polymer chains and organizes them in manner to improve the chain orientation which is reflected in an improved crystallinity and increased size of the PAN crystallites (Figure 2b).

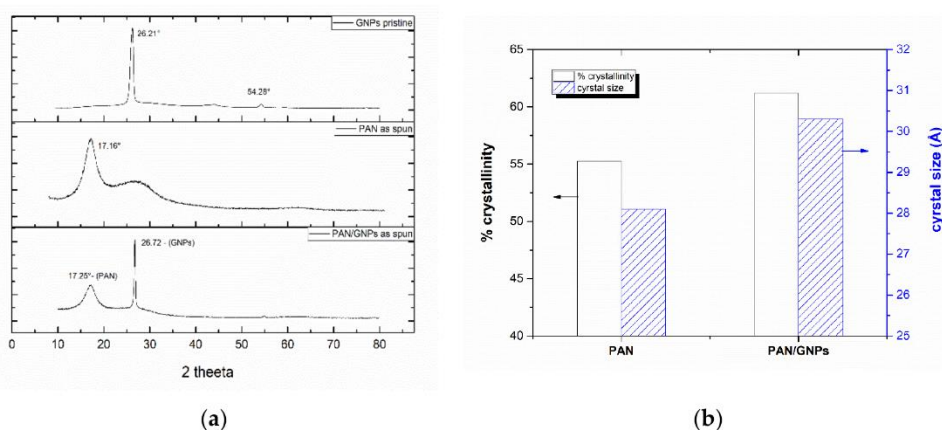


Figure 2. (a) X-ray diffractograms (XRD) for pristine GNPs, PAN and PAN/GNPs as-spun nanofibers; (b) crystallinity and crystal size for as spun PAN and PAN/GNPs nanofibers computed from XRD diffractograms.

Characteristic IR spectra of as-spun and stabilized mats are shown in Figure 3a,b. The typical signature for PAN is the nitrile band ($C\equiv N$) at 2243 cm^{-1} . The absorption observed at 2871 cm^{-1} and 2938 cm^{-1} corresponds to CH_2 symmetric and asymmetric stretch modes, while other main intensity lines represent $C=O$ stretch (1732 cm^{-1}), $C=C$ stretch (1665 cm^{-1}) and $C-O$ (1173 cm^{-1}) vibrations. With the addition of GNPs, there is a small shift in $C=O$ stretching and from 1732 cm^{-1} to 1734 cm^{-1} with a reduction in intensity, while the intensity line for 1663 cm^{-1} is increased. The changes in bands at higher wave numbers and especially at 1732 cm^{-1} hints towards an interaction of graphene platelets with the backbone $C=O$ group. After stabilizing at 250°C for 10 h, the evolution of the $C=N$ band at $\sim 1591\text{ cm}^{-1}$ takes place while the band at 2243 cm^{-1} is almost disappeared. This shows that the cyclization process has taken place and $C\equiv N$ has been transformed to $C=N$, forming a ring like ladder structure. Ring cyclization index (RCI) showed the value of $\sim 95\%$ for both PAN and PAN/GNPs. The appearance of a peak at 806 cm^{-1} shows that the dehydrogenation has also taken place. For the cyclized mats, the shift in $C=N$ can be observed which also points towards strong interaction of GNPs with PAN.

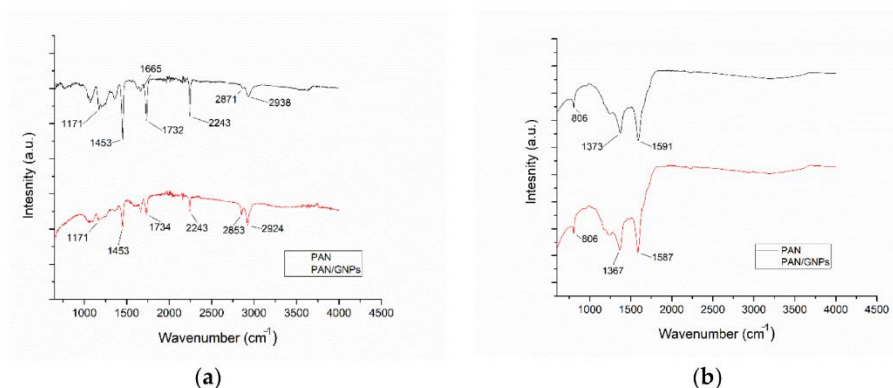


Figure 3. (a) Infrared (IR) spectra for as-spun PAN and PAN/GNPs nanofibers; (b) IR spectra for PAN and PAN/GNPs nanofibers stabilized at 250 °C for 10 h in air.

3.2. Carbonization and Graphitic Structure of PAN and GNPs Doped PAN

The carbonization of non-creep stress stabilized PAN and PAN/GNPs were performed at four different temperatures (1000 °C, 1200 °C, 1500 °C and 1700 °C). To investigate the graphitic structure and crystallinity, Raman spectroscopy and XRD measurements were performed. Typical Raman spectra for the pristine GNPs, PAN and PAN/GNPs carbonized at 1000 °C and 1700 °C are shown in Figure 4a. The two major peaks centering nearly at 1360 cm^{-1} and 1585 cm^{-1} in the spectrum are referred to as D- and G-band. The G-band is attributed to an in-plane stretching mode of sp^2 carbon bonds, while the D-band is due to hybridized vibrational mode related to the graphene layer edges, indicating the number of defects in the graphitic structure [22]. At lower temperatures of 1000 °C, the region in the range 2500–3000 cm^{-1} is majorly a hump with no sharp bands, however at higher temperature of 1700 °C the evolution of additional bands, 2D and D + D' take place due to a two phonon process. The integral intensity ratio of D- and G-bands is indicative of the graphitic quality of samples and defects while the FWHM of G-band reflects the degree of graphitization [24]. As the temperature is increased, I_D/I_G ratio and FWHM of G peak decreases (Figure 4b,d). The FWHM of G peak decreases for PAN doped with GNPs (e.g., at 1700 °C; from 67.0 to 59.7 cm^{-1}). The L_a (domain crystal size along basal plane) shown in Figure 4c is also increased for GNPs doped PAN at all temperatures. All these changes are attributed to an enrichment of sp^2 hybridized carbon and transformation of amorphous carbon into crystalline carbon. XRD results for PAN and PAN/GNPs are shown in Table 1. The FWHM of (002) peak decreases and the stacking size of crystal plane ' L_c ' increases (e.g., at 1700 °C, 2.03 nm for PAN and 2.47 nm for PAN/GNPs) which also suggests an increase of the carbon crystallinity. XPS was performed on pristine PAN and PAN/GNPs nanofibers at 1000 °C and 1700 °C. Typical XPS spectra for PAN and PAN/GNPs at 1000 °C and 1700 °C is shown in Figure 5. The sp^2 content increases from nearly 55% to 59% upon doping with graphene platelets at 1000 °C and from 62% to 64% at 1700 °C (Table 2). The improved degree of graphitization supports the findings from Raman and XRD.

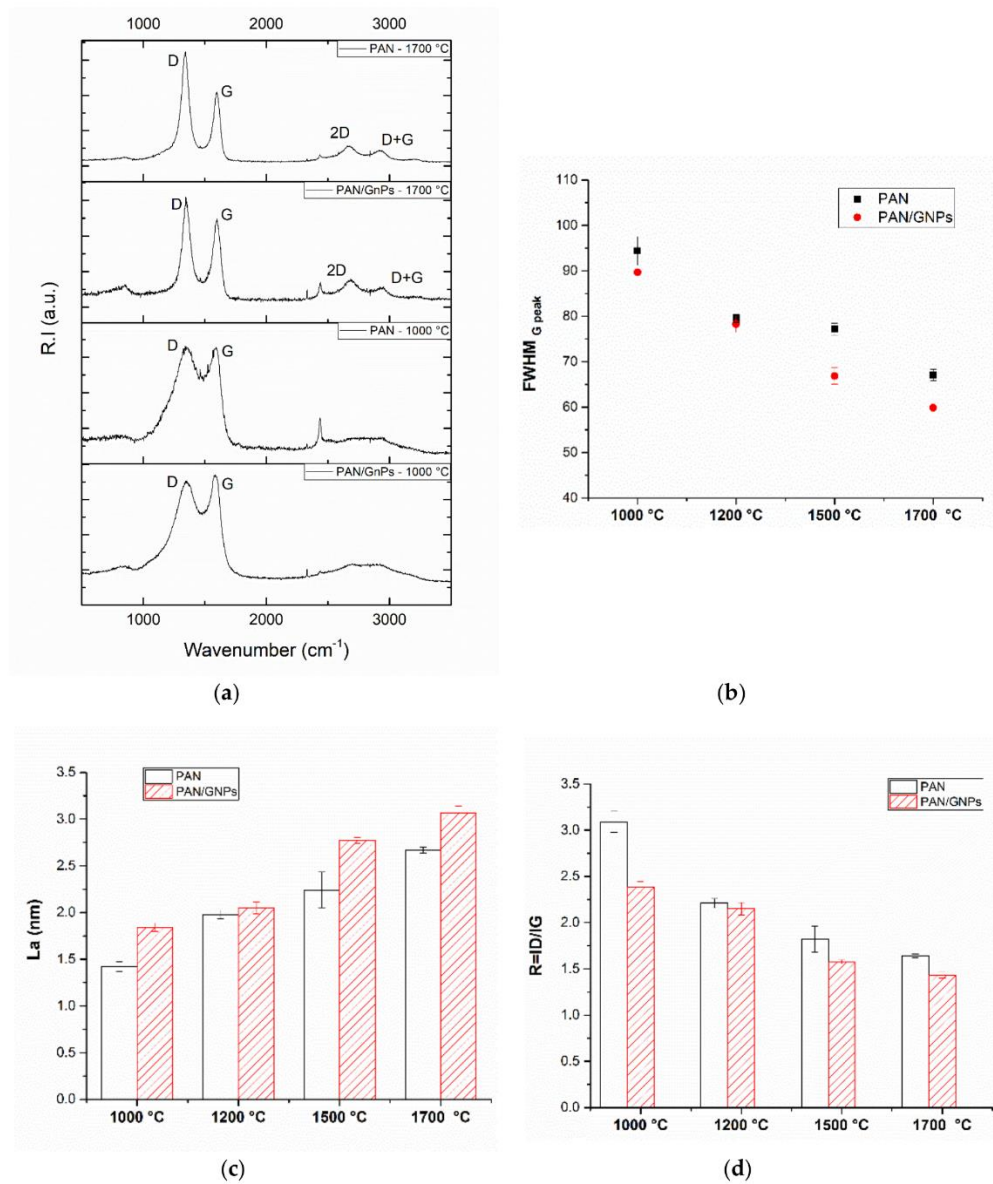


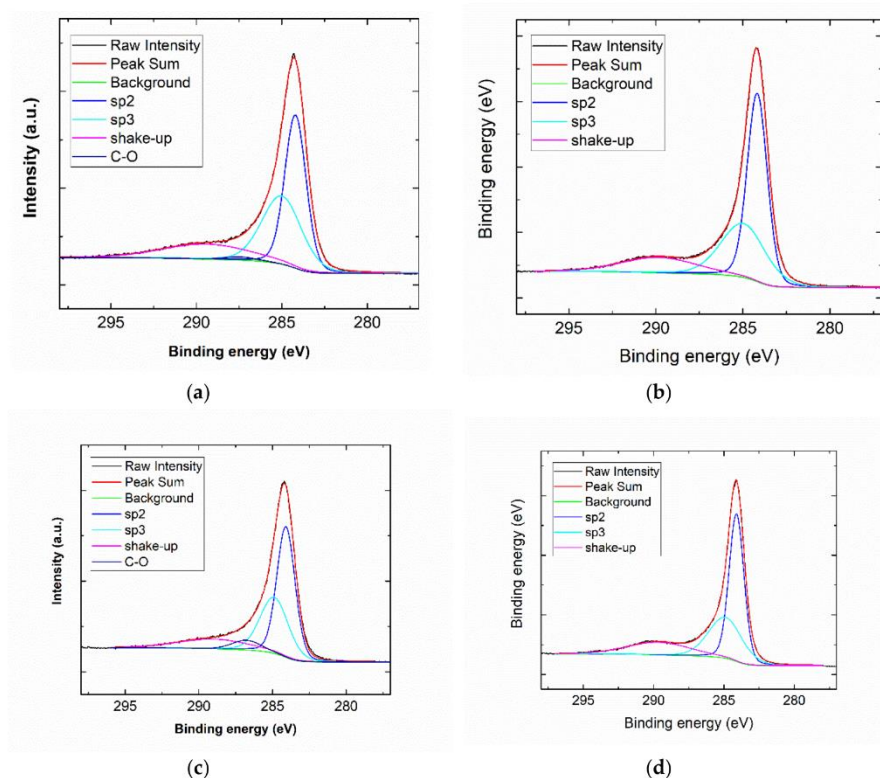
Figure 4. (a) Typical Raman spectra for PAN and PAN/GNPs carbonized at 1000 °C and 1700 °C; (b) FWHM_{G-peak}; (c) L_a and (d) R = (I_D/I_G) for PAN and PAN/GNPs doped nanofibers at different temperatures.

Table 1. The full width at half maximum (FWHM)₍₀₀₂₎ and the crystallite size ' L_c ' for PAN and PAN/GNPs carbonized at different temperatures, as calculated from XRD results.

Sample	L_c (nm)	FWHM ₍₀₀₂₎
PAN-1000 °C	1.38	5.82
PAN-1200 °C	1.96	5.01
PAN-1500 °C	2.01	4.65
PAN-1700 °C	2.03	3.98
PAN/GNPs-1000 °C	1.68	5.14
PAN/GNPs-1200 °C	2.2	3.64
PAN/GNPs-1500 °C	2.33	3.45
PAN/GNPs-1700 °C	2.47	3.25
PAN-1700 °C-T	2.07	3.88
PAN/GNPs-1700 °C-T	2.58	3.12

Table 2. sp^2 fraction and sp^2/sp^3 ratio for PAN and PAN/GNPs at 1000 °C and 1700 °C, as evaluated from de-convolution of C1s spectra for X-ray photoelectron spectroscopy (XPS) results.

Sample	sp^2/sp^3 Ratio	sp^2 Fraction
PAN-1000 °C	1.22	54.8%
PAN/GNPs-1000 °C	1.50	59%
PAN-1700 °C	1.57	61.89%
PAN/GNPs-1700 °C	1.81	64.45%

**Figure 5.** (a,b) Typical XPS spectra of de-convoluted C1s peak for pristine PAN and (c,d) PAN/GNPs at 1000 °C and 1700 °C.

The above results are obtained for carbonized PAN and PAN/GNPs, which were cyclized by only fixing both ends of fiber mats (non-creep stress stabilized mats). To observe the impact of the creep stress, the carbonization was done at 1700 °C. The results of the Raman analysis are plotted in Figure 6a. It can be seen that the I_D/I_G ratio is further decreased and L_a is increased for the samples stabilized with creep stress for both pristine PAN and PAN/GNPs. This shows that the graphitization is further enhanced and the crystallinity is increased. Moreover, it was found that the evolution of an intense and symmetric 2D peak takes place for 'T' samples (Figure 6b), while the FWHM of the 2D peak decreases (~195 cm) for both PAN-T and PAN/GNPs-T compared to (~370 cm) PAN and PAN/GNPs hinting towards ordering graphitic crystals. The 2D band is active due to a double resonance mechanism and is often used in general, for inferring the number of graphene layers for single, bilayer and multilayer graphene by calculation of I_{2D}/I_G ratio [24]. XRD results (Table 1) shows increased stacking size L_c and decreased FWHM for the (002) peak.

The application of creep stress during the stabilization process not only helps to avoid the entropic shrinkage, but also ensures a high degree of chain alignment that prevents the curvature in carbon planes and eventually paves the way for an improved alignment of graphitic domains [11,25]. According to Haris et al. [26,27], the graphitizable carbons and non-graphitizable carbons differ in extent of fullerenic formation during the pyrolysis of polymer precursor. During the pyrolysis of PAN, the ribbon-like graphene ribbon is formed [28]. In these ribbons, along with the formation of six membered rings, the non-six membered heptane- and penta-rings fragments are also present. These majority of non-six membered rings fragments introduce a curvature in carbon plane which results in formation of a fullerenic structure. The introduction of curvature and curls in carbon planes prevents the long range stacking during the high temperature pyrolysis and is hindering the full graphitization process

To summarize this part, both the diffraction and the Raman analysis showed that GNPs act as nucleation centers for the growth of graphitic carbon. The presence of GNPs promotes graphitization of PAN. Furthermore, even without the application of creep stress during the oxidative stabilization process, the PAN/GNPs doped fibers showed a greater extent of graphitization and crystallinity. In absence of external stress, the GNPs act as anchoring units for the alignment of PAN chains. From the SEM images (Figure 1d), it can be observed that these GNPs are embedded in PAN nanofiber mats and at discrete locations where they acts as possible fastening units that stretch PAN chains. These units of GNPs spun between the nanofibers prevent the loss of chain alignment during the stabilization process, which results in an improved degree of graphitization as compared to pristine PAN system. It is known, that during pyrolysis the polymer backbone serves as a nucleation point for growth of graphene ribbons [30]. The stronger interaction of GNPs with the PAN backbone supplemented by mechanical action of these GNPs in inducing stress in PAN chains is instrumental in preventing the curvature in carbon planes and maintaining long range order, which translates into improved graphitization of PAN. As evident, the sample cyclized under creep stress showed improved graphitization compared to non-creep stress cyclized samples, both for PAN and PAN/GNPs. [29].

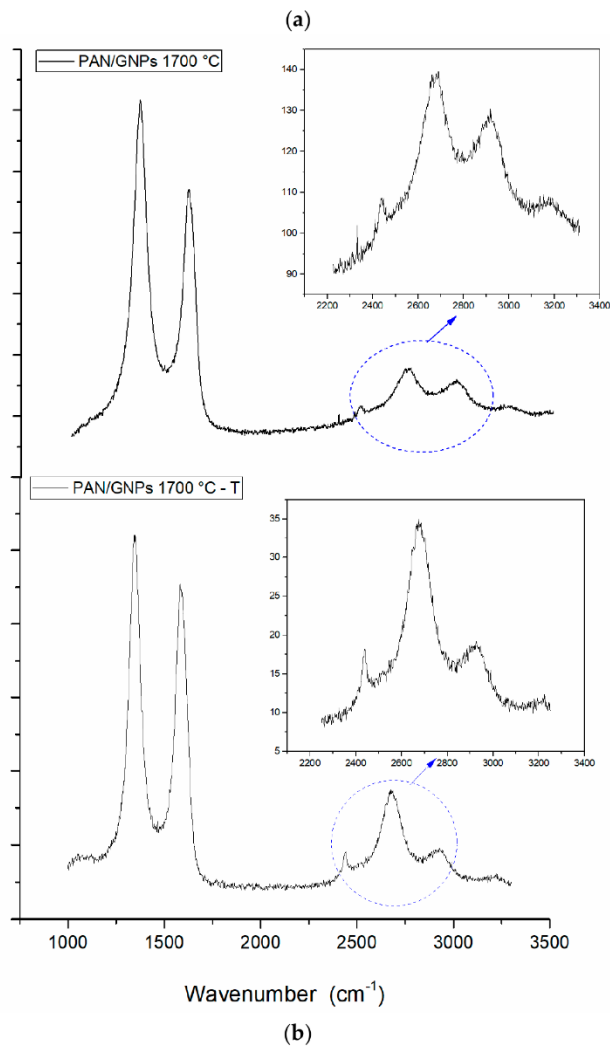
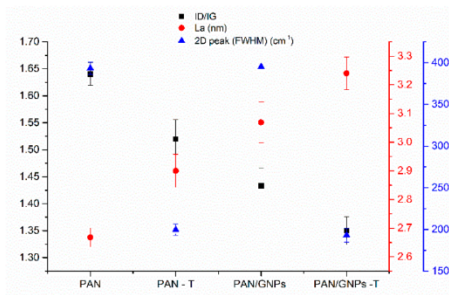


Figure 6. (a) I_D/I_G , L_a and FWHM of 2D peak for spectra for PAN and PAN/GNPs stabilized with and without creep stress after carbonization at 1700 °C; (b) typical Raman spectra for PAN/GNPs stabilized with creep stress (PAN/GNPs 1700 °C-T) and without creep stress (PAN/GNPs 1700 °C) after carbonization at 1700 °C.

3.3. Electrical Conductivity of Pristine and GNPs Doped PAN Nanofiber Mats

The results of electrical conductivity measurements of PAN and PAN/GNPs are shown in Figure 7a,b. The transport was measured along and across the nanofiber axis direction for both types of samples. It can be seen that for all temperatures, doping with GNPs enhances the conductivity along the fiber direction. At 1000 °C, the electrical conductivity is increased by almost 60% along the fiber axis. Similarly, a 24% increase in electrical conductivity was observed at 1700 °C, suggesting that microstructure becomes more graphitic as supported by Raman and XRD results. A greater increment in conductivity at lower temperatures as compared to higher temperatures upon doping with GNPs can be attributed to the fact that the templating effect of nano-carbons is more pronounced at lower carbonization temperatures where a large portion of carbon is more amorphous [31]. Conductivity across the fiber directions is lower as compared to in fiber direction (e.g., at 1000 °C from average of 77 S/cm in fiber direction to 8 S/cm across the fiber direction). Such a large discrepancy in electrical conductivities across and along fiber direction is obvious as there are fewer interconnects available for electrons. Fibers make occasional contacts even when they are not stretched however they are aligned in one direction due to use of rotating collector after spinning. Interestingly for PAN/GNPs, the anisotropy in electrical conductivity is decreased as compared to pristine CNF. In the case of pristine CNFs, there are fewer paths for electron flowing in the perpendicular direction, however with incorporation of GNPs into CNFs, there are more conductive network like pathways across nanofibers. Uniformly distributed GNPs in fiber matrix at different locations provide a path due to which the anisotropy in conductivity is reduced as compared to pristine CNF (Figure 8). The anisotropy of the electrical conductivity is much higher for 1700 °C–T as compared to 1700 °C samples (Figure 7d). The average electrical conductivity parallel to fiber direction is 590.8 S/cm, however, across the fiber direction is 40.5 S/cm for PAN–1700 °C–T, i.e., 15 times lower. Similarly, a high anisotropy in electrical conductivity was reported earlier by us for creep stress cyclized PAN system [32]. For PAN/GNPs–1700 °C–T, the anisotropy in electrical conductivity is greatly reduced compared to PAN–1700 °C–T. The above finding suggest that the presence of GNPs triggers the formation of a 2D electrically conductive network by interfacial contacts between different fibers. GNPs acts as a bridge between the conductive fiber lines, not only by themselves, but also a network of nanofiber cross connections was observed where the GNPs are embedded in nanofibers (Figure 8a,b). Due to this, the conductivity is fairly enhanced across the fiber direction providing electrical paths. Carbon nanofibers are bridged across the nanofiber alignment direction where GNPs are present. It is important to mention here that the conductivity of carbon nanofiber mats or assemblies cannot be directly interpreted as the electrical conductivity of single carbon nanofiber due to the fact that in addition to the conductivity of a single nanofiber, the entanglements and interconnects between the nanofibers also influence the electron flow. Our earlier studies have reported that the cross connections act as scattering centers for electron flow, details of which can be looked over [32].

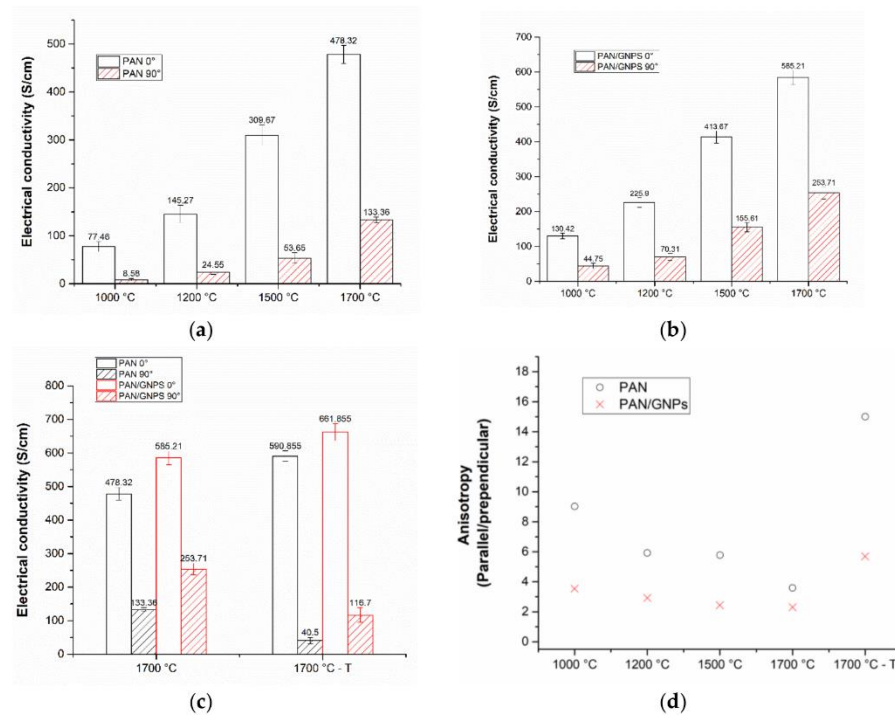


Figure 7. (a) Electrical conductivities of (a) PAN and (b) PAN/GNPs nanofiber mat after carbonization at different temperatures in parallel and perpendicular direction; (c) electrical conductivities of creep stress stabilized and non-creep stress stabilized PAN and PAN/GNPs nanofiber mats at 1700 °C in parallel and perpendicular directions; (d) anisotropy in electrical conductivity of carbonized PAN and PAN/GNPs.

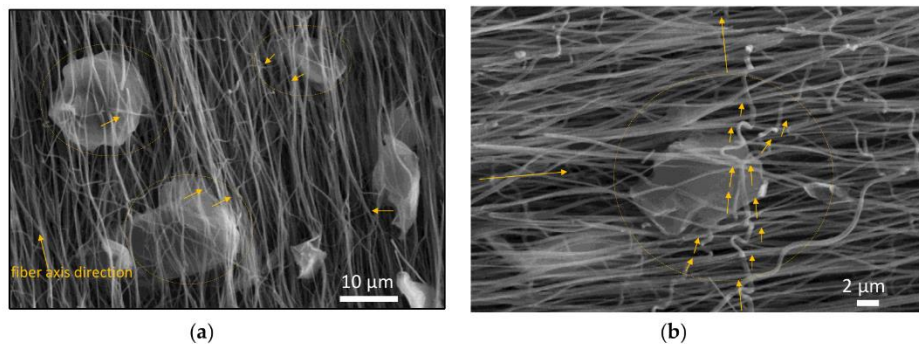


Figure 8. (a,b) SEM Images showing the bridging effect of GNPs between the individual nanofibers that mediates the presence of path ways for electrical conductivity in perpendicular.

In conventional carbon fiber fabrication process, the improved graphitization degree is closely associated with orientation of polymer chains in PAN precursor fiber. Carbon fibers are stabilized under constant tension in order to avoid the relaxation in amorphous region before carbonization. Stabilization under constant tension has proven to be an effective technique to reduce the entropic shrinkage and prevent the loss of polymer chain alignment especially in the amorphous region. It is interesting to observe that by adding GNPs, high graphitic content can be achieved even with absence of tension applied during the stabilization process. GNPs beaded carbon nanofiber can not only help

to counter the absence of external tension as they anchors the polymer chain and prevent loss of chain orientation but also serve as templating agent, providing nucleation sites for growth of graphitic crystal. In other words, the GNPs embedded in nanofiber matrix can pre-organize the polymer chain into aligned structures which translates into highly orientated graphitic crystallite during carbonization.

4. Conclusions

In this study, pristine CNFs and GNPs doped CNFs were prepared via electrospinning followed by oxidative stabilization and carbonization. Stabilization at 250 °C for 10 h was performed without application of creep stress but with mechanical fixing of nanofiber mat ends for both pristine PAN and PAN doped with GNPs at four different carbonization temperatures. To observe and compare the effect of incorporated creep stress in the presence of nano-carbon doped PAN, the stabilization was also performed with the application of creep stress for PAN and PAN/GNPs at 250 °C for 10 h. These samples were carbonized at 1700 °C. The microstructure, graphitization and electrical conductivity was systematically investigated for these sets of samples. Our results revealed that the doping of CNFs with GNPs improves the crystalline structure and graphitization degree of polyacrylonitrile as confirmed by the decrease of the I_D/I_G ratio, FWHM for G peak and increased crystallite size L_a and at all carbonization temperatures. GNPs are instrumental in providing bi-fold advantage, (1) doping GNPs enhances the graphitization of PAN by a templating effect of nano-carbon, (2) the presence of GNPs even during the absence of externally applied creep stress helps to maintain a certain degree of stress during the cyclization process which translates into improved alignment of graphitic domains resulting in higher degree of graphitization. GNPs in-situ act as stress units, engraved in nanofiber mats, which to reduce the shrinkage, in case no tension is applied. Furthermore, during the electrospinning process, additional electrostatic force acts on polymer solution jet due to GNPs which exerts shear to the polymer chains, resulting in prior alignment which translates into improved ordering during carbonization process. The application of creep stress in both PAN and PAN/GNPs result in an improved graphitization of the polymer. The transport experiments reveal highly anisotropic conductivities for PAN and PAN-T compared to PAN/GNPs and PAN/GNPs-T samples in perpendicular and parallel to fiber direction. GNPs, embedded in nanofibers, bridge the nanofibers across the nanofiber direction and forms a conductive network across the fiber alignment direction due to which the conductivity in perpendicular direction is increased. In absence of GNPs, there are fewer paths for electrical current flow across the fiber alignment direction and electron flow is impeded. The graphene nanoplatelets in continuous carbon nanofiber can provide a unique chemical structure with highly conductive network due to excellent 2D nanostructure and electrical conductivity of GNPs. Further doping schemes will be worked out in the future in order to produce porous carbon nanofibers beaded with GNPs that can be stabilized without a tension yet still able to provide with appreciable degree of graphitization at lower carbonization temperatures. This could lead to a production of highly conductive electrodes for energy storage and conversion still with porosity and defects which otherwise is a compromise, as defects and porosity undermines electrical transport.

Author Contributions: Concept and idea frame work, A.B.A., R.S., C.T. and R.S.; experiment conducted, A.B.A. and J.K. (XPS characterization and analysis); writing—original draft preparation, A.B.A.; writing—review and editing, C.T., R.S. and F.R. All authors have read and agree to the published version of the manuscript.

Acknowledgments: The authors are grateful to Hannover School for Nanotechnology (HSN) and Deutsche Forschungsgemeinschaft (DFG) for their financial support under grant number, 21-78904-63-7/16, by Niedersächsisches Ministerium für Wissenschaft und Kultur (Ministry of Science and Culture of Lower Saxony/Germany).

Conflicts of Interest: The authors declare no conflict of interest.

References

1. Hammel, E.; Tang, X.; Trampert, M.; Schmitt, T.; Mauthner, K.; Eder, A.; Pötschke, P. Carbon nanofibers for composite applications. *Carbon* **2004**, *42*, 1153–1158. [[CrossRef](#)]

2. Rath, T. Carbon Nanofibers: Synthesis, Properties and Applications. In *Polymer Nanocomposites Based on Inorganic and Organic Nanomaterials*; John Wiley & Sons: Hoboken, NJ, USA, 2015; pp. 63–88.
3. Prilutsky, S.; Zussman, E.; Cohen, Y. Carbonization of electrospun poly (acrylonitrile) nanofibers containing multiwalled carbon nanotubes observed by transmission electron microscope with in situ heating. *J. Polym. Sci. Part B Polym. Phys.* **2010**, *48*, 2121–2128. [[CrossRef](#)]
4. Greil, P. Perspectives of nano-carbon based engineering materials. *Adv. Eng. Mater.* **2015**, *17*, 124–137. [[CrossRef](#)]
5. Nadiv, R.; Shachar, G.; Peretz-Damari, S.; Varenik, M.; Levy, I.; Buzaglo, M.; Ruse, E.; Regev, O. Performance of nano-carbon loaded polymer composites: Dimensionality matters. *Carbon* **2018**, *126*, 410–418. [[CrossRef](#)]
6. Liu, Y.; Kumar, S. Recent progress in fabrication, structure, and properties of carbon fibers. *Polym. Rev.* **2012**, *52*, 234–258. [[CrossRef](#)]
7. Inagaki, M.; Yang, Y.; Kang, F. Carbon nanofibers prepared via electrospinning. *Adv. Mater.* **2012**, *24*, 2547–2566. [[CrossRef](#)] [[PubMed](#)]
8. Liu, C.K.; Lai, K.; Liu, W.; Yao, M.; Sun, R.J. Preparation of carbon nanofibres through electrospinning and thermal treatment. *Polym. Int.* **2009**, *58*, 1341–1349. [[CrossRef](#)]
9. Nataraj, S.; Yang, K.; Aminabhavi, T. Polyacrylonitrile-based nanofibers—A state-of-the-art review. *Prog. Polym. Sci.* **2012**, *37*, 487–513. [[CrossRef](#)]
10. Ko, T.H.; Ting, H.Y.; Lin, C.H. Thermal stabilization of polyacrylonitrile fibers. *J. Appl. Polym. Sci.* **1988**, *35*, 631–640. [[CrossRef](#)]
11. Ali, A.B.; Dreyer, B.; Renz, F.; Tegenkamp, C.; Sindelar, R. Electrospun Polyacrylonitrile Based Carbon Nanofibers: The Role of Creep Stress towards Cyclization and Graphitization. *J. Mater. Sci. Eng.* **2018**, *7*, 1–8.
12. Cai, J.; Naraghi, M. Effect of templating graphitization on electrical conductivity of electrospun carbon nanofiber. In Proceedings of the 58th AIAA/ASCE/AHS/ASC Structures, Structural Dynamics, and Materials Conference, Grapevine, TX, USA, 9–13 January 2017; p. 0796.
13. Chawla, S.; Cai, J.; Naraghi, M. Mechanical tests on individual carbon nanofibers reveals the strong effect of graphitic alignment achieved via precursor hot-drawing. *Carbon* **2017**, *117*, 208–219. [[CrossRef](#)]
14. Vilatela, J.J.; Eder, D. Nanocarbon composites and hybrids in sustainability: A review. *ChemSusChem* **2012**, *5*, 456–478. [[CrossRef](#)] [[PubMed](#)]
15. Li, X.; Yang, Y.; Zhao, Y.; Lou, J.; Zhao, X.; Wang, R.; Liang, Q.; Huang, Z. Electrospinning fabrication and in situ mechanical investigation of individual graphene nanoribbon reinforced carbon nanofiber. *Carbon* **2017**, *114*, 717–723. [[CrossRef](#)]
16. Papkov, D.; Beese, A.M.; Goponenko, A.; Zou, Y.; Naraghi, M.; Espinosa, H.D.; Saha, B.; Schatz, G.C.; Moravsky, A.; Loutfy, R. Extraordinary improvement of the graphitic structure of continuous carbon nanofibers templated with double wall carbon nanotubes. *ACS Nano* **2012**, *7*, 126–142. [[CrossRef](#)]
17. Papkov, D.; Goponenko, A.; Compton, O.C.; An, Z.; Moravsky, A.; Li, X.Z.; Nguyen, S.T.; Dzenis, Y.A. Improved graphitic structure of continuous carbon nanofibers via graphene oxide templating. *Adv. Funct. Mater.* **2013**, *23*, 5763–5770. [[CrossRef](#)]
18. Ra, E.J.; An, K.H.; Kim, K.K.; Jeong, S.Y.; Lee, Y.H. Anisotropic electrical conductivity of MWCNT/PAN nanofiber paper. *Chem. Phys. Lett.* **2005**, *413*, 188–193. [[CrossRef](#)]
19. Burchell, T.D. *Carbon Materials for Advanced Technologies*; Elsevier: Oak Ridge, TN, USA, 1999.
20. Tiwari, A.; Syväjärvi, M. *Graphene Materials: Fundamentals and Emerging Applications*; John Wiley & Sons: Hoboken, NJ, USA, 2015.
21. Wu, X.; Mahalingam, S.; Amir, A.; Porwal, H.; Reece, M.J.; Naglieri, V.; Colombo, P.; Edirisinghe, M. Novel preparation, microstructure, and properties of polyacrylonitrile-based carbon nanofiber–graphene nanoplatelet materials. *ACS Omega* **2016**, *1*, 202–211. [[CrossRef](#)]
22. Reich, S.; Thomsen, C. Raman spectroscopy of graphite. *Philos. Trans. R. Soc. A* **2004**, *362*, 2271–2288. [[CrossRef](#)]
23. Merel, P.; Tabbal, M.; Chaker, M.; Moisa, S.; Margot, J. Direct evaluation of the sp³ content in diamond-like-carbon films by XPS. *Appl. Surf. Sci.* **1998**, *136*, 105–110. [[CrossRef](#)]
24. Ferrari, A.C.; Meyer, J.; Scardaci, V.; Casiraghi, C.; Lazzeri, M.; Mauri, F.; Piscanec, S.; Jiang, D.; Novoselov, K.; Roth, S. Raman spectrum of graphene and graphene layers. *Phys. Rev. Lett.* **2006**, *97*, 187401. [[CrossRef](#)]
25. Wu, G.; Lu, C.; Ling, L.; Hao, A.; He, F. Influence of tension on the oxidative stabilization process of polyacrylonitrile fibers. *J. Appl. Polym. Sci.* **2005**, *96*, 1029–1034. [[CrossRef](#)]

26. Harris, P.J. New perspectives on the structure of graphitic carbons. *Crit. Rev. Solid State Mater. Sci.* **2005**, *30*, 235–253. [[CrossRef](#)]
27. Harris, P.J.; Tsang, S.C. High-resolution electron microscopy studies of non-graphitizing carbons. *Philos. Mag. A* **1997**, *76*, 667–677. [[CrossRef](#)]
28. Rahaman, M.S.A.; Ismail, A.F.; Mustafa, A. A review of heat treatment on polyacrylonitrile fiber. *Polym. Degrad. Stab.* **2007**, *92*, 1421–1432. [[CrossRef](#)]
29. Sharma, S.; Kumar, C.S.; Korvink, J.G.; Kübel, C. Evolution of glassy carbon microstructure: In situ transmission electron microscopy of the pyrolysis process. *Sci. Rep.* **2018**, *8*, 16282. [[CrossRef](#)] [[PubMed](#)]
30. Pesin, L. Review Structure and properties of glass-like carbon. *J. Mater. Sci.* **2002**, *37*, 1–28. [[CrossRef](#)]
31. Ramos, A.; Cameán, I.; García, A.B. Graphitization thermal treatment of carbon nanofibers. *Carbon* **2013**, *59*, 2–32. [[CrossRef](#)]
32. Aprojanz, J.; Dreyer, B.; Wehr, M.; Wiegand, J.; Baringhaus, J.; Koch, J.; Renz, F.; Sindelar, R.; Tegenkamp, C. Highly anisotropic electric conductivity in PAN-based carbon nanofibers. *J. Phys. Condens. Matter* **2017**, *29*, 494002. [[CrossRef](#)]



© 2020 by the authors. Licensee MDPI, Basel, Switzerland. This article is an open access article distributed under the terms and conditions of the Creative Commons Attribution (CC BY) license (<http://creativecommons.org/licenses/by/4.0/>).

4.4 Synergistic effect of nanocarbon inclusion (CNTs) and creep assisted stabilization on 1) graphitization in PAN and 2) electrical transport in low dimensional carbon - Cumulative and independent effect of approach 1 and 2

4.4.1 Preface and Summary

In the 2nd and 3rd phase of the project, the effect of creep stress induced cyclization and carbonization and the effect of graphene platelet as nanocarbon reinforcement on the graphitic growth and electrical transport in PAN nanofibers was investigated. Up to this point, both the effect of creep stress (hot drawing assisted stabilization of PAN precursor) was explored, and findings showed that application of creep stress and nanocarbon inclusion (GNPs) improve the degree of graphitization of PAN. It was found that the degree of graphitization was influenced by both the factors and previous literature had also reported findings of nanocarbons doped templated graphitic structure in carbon fibers / carbon nanofibers. However, the basic research question of the limiting factor for electrical transport in carbon nanofibers remained unanswered.

Henceforth, in the last phase of project, the synergistic effect of both the nanocarbon doping and the application of creep stress was explored on 1) graphitic structure of PAN and 2) electrical transport in PAN based carbon nanofibers. Multi-walled carbon nanotubes (CNTs) were used as nanocarbon inclusion. Additionally, as CNTs are smaller in dimensions compared to graphene platelets, they were positioned inside a carbon nanofiber (100 - 300 nm). To holistically explore the electrical transport properties, the electrical transport properties of single carbon nanofiber/nanofilament were investigated for each case, i.e., 1) creep stress stabilized and 2) CNTs doped and their respective synergistic effects. Based on these findings from each case, the transport phenomena in carbon nanofibers were proposed. Presently, this is the only work as per author's knowledge that reported the electrical transport properties of single carbon nanofibers

and discussed in detail about the dictating factor in transport. The work has been recently published in Carbon – Elsevier (DOI: <https://doi.org/10.1016/j.carbon.2020.10.033>).

Nanofiber mats stabilized with creep stress applied during the cyclization process were denoted with suffix T (e.g., PAN - T and PAN/CNT - T) while the other stabilized without creep stress were denoted as PAN and PAN/CNT.

The findings revealed that doping of CNTs improve the degree of graphitization and crystalline structure of PAN as evidenced with decrease in I_D/I_G ratio, increase in L_a , L_c and sp^2 fraction and decrease in FWHM. Characterization of graphitic structure from TEM showed that doping of CNTs to PAN for non-creep stress cyclized samples resulted in avoiding the formation of curved carbon planes and random orientation of graphene layers. The pristine PAN showed nearly no preferable alignment of graphene layers and curled graphene planes were observed. However, for the PAN cyclized with creep stress (PAN - T), highly aligned graphitic domains were observed. For PAN/CNTs stabilized with creep stress (PAN/CNTs - T), the graphene layers lost the preferential alignment along the fiber axis. Electrical transport probed via 4PP STM/SEM on fiber mats showed an increased anisotropy for samples cyclized with creep stress. Measurement on the isolated single nanofibers showed that CNTs doping to PAN decreases the resistivity of PAN for non-creep cyclized systems. The resistivity was further reduced for creep stress cyclized PAN (PAN - T), however for CNTs doped samples with creep stress (PAN/CNT - T), the resistivity showed an increased value compared to PAN - T. Our findings disclosed that the transport properties in 1D CNF structures were strongly dependent on the size, interaction, and alignment of the local graphitic domains (sp^2 - sp^2 cluster). The structural and electronic properties of PAN-based CNFs can be tuned by the addition of CNTs and the application of creep stress. However, the addition of other nanostructures feedback to the structure and influence mutually hopping and band mobilities. The electrical transport properties of these 1D nanostructures could be understood as a cumulative effect of electron hopping and band-based transport

along different crystalline and sub crystalline units along the surface. The electron path along the surface was hindered with disruption in graphene planes alignment.

The author performed all the fabrication work for PAN and PAN/CNT nanofiber mats and single nanofiber isolation. Moreover, the conceptualization of the research-theme was performed by the author himself. XRD, Raman, FTIR and SEM analysis was also conducted by the author himself. XPS experiments were conducted by JULIAN KOCHER from the solid-state physics department, LUH. TEM was conducted by ANJA SCHLOSSER. However, the investigations and analysis on TEM were made by the author. The 4pp STM/SEM measurements were carried out by DAINA SLAWIG. All the analysis and results were analyzed by the author together with DR. FRANZ RENZ, DR. CHRISTOPH TEGENKAMP and DR. RALF SINDELAR.

The author wrote the manuscript on his own and it was edited and reviewed by the DR. FRANZ RENZ, DR. CHRISTOPH TEGENKAMP and DR. RALF SINDELAR.



Contents lists available at ScienceDirect

Carbon

journal homepage: www.elsevier.com/locate/carbon

Research Article

Polyacrylonitrile (PAN) based electrospun carbon nanofibers (ECNFs): Probing the synergistic effects of creep assisted stabilization and CNTs addition on graphitization and low dimensional electrical transport



A.B. Ali ^{a, b, c, *}, D. Slawig ^{b, e}, A. Schlosser ^{b, f}, J. Koch ^d, N.C. Bigall ^{b, f}, F. Renz ^{a, b}, C. Tegenkamp ^{b, d, e}, R. Sindelar ^{b, c}

^a Institut für Anorganische Chemie, Leibniz Universität Hannover, Callinstr. 7, 30167, Hannover, Germany

^b Laboratorium für Nano und Quantenengineering (LNQE), Leibniz Universität Hannover, Schneiderberg 39, 30167, Hannover, Germany

^c University of Applied Sciences and Arts, Faculty II, Hochschule Hannover, Ricklinger Stadtweg 120, 30459, Hannover, Germany

^d Institut für Festkörperphysik, Leibniz Universität Hannover, Appelstraße 2, 30167, Hannover, Germany

^e Institut für Physik, Technische Universität Chemnitz, Reichenhainer Str. 70, 09126, Chemnitz, Germany

^f Institut für Physikalische Chemie und Elektrochemie, Leibniz Universität Hannover, Callinstr. 3A, 30167, Hannover, Germany

ARTICLE INFO

Article history:

Received 28 July 2020

Received in revised form

5 October 2020

Accepted 6 October 2020

Available online 9 October 2020

Keywords:

Aligned graphitic domains

Anisotropic conductivity

Creep stress assisted cyclization

Carbon nanofibers

Graphitization

ABSTRACT

We report on the fabrication of Polyacrylonitrile (PAN) based electrospun carbon nanofiber (ECNF) reinforced with multi-walled carbon nanotubes (MWCNTs) and characterization of the graphitic structure as well as electrical transport properties for four different ECNF systems. The different systems were obtained by the combination of two different ways of cyclization for pristine PAN and PAN with CNTs addition (PAN/CNT), typically by the application of constant creep stress and a constraint fixing. The addition of CNTs improved the graphitic structure of PAN. For the detailed analysis of different systems, carbonization was performed at 1700 °C and the graphitic structures were characterized. The CNTs improve the alignment of graphitic domains even for non-creep cyclized systems. The application of creep stress during cyclization results in highly aligned graphene planes. However, the creep stress cyclized PAN/CNT system exhibited a reduction in the alignment of graphene planes coming along with the observation of discontinuous, randomly orientated domains and a reduced conductivity. The electrical anisotropy increased for creep cyclized PAN and PAN/CNT compared to non-creep stress cyclized system. Our findings reveal that electrical transport in carbon nanofibers need to be considered as a cumulative effect of hopping and band transport along chemically and structurally inhomogeneous ECNFs.

© 2020 Elsevier Ltd. All rights reserved.

1. Introduction

Carbon nanomaterials have been synthesized and exploited in a wide range of applications due to their versatile properties. Nanostructured carbon materials exist in different allotropic forms, e.g. 0 dimensional (0D) fullerenes such as C60, 1D carbon nanotubes

(CNTs) and carbon nanofibers (CNFs), 2D graphene nano-sheets, etc. Each specific allotrope provide a unique shape, dimension, structure and characteristic properties. These various allotropes and combinations of them are currently used as building blocks to synthesize new hybrid materials with unique properties [1–4]. Thereby, not only the coupling between the allotropes is important, but also the distribution within the composite material, in particular, if the transport properties are of interest. This is even more severe for low dimensional systems, like the functionalized CNFs of this study.

Among low dimensional carbon nanostructures, 1D carbon nanofibers (CNF) are prominent candidates due to their simple fabrication, low densities accompanied with a high temperature tolerance, chemical stability, mechanical integrity and comparably

Abbreviations: PAN, Polyacrylonitrile; ECNF, Electrospun Carbon nanofiber; CNT, Carbon nanotube; FTIR, Fourier transform infra-red spectroscopy; XRD, X-ray diffraction; SEM, Scanning electron microscopy; STM, Scanning tunneling microscopy; TEM, Transmission electron microscopy; RCI, Ring cyclization index; FWH, Full width at half maxima; 4pp, Four-point probe.

* Corresponding author. University of Applied Sciences and Arts, Faculty II, Hochschule Hannover, Ricklinger Stadtweg 120, 30459, Hannover, Germany.

E-mail address: annas.bin.ali@acd.uni-hannover.de (A.B. Ali).

<https://doi.org/10.1016/j.carbon.2020.10.033>

0008-6223/© 2020 Elsevier Ltd. All rights reserved.

high electrical conductivity [5,6]. The carbon fiber market is expected to reach ~3.7 billion \$ by 2025, which reflects the high expectations of applications. Since 1980s, extensive research has been done setting up a scalable production of micron-sized carbon fibers. While different methods have been employed over decades to fabricate CNFs, carbonization of polyacrylonitrile (PAN) is the most recognized and facile method. Among other contemporary precursor materials such as pitch, rayon and lignin, PAN is the most used material owing to its high yield and comparatively better graphitic structure after the high temperature carbonization process [7,8]. By electrospinning of the polymer solution and control of the process parameters, fibers of various micron and sub-micron diameters can be produced, subsequently followed by a stabilization in air and the carbonization in inert atmosphere at high temperatures.

Thereby, achieving a better graphitic structure is the key point for improving the properties of CNFs in order to be used in different applications such as micro-electro-mechanical or nano-electronic devices. Indeed, graphitization at higher temperatures is desirable to achieve an improved graphitic structure, however, even at high temperatures (<2400 °C), the formation of highly aligned graphitic domains is limited by the formation of so-called graphitic loops and disorder within the carbon planes, based on the structure of the polymer precursor material [9,10]. For this reason, the controlled addition of carbon-based nanostructures, graphene, nano-ribbons or graphene platelets to CNFs is a promising approach for further improving the structure. It is known that introduction of small portions with these nanocarbons to polyacrylonitrile results in the formation of graphitic domains, already at much lower temperatures [11–19]. In particular, the addition of CNTs to PAN assists the conversion into a highly ordered ladder structure, lesser polymer chain terminations and the formation of extended interphase structures in the vicinity of the CNTs. Studies have shown that CNTs help to reduce the entropic and reaction shrinkage in the PAN films during the stabilization both in inert and oxidative environments [11,20,21]. The stabilization process is the most critical step in the carbon fiber production cycle, i.e. cyclization, dehydrogenation as well as cross linkage. This process serves as a basis for growth of ribbon like graphite structure later in the carbonization process. The entropic shrinkage during the oxidative stabilization process comes along with the relaxation of the PAN molecular orientation which deteriorates the formation of aligned graphitic domains during carbonization [22,23]. Hence, as a approach to achieve a highly graphitic structure, the application of tension is imperative during the stabilization which results in an increased alignment of graphitic domains and in turn improved mechanical and electrical properties.

In this work, adding CNTs as a templating agent and application of constant creep stress throughout the whole stabilization process has been explored. Moreover, the effect on the graphitic structure and electrical transport properties of bundles/assemblies as well as of isolated single carbon nanofibers (~100–200 nm in diameter) are investigated. First, the PAN nanofibers and PAN nanofibers reinforced with CNTs (PAN/CNT) were electrospun and were stabilized without an external creep stress (only shrinkage stress) and subsequently carbonized at different temperatures to examine the graphitization of CNTs templated structure in comparison to pristine ECNFs. Second, the pristine PAN and PAN/CNT nanofibers were stabilized with creep stress and carbonized at 1700 °C in order to observe the combined effect of CNTs templated structure and creep stress on the PAN graphitic structure. The chemical and structural properties on the atomic scale were investigated by IR, SEM, XRD, Raman, XPS and TEM. In the last part, the electrical transport properties of pristine PAN and PAN/CNT systems as well as single fibers, cyclized with and without creep stress, were studied. The

conceptual insight addresses the synergistic effect of CNT addition and creep stress assisted stabilization on PAN graphitic structure how this affects the electrical transport properties of single nanofibers.

2. Material & methods

2.1. Materials

Polyacrylonitrile (PAN, average molecular weight 150,000 M_w) was purchased from Sigma Aldrich. Dimethylformamide (DMF) was used as solvent for dissolving PAN as received by Carl Roth. The multi walled carbon nanotubes (MWCNTs) were obtained from ABCR GmbH. A mixture of 2% H_2 /98% Ar supplied by Westfalen AG was used for carbonization process.

2.2. Fabrication of ECNF and CNTs reinforced ECNF assemblies

A three stage process, comprised of electrospinning, stabilization in air and high temperature carbonization in reducing atmosphere, was used to fabricate pristine carbon nanofibers and CNT added carbon nanofibers.

The fabrication process is schematically shown in Fig. 1. First, PAN was dissolved in DMF by 16 wt% (1.8 g in 10 ml DMF) and then stirred over night for a period of 12 h to obtain a homogeneous solution. About 1 wt% of CNTs were added w.r.t to the whole mixture PAN/CNT/DMF (hence the total solute composition in spinning solution is: PAN/CNT ~ 94.0/6.0 wt %) and ultrasonicated for 1 h with 15 min intervals and dwell time for the dissipation of heat. Subsequently, the PAN was added stepwise to the solution and stirring was done for 12 h. Both solutions, PAN-DMF and PAN/CNT-DMF were electrospun at 17 kV, 1 ml/h and 10 m/s collector speed while the fibers were collected on an aluminum foil. In the second step, the stabilization was performed (250 °C for 10 h) on pristine PAN mats and PAN/CNT bundles in two different ways. For one set of samples, the ends of as spun nanofiber mats were clamped during the cyclization process to avoid the free relaxation of PAN, hence the only stress is the inherent shrinkage stress. These samples were carbonized at various temperatures (1000 °C, 1200 °C, 1500 °C, and 1700 °C) for studying the effect of addition of CNTs to PAN. The second set of nanofiber mats were clamped and constant creep stress was applied for the entire duration of stabilization (10 h). These nanofiber mats were carbonized at 1700 °C. The graphitic structure and electrical transport properties were then compared with non-creep stress stabilized PAN samples. Nanofiber mats cyclized with creep stress applied during the cyclization process were denoted with suffix T (e.g. PAN - T and PAN/CNT - T).

2.3. Characterizations

Diffraction patterns (Bruker D2 Phaser) were recorded from 10° to 80° with a step size of 0.03° using Cu- K_{α} photons ($\lambda = 1.5406 \text{ \AA}$) to analyze structural details of carbonized pristine and modified nanofibers. The interlayer spacing, $d_{(002)}$ was calculated using Bragg law, $d = (\lambda/2 \sin\theta)$, where θ is the Bragg angle. The crystallite sizes were estimated using the Scherrer equation, $L_c = (K \lambda/\beta \cos\theta)$, where K is the shape factor (0.89 for L_c) and β is the full width at half maximum (FWHM). Raman spectroscopy (DXR2, Thermo Fisher) was used to obtain information about graphitic structure and disorder in the nanofiber mats. Raman spectra were recorded using a laser wavelength of 532 nm as an excitation source in the range of 1000–3000 cm^{-1} with an incident laser power of 1 mW. Five spectra were recorded on different samples. The D- and G-bands in the spectra were deconvoluted using

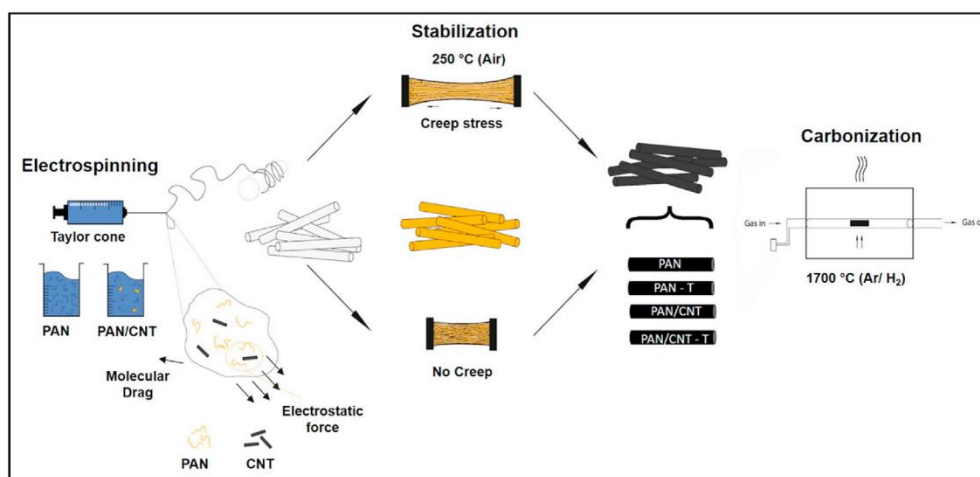


Fig. 1. Schematic illustration of complete carbon nanofiber (PAN, PAN/CNT) fabrication process.

Lorentz fitting via Origin lab pro and I_D and I_G , the integral ratios of respective D- and G-band were calculated. Moreover, the crystal size L_a (apparent crystallite size along the basal plane) of carbon nanostructures were calculated via L_a (nm) = $(2.4 \times 10^{-10}) \lambda^4_{laser} (I_D/I_G)^{-1}$ [24]. Polarization Raman was performed to characterize the orientation of graphene planes in ECNFs, by polarizing the laser parallel and perpendicular to nanofiber axis. Fourier transform infrared spectroscopy (Perkin Spectrum Two) was used to monitor the structural changes in PAN fibers during stabilization stage via a spectrometer operating in the wavenumber regime of 500–4000 cm^{-1} . The ring cyclization index (RCI) was calculated in order to estimate the amount of the crosslink ladder polymer conversion by measuring the integral intensity of absorbed IR, $\text{C}\equiv\text{N}$ (2240 cm^{-1}) and $\text{C}=\text{N}$ (1600 cm^{-1}) peaks ($\text{RCI} = \frac{I_{\text{C}=\text{N}}}{I_{\text{C}\equiv\text{N}} + I_{\text{C}=\text{N}}}$). X ray photoelectron spectroscopy (XPS, SPECS) experiments were performed using an Al K_{α} emission source and recorded with Phoibos 100 spectrometer equipped with an MCD-5 detector at a pass energy of 20 eV. The C1s spectra were fitted using symmetric Gaussian-Lorentzian sum functions including the Shirley background, under a limitation that the energy difference between the sp^2 - and the sp^3 -peak is 0.8 eV [25]. Scanning electron microscopy (SEM, Zeiss LEO 1455VP) was done to analyze the morphology of as spun and carbonized nanofiber mats using acceleration voltage of 15 kV and emission current of 1 nA. Transmission electron microscopy (TEM, FEI Tecnai G2 F20) imaging was carried out using field emission gun operating at 200 kV acceleration voltage in bright field mode. The TEM samples were prepared by ultrasonically small pieces of the fiber mats in 500 μl of ethanol for 15 min. Subsequently, the majority of the solvent was removed in an air flow and 10 μl of the concentrated ethanol solution containing the fibers was drop-casted onto a carbon coated copper grid (Quantifoil, 300 mesh). Electrical transport measurements were performed using a 4-tip scanning tunneling/scanning electron microscope (STM/SEM, Omicron) operating under ultrahigh vacuum conditions [26]. The independent operation of the tips allows probing local electrical characterization down to nanoscale. The SEM enables the precise navigation and positioning of the electrochemically etched W tips with typical apex radii of 20–70 nm. Both fiber mats/assemblies and single nanofibers deposited on SiO_2 samples were investigated.

3. Results and discussions

3.1. Nanofiber morphology

Fig. 2a-c shows the morphology of as spun and carbonized PAN nanofibers and PAN/CNT nanofibers with histograms of their diameter distributions. In general, the as spun PAN nanofibers and PAN/CNT nanofiber appear quite homogenous. However, a rare formation of beads/spindles were observed for PAN/CNT samples, which suggests that the addition of CNTs have reduced the viscosity of the solution as also perceived during the electrospinning process. The slight reduction in the mean diameters of as spun PAN/CNT nanofibers (~311 nm) as compared to pristine PAN nanofibers (~390 nm) is attributed to the enhanced conductivity of the polymer solution due to the presence of CNTs [27]. Additionally, it was found that the carbonization at 1700 °C causes reduction in diameter of the fibers, ascribed to the evaporation of volatile species during the stabilization and carbonization process. Carbon yield calculated for carbonized samples decreases as the temperature is increased (Table S1). The PAN/CNTs carbonized at 1700 °C showed carbon yield of ~46% while pristine PAN showed reduced value, ~39%, furthermore, an average percentage size reduction (% SR) of 47% was observed for pristine PAN compared to 20% for PAN/CNT (Fig. 2c). This suggests that the admixture of CNTs is apparently improving the thermal stability of PAN nanofibers. The PAN chains interacting with CNTs are not free to shrink as CNTs anchor the polymer chains during the shrinkage in cyclization and carbonization process. This reduced shrinkage of PAN/CNT nanofibers indicates the reasonable interaction of CNTs with PAN.

3.2. Structure and chemical composition of as spun and cyclized nanofibers

Characteristic IR spectra of as spun PAN and PAN/CNT nanofibers are shown in Fig. 3a. For both as spun nanofibers, a band is observed at $\sim 2240 \text{ cm}^{-1}$, which is characteristic for PAN, indicating the presence of a nitrile group ($-\text{C}\equiv\text{N}$). The band at 2938 cm^{-1} corresponds to symmetric CH_2 stretch modes, while in the low wavenumber regime (1000 - 1500 cm^{-1}) various bands can be attributed to C–C, C–O, C–N and C–H bonds. For the PAN/CNT, the

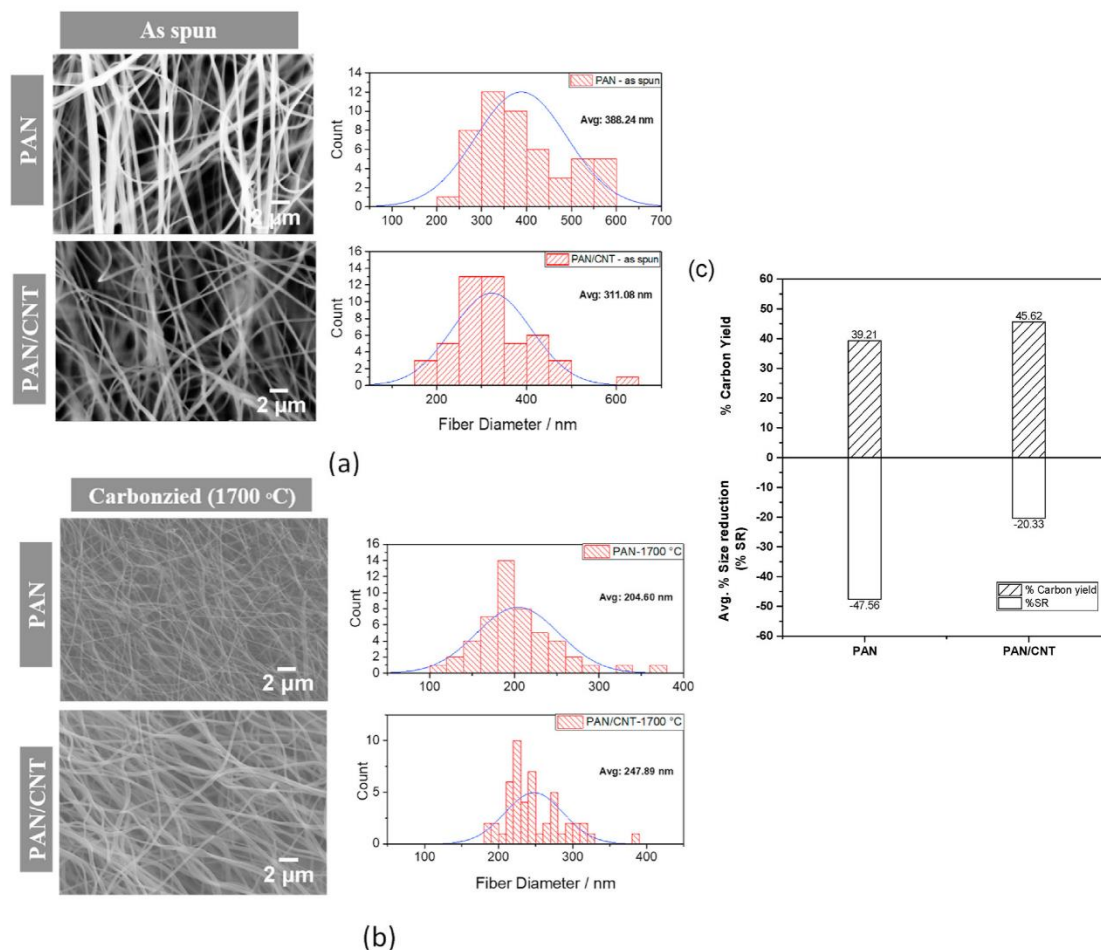


Fig. 2. SEM images and histogram of diameter distribution for (a) as spun and (b) carbonized (1700 °C) pristine PAN nanofibers and PAN/CNT nanofibers. (c) Percentage size reduction and carbon yield for carbonized (1700 °C) PAN and PAN/CNT nanofiber.

intensity line at 1730 cm^{-1} (C=O stretch) is decreased while a sharp increase in intensity is observed for the mode at 1660 cm^{-1} (C=C stretch), which is most likely due to the interaction of the CNT with the C=O backbone structure. Raman spectroscopy was also performed on as spun PAN and PAN/CNT nanofiber mats (Fig. 3b). A sharp peak at Raman shift of 2252 cm^{-1} is observed corresponding to nitrile group, which is also found for PAN/CNT at 2251 cm^{-1} . The additional peaks in PAN/CNT at Raman shift of 1363 cm^{-1} , 1592 cm^{-1} and 2710 cm^{-1} correspond to the characteristic D-, G- and 2D-bands, respectively, showing the presence of CNTs in nanofiber mats. After cyclization, an evolution of the band at 1590 cm^{-1} takes place corresponding to a C=N mode, while the nitrile group intensity at 2243 cm^{-1} is strongly reduced as measured by IR absorption spectroscopy (Fig. 3c). The presence of a band at 1590 cm^{-1} is due to the formation of a ladder structure that enables PAN to withstand the high temperature carbonization process without fusion. Similarly, the appearance of a sharp band at 807 cm^{-1} (C=C=H) is found, indicating that

dehydrogenation has also taken place. The ring cyclization index (RCI) showed a value of ~94% for PAN and PAN/CNT nanofiber. PAN and PAN/CNT composites cyclized with creep stress demonstrated very similar values for the degree of cyclization. We showed in a previous study, that the utilization of creep stress during the cyclization process at lower temperatures for a shorter time promotes effectively the cyclization of nitrile groups, which in turn increases the RCI. However, at higher temperatures (230 °C) for a longer duration of 10 h, the RCI showed nearly no difference for creep stressed and non-creep stressed PAN nanofibers [28].

3.3. Carbonization: graphitic structure of pristine PAN and PAN/CNT nanofibers

Typical Raman spectra of PAN and PAN/CNT nanofiber mats carbonized at 1000 °C are shown in Fig. 4a. The main bands, i.e. the D- ($\sim 1340\text{--}1400\text{ cm}^{-1}$) and G-band ($\sim 1560\text{--}1600\text{ cm}^{-1}$), are ascribed to defects in graphitic structure and graphitic carbon

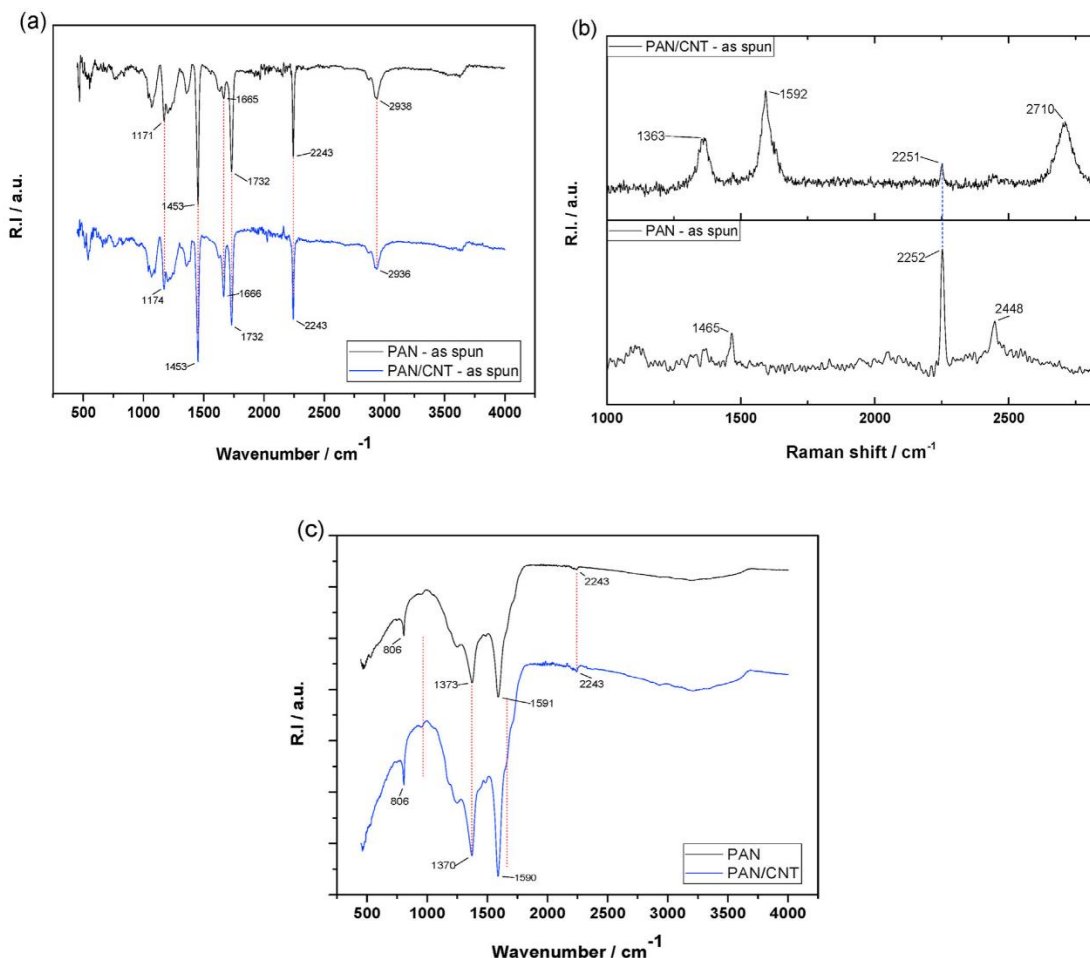


Fig. 3. (a) IR spectra for as-spun PAN and PAN/CNT nanofibers. (b) Raman spectra for as spun PAN and PAN/CNT nanofibers. (c) IR spectra for cyclized PAN and PAN/CNT nanofibers at 250 °C for 10 h in air. (A colour version of this figure can be viewed online.)

nanocrystallites. Both the D- and G-bands are first order Raman bands for carbon materials. A broad band around ($\sim 1521 - 1550 \text{ cm}^{-1}$) is also observed which is attributed to amorphous carbon, and presence of hetero-atoms as impurities in the carbon lattice. The R value, i.e., the I_D/I_G intensity, depends on the concentration of defects in the carbon system, including grain boundaries, edges as well as the degree of graphitization, and can be used to quantify the crystal structure of carbon materials [24]. In general, it is found that with increase in the carbonization temperature, the R value is decreased for pristine PAN and PAN/CNT from ~ 3.2 to 1.5, which suggests that the portion of amorphous carbon is reduced at the expense of an increased crystallinity (Fig. 4b). Furthermore, for all temperatures investigated here, the I_D/I_G is lower for PAN/CNT fibers, i.e. the crystallinity in the fibers can be increased by the admixture of CNTs. The L_a (domain crystal size along basal plane) is increased with the rise in carbonization temperature (Fig. 4c), L_a is increased by $\sim 45\%$ from 1000 °C to 1700 °C for PAN nanofibers. Similarly, for the CNT templated

systems, the L_a increased as compared to the pristine PAN system at all temperatures. The FWHM value for G-band is decreased with increasing temperature and addition of CNTs, which suggests growth of carbon nanocrystallites takes place (Fig. 4d). The stacking size of crystal planes (L_c) and FWHM of (002) reflection of carbon crystal as evaluated from XRD data shows that the FWHM₀₀₂ is decreased and L_c is increased for PAN/CNT as compared to pristine PAN systems (Table 1).

Furthermore, XPS was performed on PAN and PAN/CNT fiber mats carbonized at 1000 °C and 1700 °C to quantify the ratio of sp^2/sp^3 hybridized carbon. Typical C1s XPS spectra for PAN carbonized at 1000 °C and 1700 °C are shown in Fig. 5. Carbonization at 1700 °C leads to fiber mats consisting $\sim 99\%$ of Carbon and the non-carbon elements present at 1000 °C are completely removed (Fig. S1). The C1s-spectra are deconvoluted considering 3 major contributions, namely the shake-up emission at 290.7 eV, sp^2 hybridized carbon atoms at 284.4 eV and sp^3 hybridized carbon at 285.2 eV. From this the sp^2 fraction and sp^2/sp^3 ratio are evaluated and are

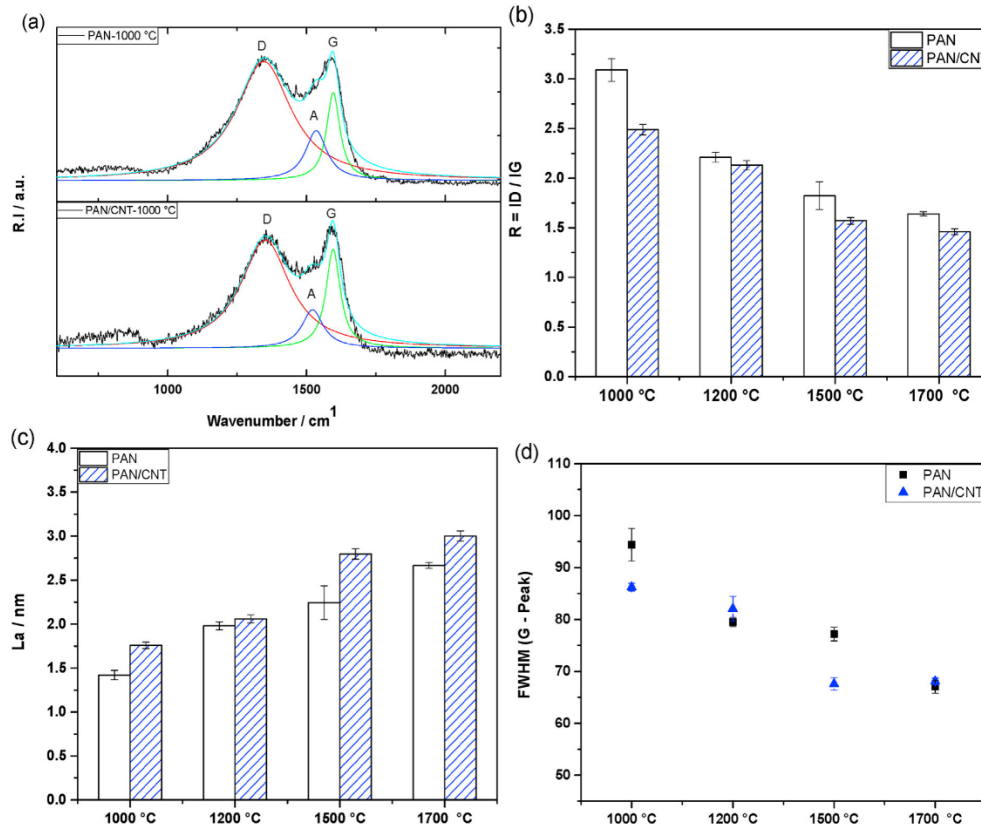


Fig. 4. (a) Typical Raman spectra for PAN and PAN/CNT carbonized at 1000 °C. (b) R (ID/IG), (c) La and (d) FWHM-G PAN and PAN/CNT nanofibers at various carbonization temperatures. (A colour version of this figure can be viewed online.)

shown in Table 2. The sp^2 fraction of PAN increased from 54% to 58% at 1000 °C while from 61% to 63% at 1700 °C upon addition of CNTs. The amount of sp^2 hybridized carbon increases and the portion of amorphous carbon is reduced. In general, the reduced sp^2 fraction even at 1700 °C is related to the inherent PAN structure and formation of thermodynamically stable penta-hepta-rings and fullerene fragments during stabilization which results in lack of oriented graphenic clusters as observed for pyrolytic graphite (discussed in next section). The XPS results support the finding from Raman and XRD, where the I_D/I_G ratio and FWHM-G peak

Table 1
The average crystallite size ' L_c ' and 'FWHM (002)' for PAN and PAN/CNT fibers carbonized at different temperatures, as calculated from X-ray diffractograms.

Sample	L_c (nm)	FWHM (002)
PAN - 1000 °C	1.38	5.82
PAN - 1200 °C	1.96	5.01
PAN - 1500 °C	2.01	4.65
PAN - 1700 °C	2.03	3.98
PAN/CNT - 1000 °C	1.54	5.20
PAN/CNT - 1200 °C	2.03	3.88
PAN/CNT - 1500 °C	1.98	3.96
PAN/CNT - 1700 °C	2.24	3.58
PAN - 1700 °C - T	2.07	3.88
PAN/CNT - 1700 °C - T	2.34	3.43

showed that the ordering of carbon crystallite takes place and graphitic crystal grows as observed from L_c and L_a values. It is worth mentioning here that, since the information depth of Raman are comparable to the diameter of ECNFs, the finding of an increased crystallinity and graphitization from Raman reflect mainly the core of nanofibers. Contrary to this, XPS is more a surface sensitive with a mean free path length of nearly 10 monolayers. Hence, the complementary findings from the surface and the core of nanofiber for samples carbonized at 1700 °C, show a graphitic homogeneity of PAN and PAN/CNT nanofiber mats throughout the whole nanostructure.

The above findings suggest that the addition of CNTs promote the graphitization of PAN nanofibers. Studies have shown that CNTs help in the formation of graphite in glassy carbon due to the confinement of matrix in the vicinity of CNTs [16,29], also the induction of stress during graphitization in the surrounding matrix by nanocarbon inclusions such as CNTs has been reported [30]. Due to intrinsic high thermal conductivity of CNTs, they enhance the thermal conductivity of the polymer matrix, which possibly could act as nucleation sites for formation of graphitic crystal.

3.3.1. Effect of creep and CNTs addition to graphitic structure of PAN

To compare the effect of creep stress, the carbonization of creep stress cyclized nanofibers (PAN -T and PAN/CNT - T) was performed

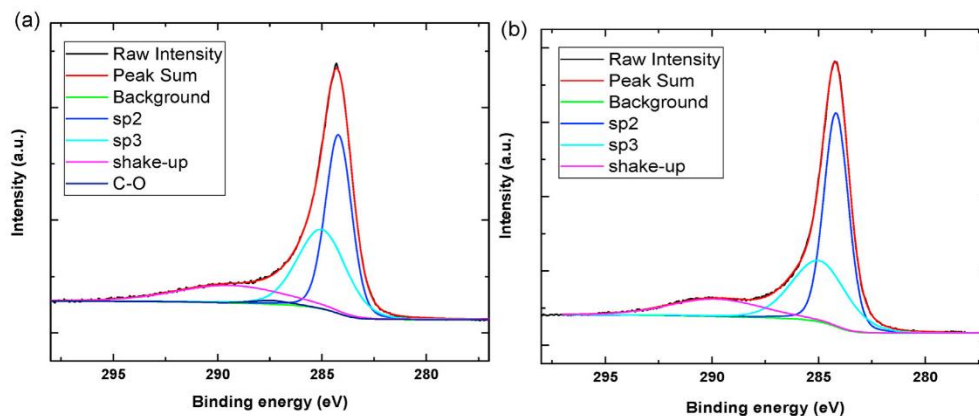


Fig. 5. Typical XPS spectra of de-convoluted C1s peak for pristine PAN at (a) 1000 °C and (b) at 1700 °C. (A colour version of this figure can be viewed online.)

Table 2

sp² fraction and sp²/sp³ ratio for PAN and PAN/CNT fibers carbonized at 1000 °C and 1700 °C, as evaluated from de-convolution of C1s spectra of XPS.

Sample	sp ² /sp ³ ratio	sp ² fraction
PAN - 1000 °C	1.22	54.8%
PAN/CNT - 1000 °C	1.50	58.6%
PAN - 1700 °C	1.57	61.89%
PAN/CNT - 1700 °C	1.78	63.95%

at 1700 °C and the structural characterizations of these samples were compared to non-creep stress samples (PAN and PAN/CNT). It can be seen that the I_D/I_G ratio is further decreased and, concomitantly, L_a is increased for creep stress stabilized PAN and PAN/CNT nanofibers (Fig. 6a). For samples cyclized with creep stress (PAN - T and PAN/CNT - T), an evolution of a more dominant symmetrical peak for second order 2D-band ($\sim 2662\text{--}2686\text{ cm}^{-1}$) is observed [Fig. 6 (b, c)]. The 2D band is not a defect induced band as the D-band, rather is active due to a phonon double resonance mechanism [24]. The FWHM of 2D peak is reduced for PAN/T and PAN/CNT - T ($\sim 196\text{ cm}^{-1}$) as compared to PAN and PAN/CNT ($\sim 380\text{ cm}^{-1}$), which hints towards the formation of nanocrystalline graphite. Moreover, for the G-band a gradual red shift is observed (Fig. 6d), reaching almost the value reported for the G-band of crystalline graphite ($\sim 1580\text{ cm}^{-1}$) [31]. However, for PAN/CNT - T, the G-band revealed a pronounced asymmetry. The G-band peak splits into two sub-bands namely G⁻ at 1577 cm^{-1} and G⁺ at 1604 cm^{-1} (Fig. 6e). For instance, this splitting of G peak in two sub-band is observed for CNTs and graphene as a result of curvature and electron confinement. It has been reported that, the pure curvature splits the graphene E_{2g} mode in a component one parallel and one perpendicular to the applied strain [32,33]. Also with increasing strain, the splitting of G band is reported to increase for graphene and carbon fibers. No splitting of G peak was observed for PAN/CNT and PAN - T, hence this can be attributed to an increased strain and curvature in CNTs embedded into a creep stress cyclized PAN matrix [34].

To reveal an atomistic insight regarding the alignment of carbon planes, TEM was performed both on creep stress stabilized (PAN and PAN/CNT) and non-creep stress stabilized (PAN and PAN/CNT) nanofibers, carbonized at 1700 °C. It can be seen that the graphitic domains for non-creep stress stabilized (PAN - 1700 °C) reveal no preferred alignment and the graphene layers are majorly curved resembling fragments of fullerene related structures

(Fig. 7a). More apparent in the skeletonized image (Fig. 7b), the curvature in carbon planes and ripples of graphene like layers are observed. Compared to PAN, the graphitic domains in PAN/CNT are comparatively well aligned and no ring like fullerene segmented motifs were observed [Fig. 7 (c, d)]. For creep stress stabilized PAN (PAN - T), the size of graphitic zone increases, they are highly aligned along the nanofiber axis [Fig. 7 (e, f)]. The tortuosity in graphene layers is prevented by the application of creep stress during the stabilization process and rather more continuous domains are observed. However, for PAN/CNT - T, the graphitic domains appear to be slightly fragmented/discontinuous and their alignment is reduced compared to PAN/CNT and PAN - T [Fig. 7 (g, h)]. The directional analysis and distribution of orientation is also performed on TEM images to have additional insight, using Orientation J plug-in of Image J software (Fig. S2) [35]. To further have a holistic insight of orientation of graphene planes, the polarized Raman was performed with polarization of incident light parallel and perpendicular to fiber axis. The G-band is sensitive to the laser polarization, hence by evaluating the difference in intensity of G-band for both cases, the orientation is evaluated. The results from polarized Raman supported the TEM findings, the factor ' $I_G // I'_{\perp}$ ' (intensity ratio of G-band obtained for polarization of laser parallel and perpendicular to fiber axis) showed increased values specifically for PAN - T and PAN/CNT samples, indicating improved alignment of graphitic domains (Fig. S3).

In a constrained system, where an external force against the entropic shrinkage is not present, the alignment of polymer chain is reduced during the oxidative stabilization process. The ladder structure of PAN tends to loose N groups and the formation of thermodynamically stable penta- and hepta-rings takes place along with hexagonal rings [36]. These defects, named as 'Stone Wales defects' in graphene [37], tend to impart bending and curvature to the carbon planes unless not balanced by the application of external stress that prevents the bending/curling of graphene layers and formation of cage like geometries typically observed for glassy carbons [38–40]. The improved alignment of graphene layers in PAN - T is attributed to the applied creep stress during the process. For the PAN/CNT system, although no creep stress is present but still the presence of CNTs act as anchoring centers for holding the polymer chains, the effect of entropic shrinkage is reduced. This results in evading the loss of chain alignment and later tortuosity in graphene planes during the carbonization process. Apparently, slightly reduced alignment of PAN/CNT - T

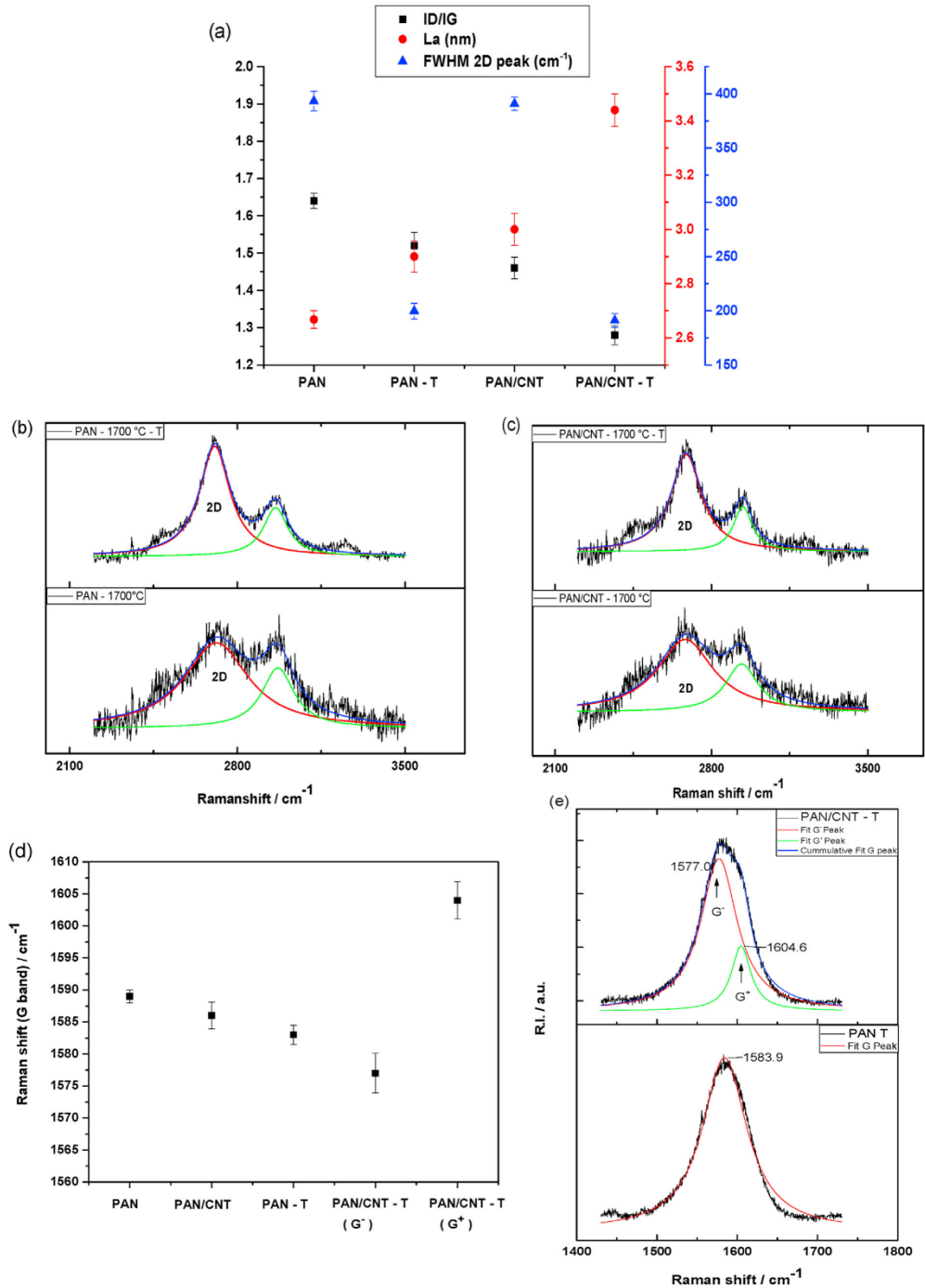


Fig. 6. (a) I_D/I_G , L_a and FWHM of 2D-peak evaluated from Raman spectra of respective samples. 2D-band typical spectra for creep stress stabilized and non-creep stress stabilized (b) PAN and (c) PAN/CNT nanofibers after carbonization at 1700 °C. (d) Raman shift of G-band for respective samples. (e) G-band peak fitting for PAN - T and PAN/CNT - T. (A colour version of this figure can be viewed online.)

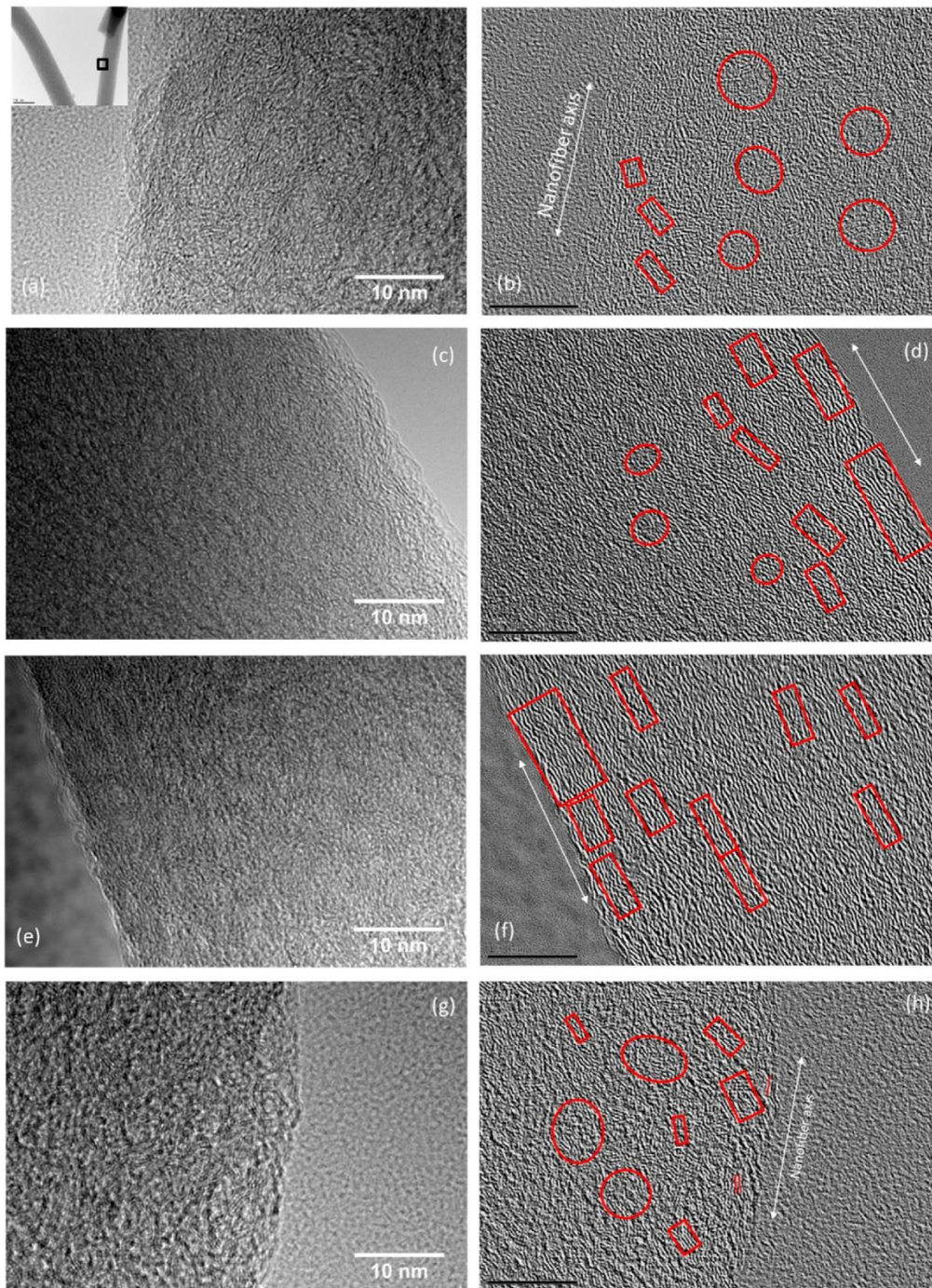


Fig. 7. HR-TEM images: (a) PAN - 1700 °C, (c) PAN/CNT - 1700 °C, (e) PAN - 1700 °C, (g) PAN/CNT - 1700 °C - T and (b, d, f, h) are corresponding skeletonized processed images of (a, c, e, g). The marked rectangular areas highlights the aligned domains while the circles highlight areas of randomly oriented graphitic domains. (A colour version of this figure can be viewed online.)

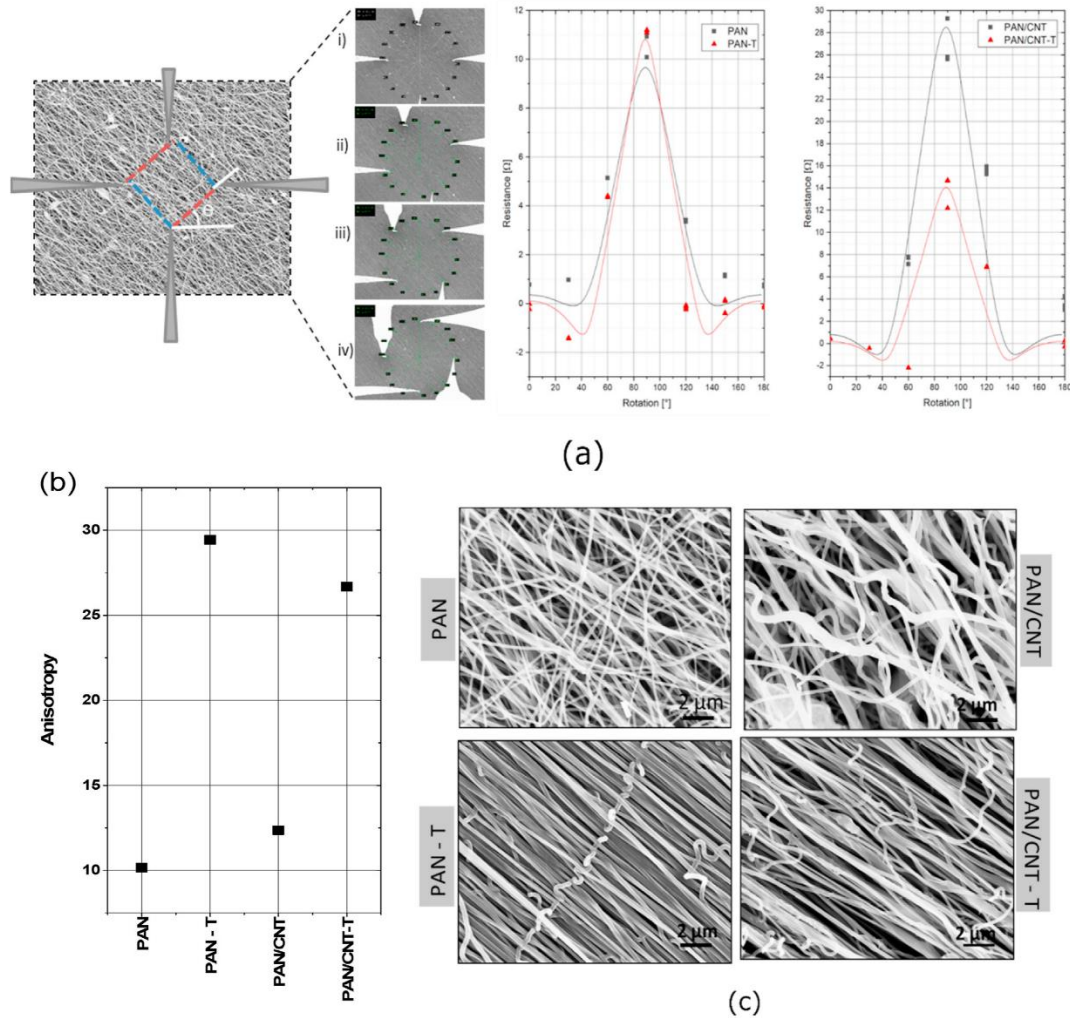


Fig. 8. (a) Resistance measured as function of rotation angle and (b) Anisotropy for four different nanofiber mats (PAN, PAN/CNT, PAN - T, PAN/CNT - T) using a 4Pp STM/SEM system. (c) SEM images for creep stress (T) and non-creep stress stabilized PAN and PAN/CNT after carbonization. (A colour version of this figure can be viewed online.)

indicates that the admixture of CNTs is counteracting on the improved local alignment of the graphene-like planes in creep-stressed PAN. This can be linked to the anchoring function of CNTs to the PAN chains, for the constrained system, where no global order exists, CNTs are instrumental in preventing the loss of orientation by holding the PAN chains during the stabilization. However for the creep stress system, the PAN chains are aligned externally by drawing and the anchoring function of CNTs limits the further alignment of interacting PAN chains and rather at some locations possibly counteracting.

3.4. Electrical transport properties of carbonized PAN and PAN/CNT

In-situ 4pp (four-point probe) SEM/STM transport measurements were performed on four different samples, i.e. creep stress

and non-creep stress cyclized pristine PAN and PAN/CNT. This local method was shown to be suitable tool to study transport on individual nano fibers and to address the aspect of fiber alignment in ECNF mats without the need of any fabrication of contacts, e.g. by lithography [37]. Linear I–V curves were recorded for different angles with respect to fiber mat preferential alignment direction, depicting an ohmic behaviour (Fig. S4). Anisotropy measurements have shown to be a good tool to determine the impact of the fiber orientation within the mat composition and to quantify the package density of the single fibers. For an homogenous but anisotropic ECNF-mat sample, the corresponding conductivity values can be derived accurately, as explained in detail in Ref. [41]. Nevertheless, as obvious from the SEM images (Fig. 8c) the ensemble lacks of a defined homogeneity, thus we will use the rotational square method here mainly in order to quantify the anisotropy for

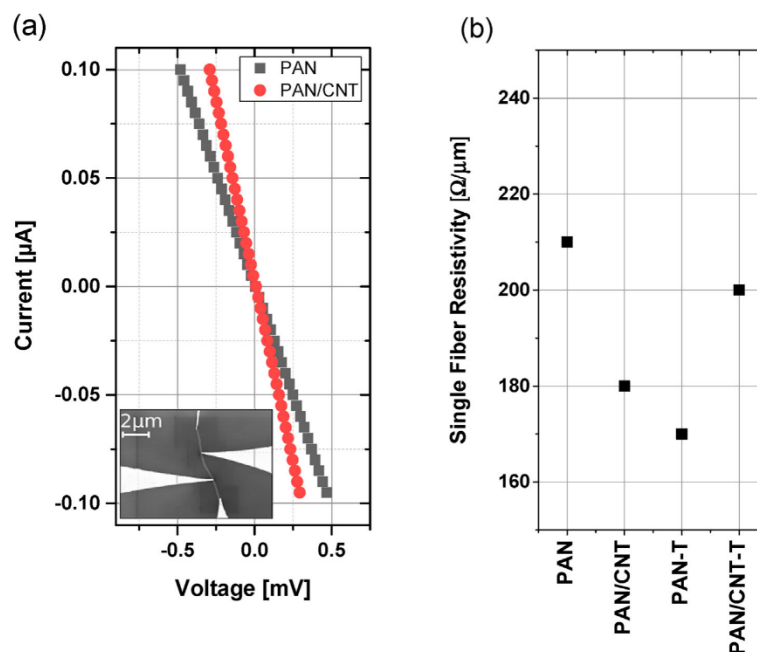


Fig. 9. (a) Typical I–V linear curve from measurement on single PAN and PAN/CNT nanofiber (included images is for PAN/CNT) using 4-tip measurement, inset shows single nanofiber on Si wafer during measurement. (b) Resistance measurements on single nanofibers for all four different types of sample (PAN, PAN/CNT, PAN - T, PAN/CNT - T) performed in 4-tip configuration. (A colour version of this figure can be viewed online.)

differently treated ECNF-mat systems. Thereby, the squared 4pp geometry is sequentially rotated with respect to the sample. The resistances measured for the current injected parallel and perpendicular to the overall orientation of the ECNFs is shown in Fig. 8a.

In general, the creep stress cyclized fibers show a much higher anisotropy than the non-creep stress cyclized sample (Fig. 8a). Thereby, the anisotropy values are increased from 10 to 29 with the application of creep stress for PAN fibers and from 12 to 27 for the templated samples (Fig. 8b). In general, both for the PAN and PAN/CNT nanofiber mats, the anisotropy of the creep stress cyclized fibers is significantly lower than non-creep stress cyclized system. This is expected since the application of creep stress results in an improved alignment of fibers along the stretching direction and fewer paths are available for current to flow across the fiber alignment direction. In accordance with our prior study [42], we therefore conclude that fiber crossings act as scattering centers indicating the transport channels are located near the surface of the nanofibers in all four measured samples.

Because of the above mentioned inhomogeneity of the 3D ECNF network, a determination of the conductivity from the anisotropy is prone to errors. The conductivity of the ECNFs was therefore determined from individual wires, considering their lengths and cross sections. For the fabrication of single nanofibers, the fiber mats were dissolved in isopropanol by ultra-sonication. The fiber solution was dropped onto oxidized silicon wafers to assure an electric decoupling of the ECNFs to the surrounding. Single nanofibers up to a length of 80 μm were placed by this method on the Si wafer (inset Fig. 9a). This simple way of separation provides single nanofibers with intact surfaces. On these nanostructures, four tip measurements were performed in order to minimize the issue of

contact resistance. The measurements showed a highly linear I(V)-curve indicating clearly an ohmic behavior for all four types of samples and supporting our assignment made for the transport measurements on entire mat structures. Fig. 9a shows the linear I(V) curve for PAN single PAN and PAN/CNT fiber. This indicates a conservation of the main transport mechanism upon templating, nevertheless the resistivity is influenced by these structural changes. The corresponding resistivities are plotted in Fig. 9b. The measurements done on single fibers show, that also the (local) resistivity is improved by around 20%, e.g. drops from 210 $\Omega\mu\text{m}$ for PAN to 170 $\Omega\mu\text{m}$ for PAN - T, thus the application of creep stress also improves the microscopic alignment of the graphitic units within a single fiber. For the non-creep cyclized samples, the resistivity is decreased from 210 $\Omega\mu\text{m}$ for PAN to 180 $\Omega\mu\text{m}$ for PAN/CNT. Apparently, the admixture of conductive CNTs is improving also the electronic properties without applying any creep stress. This effect is reversed for the creep cyclized samples, where the resistivity is increased from 170 $\Omega\mu\text{m}$ for PAN - T to 200 $\Omega\mu\text{m}$ for PAN/CNT - T (see Fig. 9).

The electrical transport properties of our 1D carbon structures can be explained by considering the cumulative effect of connection of different crystalline units/ sp^2 clusters and sub-crystalline units in sp^3 insulating matrix (schematic Fig. 10). Therefore, the conductivity is explained as a combination of band conductivity within the perfect graphitic domains and by hopping conductivity in between these domains [43,44]. The increase in the concentration and size of these sp^2 clusters results in an improved conductivity. The transport results fit nicely to Raman and TEM, revealing an increased I_a value, a decreased I_D/I_G ratio as well as improved alignment of the graphene planes. The addition of CNTs to PAN in a constrained system, improves the alignment of graphene planes

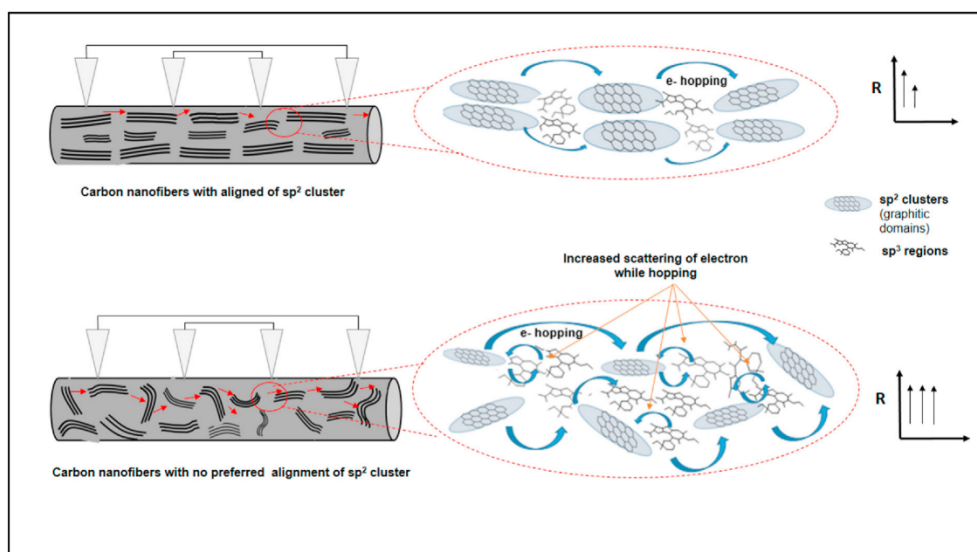


Fig. 10. Schematic illustration of possible mechanism for electrical transport in carbon nanofibers.

(Fig. 7c) and the degree of graphitization as observed from Raman and XPS (Fig. 6, Table 2), as reflected by the decrease in resistivity from $210 \Omega\mu\text{m}$ for PAN to $180 \Omega\mu\text{m}$ for PAN/CNT. An improved alignment, formation of continuous graphitic domains (sp^2 clusters) and the reduction of the torsion of carbon planes decreases the tunneling barriers for the electronic hopping process. For PAN/CNT - T, rather an increased resistivity compared to PAN - T is observed, which we relate to reduced alignment of graphene planes, as seen by TEM. Due to reduced alignment and also discontinuity of graphene planes, the band conductivity seems to be reduced, and rather more scattering takes place for electronic hopping, thus resulting in increase in the overall resistivity.

4. Summary and conclusion

Pristine and MWCNTs added carbon nanofibers have been prepared by electrospinning followed by stabilization in air and carbonization in inert atmosphere. The stabilization was performed typically by: a) clamping the ends of nanofiber mats (constraint shrinkage) and b) application of constant creep stress during the whole stabilization process. XRD, Raman and XPS measurements of non-creep stress cyclized PAN and PAN/CNT performed at various temperatures revealed that the addition of CNTs improved the degree of graphitization and the crystalline structure of PAN. To investigate the effect of creep stress stabilization in combination with the effects of CNTs introduced into the PAN graphitic structure, the carbonization of each four samples of different category (creep stress and non-creep stress cyclized pristine PAN and PAN/CNT) were performed at 1700°C . Both the PAN and PAN/CNT samples, stabilized with creep stress, showed further a reduction in the I_D/I_G ratio, $\text{FWHM}_{G\text{-peak}}$ and increased in crystallite size indicating improved graphitization compared to non-creep stress cyclized PAN and PAN/CNT. Electrical transport probed via 4pp STM/SEM on fiber mats revealed an increased anisotropy for samples cyclized with creep stress with highest observed for PAN - T. Measurement on the single isolated nanofibers showed that CNTs addition to PAN decreases the resistivity of PAN for non-creep

cyclized system. The resistivity is further reduced for creep stress cyclized PAN (PAN - T), however for CNTs added samples with creep stress (PAN/CNT - T), the resistivity showed an increased value compared to PAN - T. Our findings reveal that the transport properties in 1D ECNF structures are strongly dependent on the size, interaction and alignment of the local graphitic domains (sp^2 - sp^2 cluster). The structural and electronic properties of PAN-based ECNFs can be tuned by the addition of CNTs and the application of creep stress. However, the addition of other nanostructures feedback to the structure and influence mutually hopping and band mobilities. Only the detailed understanding on the microscopic and mesoscopic scale will provide insight into the development of carbon nanofibers with optimized properties, e.g. to employ these 1D materials in electrodes for energy storage and molecular scale sensing. Future work is intended in the mentioned direction by fabrication of nano-gap electrode using 1D carbon nanofibers and functionalization of sub-surface to connect molecules and analogous sized nanostructure to the outside world for molecular scale devices.

CRedit authorship contribution statement

A.B. Ali: Writing - original draft, Writing - review & editing, Data curation, Methodology, Formal analysis, Investigation. **D. Slawig:** Writing - original draft, Data curation, Investigation. **A. Schlosser:** Data curation, Visualization. **J. Koch:** Data curation, Visualization. **N.C. Bigall:** Resources, Validation. **F. Renz:** Resources, Validation. **C. Tegenkamp:** Conceptualization, Supervision, Writing - review & editing, Formal analysis. **R. Sindelar:** Conceptualization, Supervision, Writing - review & editing, Project administration, Funding acquisition.

Declaration of competing interest

The authors declare that they have no known competing financial interests or personal relationships that could have appeared to influence the work reported in this paper.

Acknowledgements

The authors are grateful to Hannover School for Nanotechnology (HSN) and Deutsche Forschungsgemeinschaft (DFG) for their financial support (grant number: 21-78904-63-7/16) provided by Niedersächsisches Ministerium für Wissenschaft und Kultur (Ministry of Science and Culture of Lower Saxony/Germany). N. C. B. would also like to acknowledge the DFG (Cluster of Excellence PhoenixD (EXC 2122, Project ID 390833453) and grant agreement BI 1708/4–1) and the European Research Council (European Union's Horizon 2020 research and innovation program, grant agreement 714429) for funding.

Appendix A. Supplementary data

Supplementary data to this article can be found online at <https://doi.org/10.1016/j.carbon.2020.10.033>.

References

- [1] T.D. Burchell, *Carbon Materials for Advanced Technologies*, Elsevier, 1999.
- [2] L. Dai, *Carbon Nanotechnology: Recent Developments in Chemistry, Physics, Materials Science and Device Applications*, Elsevier, 2006.
- [3] D. Jariwala, V.K. Sangwan, L.J. Lauhon, T.J. Marks, M.C. Hersam, Carbon nanomaterials for electronics, optoelectronics, photovoltaics, and sensing, *Chem. Soc. Rev.* 42 (7) (2013) 2824–2860.
- [4] J. Ni, Y. Li, Carbon nanomaterials in different dimensions for electrochemical energy storage, *Advanced Energy Materials* 6 (17) (2016) 1600278.
- [5] M. Inagaki, Y. Yang, F. Kang, Carbon nanofibers prepared via electrospinning, *Adv. Mater.* 24 (19) (2012) 2547–2566.
- [6] T. Rath, *Carbon Nanofibers: Synthesis, Properties and Applications*, Polymer Nanocomposites Based on Inorganic and Organic Nanomaterials, 2015, pp. 63–88.
- [7] B.A. Newcomb, Processing, structure, and properties of carbon fibers, *Compos. Appl. Sci. Manuf.* 91 (2016) 262–282.
- [8] E. Frank, F. Hermanutz, M.R. Buchmeiser, Carbon fibers: precursors, manufacturing, and properties, *Macromol. Mater. Eng.* 297 (6) (2012) 493–501.
- [9] A. Ramos, I. Cameán, A.B. García, Graphitization thermal treatment of carbon nanofibers, *Carbon* 59 (2013) 2–32.
- [10] F. Ko, Y. Gogotsi, A. Ali, N. Naguib, H. Ye, G. Yang, C. Li, P. Willis, Electrospinning of continuous carbon nanotube-filled nanofiber yarns, *Adv. Mater.* 15 (14) (2003) 1161–1165.
- [11] J. Cai, M. Naraghi, The formation of highly ordered graphitic interphase around embedded CNTs controls the mechanics of ultra-strong carbonized nanofibers, *Acta Mater.* 162 (2019) 46–54.
- [12] T. Maitra, S. Sharma, A. Srivastava, Y.-K. Cho, M. Madou, A. Sharma, Improved graphitization and electrical conductivity of suspended carbon nanofibers derived from carbon nanotube/polyacrylonitrile composites by directed electrospinning, *Carbon* 50 (5) (2012) 1753–1761.
- [13] J. Cai, M. Naraghi, Effect of Templating Graphitization on Electrical Conductivity of Electrospun Carbon Nanofiber, 58th AIAA/ASCE/AHS/ASC Structures, Structural Dynamics, and Materials Conference, 2017, p. 796.
- [14] B.V. Cunnning, B. Wang, T.J. Shin, R.S. Ruoff, Structure-directing effect of single crystal graphene film on polymer carbonization and graphitization, *Materials Horizons* 6 (4) (2019) 796–801.
- [15] Y. Zhang, K. Song, J. Meng, M.L. Minus, Tailoring polyacrylonitrile interfacial morphological structure by crystallization in the presence of single-wall carbon nanotubes, *ACS Appl. Mater. Interfaces* 5 (3) (2013) 807–814.
- [16] S. Prilutsky, E. Zussman, Y. Cohen, The effect of embedded carbon nanotubes on the morphological evolution during the carbonization of poly (acrylonitrile) nanofibers, *Nanotechnology* 19 (16) (2008) 165603.
- [17] X. Li, Y. Yang, Y. Zhao, J. Lou, X. Zhao, R. Wang, Q. Liang, Z. Huang, Electrospinning fabrication and in situ mechanical investigation of individual graphene nanoribbon reinforced carbon nanofiber, *Carbon* 114 (2017) 717–723.
- [18] H. Matsumoto, S. Imaizumi, Y. Konosu, M. Ashizawa, M. Minagawa, A. Tanioka, W. Lu, J.M. Tour, Electrospun composite nanofiber yarns containing oriented graphene nanoribbons, *ACS Appl. Mater. Interfaces* 5 (13) (2013) 6225–6231.
- [19] Z. Gao, J. Zhu, S. Rajabpour, K. Joshi, M. Kowalik, B. Croom, Y. Schwab, L. Zhang, C. Bumgardner, K.R. Brown, Graphene reinforced carbon fibers, *Science Advances* 6 (17) (2020) eaaz4191.
- [20] A. Benko, M. Nocuń, M. Gajewska, M. Białiewicz, Addition of carbon nanotubes to electrospun polyacrylonitrile as a way to obtain carbon nanofibers with desired properties, *Polym. Degrad. Stab.* 161 (2019) 260–276.
- [21] Y. Liu, H.G. Chae, S. Kumar, Gel-spun carbon nanotubes/polyacrylonitrile composite fibers. Part II: stabilization reaction kinetics and effect of gas environment, *Carbon* 49 (13) (2011) 4477–4486.
- [22] C. Liu, L. Hu, Y. Lu, W. Zhao, Evolution of the crystalline structure and cyclization with changing tension during the stabilization of polyacrylonitrile fibers, *J. Appl. Polym. Sci.* 132 (27) (2015).
- [23] E.N. Sabet, P. Nourpanah, S. Arbab, Quantitative analysis of entropic stress effect on the structural rearrangement during pre-stabilization of PAN precursor fibers, *Polymer* 90 (2016) 138–146.
- [24] A.C. Ferrari, D.M. Basko, Raman spectroscopy as a versatile tool for studying the properties of graphene, *Nat. Nanotechnol.* 8 (4) (2013) 235.
- [25] P. Merel, M. Tabbal, M. Chaker, S. Moisa, J. Margot, Direct evaluation of the sp³ content in diamond-like-carbon films by XPS, *Appl. Surf. Sci.* 136 (1–2) (1998) 105–110.
- [26] I. Miccolli, F. Edler, H. Pfnür, C. Tegenkamp, The 100th anniversary of the four-point probe technique: the role of probe geometries in isotropic and anisotropic systems, *J. Phys. Condens. Matter* 27 (22) (2015) 223201.
- [27] T. Ebbesen, H. Lezec, H. Hiura, J. Bennett, H. Ghaemi, T. Thio, Electrical conductivity of individual carbon nanotubes, *Nature* 382 (6586) (1996) 54–56.
- [28] A. Ali, B. Dreyer, F. Renz, C. Tegenkamp, R. Sindelar, Electrospun polyacrylonitrile based carbon nanofibers: the role of creep stress towards cyclization and graphitization, *J. Mater. Sci. Eng.* 7 (493) (2018).
- [29] Y. Zhang, N. Tajaddod, K. Song, M.L. Minus, Low temperature graphitization of interphase polyacrylonitrile (PAN), *Carbon* 91 (2015) 479–493.
- [30] L.J. Lantice-Diaz, Y. Tanabe, T. Enami, K. Nakamura, M. Endo, E. Yasuda, The effect of nanotube alignment on stress graphitization of carbon/carbon nanotube composites, *Carbon* 47 (4) (2009) 974–980.
- [31] A.C. Ferrari, Raman spectroscopy of graphene and graphite: disorder, electron–phonon coupling, doping and nonadiabatic effects, *Solid State Commun.* 143 (1–2) (2007) 47–57.
- [32] T. Mohiuddin, A. Lombardo, R. Nair, A. Bonetti, G. Savini, R. Jalil, N. Bonini, D. Basko, C. Galiotis, N. Marzari, Uniaxial strain in graphene by Raman spectroscopy: G peak splitting, Grüneisen parameters, and sample orientation, *Phys. Rev. B* 79 (20) (2009) 205433.
- [33] O. Frank, G. Tsoukleri, I. Riaz, K. Papagelis, J. Parthenios, A.C. Ferrari, A.K. Geim, K.S. Novoselov, C. Galiotis, Development of a universal stress sensor for graphene and carbon fibres, *Nat. Commun.* 2 (1) (2011) 1–7.
- [34] G. Washer, F. Blum, Raman spectroscopy for the nondestructive testing of carbon fiber, *Advances in Materials Science and Engineering* (2009) 2008.
- [35] Z. Püspöki, M. Storath, D. Sage, M. Unser, Transforms and Operators for Directional Bioimage Analysis: a Survey, *Focus on Bio-Image Informatics*, Springer, 2016, pp. 69–93.
- [36] B. Saha, G.C. Schatz, Carbonization in polyacrylonitrile (PAN) based carbon fibers studied by ReaxFF molecular dynamics simulations, *J. Phys. Chem. B* 116 (15) (2012) 4684–4692.
- [37] F. Banhart, J. Kotakoski, A.V. Krasheninnikov, Structural defects in graphene, *ACS Nano* 5 (1) (2011) 26–41.
- [38] P.J. Harris, New perspectives on the structure of graphitic carbons, *Crit. Rev. Solid State Mater. Sci.* 30 (4) (2005) 235–253.
- [39] P. Harris, Fullerene-related structure of commercial glassy carbons, *Phil. Mag.* 84 (29) (2004) 3159–3167.
- [40] S. Sharma, C.S. Kumar, J.G. Korvink, C. Kübel, Evolution of glassy carbon microstructure: in situ transmission electron microscopy of the pyrolysis process, *Sci. Rep.* 8 (1) (2018) 1–12.
- [41] T. Kanagawa, R. Hobara, I. Matsuda, T. Tanikawa, A. Natori, S. Hasegawa, Anisotropy in conductance of a quasi-one-dimensional metallic surface state measured by a square micro-four-point probe method, *Phys. Rev. Lett.* 91 (3) (2003), 036805.
- [42] J. Aprojanz, B. Dreyer, M. Wehr, J. Wiegand, J. Baringhaus, J. Koch, F. Renz, R. Sindelar, C. Tegenkamp, Highly anisotropic electric conductivity in PAN-based carbon nanofibers, *J. Phys. Condens. Matter* 29 (49) (2017) 494002.
- [43] J. Carey, S. Silva, Disorder, clustering, and localization effects in amorphous carbon, *Phys. Rev. B* 70 (23) (2004) 235417.
- [44] J. Cai, S. Chawla, M. Naraghi, Piezoresistive effect of individual electrospun carbon nanofibers for strain sensing, *Carbon* 77 (2014) 738–746.

5 Conclusion and Outlook

In this work, graphene nanostructures were explored and realized via tangible carbon nanofibers. The aim of the thesis was to investigate the graphene nanostructures along carbon nanofibers, their nucleation/growth and electrical transport properties. Therefore, the project was designated with project phases as described in Chapter 1 which were accomplished.

Firstly, the carbon nanofiber fabrication process was optimized for each sub-processes, electrospinning, stabilization, and carbonization. Electrospinning of polyacrylonitrile (PAN) was optimized to ensure the repeatability for investigation of carbon nanofibers in next stages. It was found that ~ 12 - 15 wt.% of PAN was suitable to produce nanofibers with diameter of ~ 200 - 400 nm. Increased weight percentages lead to enhanced viscosity of PAN/DMF solution, which was impossible to spin, while decreased weight percentage than 8 wt.% resulted in fibers with beads and non-uniform morphology. The solution was spun with 16 KV (applied voltage), 15 cm (needle to rotating collector distance) and 1.0 ml/h (flow rate of PAN/DMF solution). These parameters were found to be appropriate to produce nanofibers with uniform morphology. Stabilization was performed at 250 °C for 5 hours at heating rate of 1 °C/min. Carbonization was performed with temperatures from 800 °C - 1700 °C, resulting in different graphitic structures. The graphitization degree was highly dependent on the carbonization temperature and it was found that more of the amorphous carbons get ordered to form crystallites and it grows with increasing temperature (as evidenced from Raman, XRD and TEM investigations). The heating rate during the carbonization was kept constant to 5 °C/min for the rest of project phases. At least these parametric optimizations were kept constant for all the next phase investigations.

In the next stage the stabilization process was explored in detail. Stabilized structure of PAN serves as the basis for graphene like ribbon structure, hence investigation in this phase was focused on the mechano-chemical reactions. An experimental matrix was designed, whereby the stabilization was performed via; 1)

fixing the ends of spun nanofiber mats on both ends and 2) application of constant load (creep stress) during the duration of stabilization (heating-dwell-cooling). The progress of the stabilization was monitored by evaluating ring cyclization index (RCI) at different temperatures from 170 °C – 230 °C for both above cases using FTIR. We were able to show that RCI was increased with application of creep stress during the stabilization process, especially at lower temperatures, below 230 °C. At higher temperatures and for increased time, the RCI showed nearly similar values. RCI of ~ 95% was achieved by stabilizing at 250 °C for 10 hrs. These both differently stabilized structures were carbonized using the same conditions, however the graphitic structure observed for both carbon nanofibers were quite different. An increase in graphitization degree (increased crystallite size and decreased interplanar spacing) was observed from Raman and XRD for the case where PAN nanofibers were stabilized with creep stress. We concluded that though the amount of cyclized materials as estimated from RCI may show similar values, the degree of graphitization could be different which is attributed to application of stress, instrumental in avoiding the bending of carbon planes. Hence the long-range stacking of carbon planes occurred, resulting in increased graphitization degree.

Leading from this, the graphene nanostructures were explored by using the concept of templated graphitization. Thereby employing nanosized reinforcements having high surface area and graphitic order in PAN to improve the PAN chain alignment during precursor spinning, stabilization and to serves as templates for formation of ordered crystallite. This concept was explored using graphene nanoplatelets (GNPs) and carbon nanotubes (CNTs) as reinforcement. In the first phase, GNPs were introduced to PAN and spinning-stabilization-carbonization was performed. From the investigations of graphitic structure (using XPS, XRD and Raman), we were able to show that the crystallite size along lateral and basal planes (L_c and L_a) and sp^2 fraction increased while the concentration of defects were reduced (decreased I_D/I_G ratio) for CNFs reinforced with graphene nanoplatelets. The improved degree of graphitization was reflected in the enhancement of electrical conductivity of carbon nanofiber mats. e.g., the electrical conductivity of CNFs along fiber alignment direction in 1700 °C was increased from 470 S/cm to 590 S/cm

upon reinforcement with GNPs. Also, we were able to show that the percentage increase in electrical conductivity was higher for CNFs graphitized at lower temperatures of 1000 °C and 1200 °C. It was also concluded that anisotropy in electrical conductivity was reduced for CNFs reinforced with GNPs. The CNFs bridge across the nanofiber directions in the presence of GNPs, forming a conductive network, resulting in increased conductivity across the nanofiber alignment direction. It was found that for both cases of stabilization, the introduction of GNPs improve the graphitic order of carbon nanofibers and the electrical conductivity in and across the fiber direction.

In the last stage, the synergistic effect of creep stress (hot drawing) and nanocarbon inclusion was explored on the graphitic structure and electrical transport to quantify the effect of individual and combined effects. To quantify the electrical transport and understand the possible transport-mechanism in carbon nanofibers, single nanofibers were isolated, and evaluations were made on single filament. Instead of GNPs, CNTs were used as reinforcement since they are smaller in dimensions to CNFs, hence can be spun inside 1D CNFs as 1D reinforcement. This scheme allowed the investigation of templated graphitic structure and its impact on electrical transport. We concluded that addition of CNTs increased sp^2 fraction and crystallite size. However, the electrical transport didn't follow the same trend, electrical conductivity was increased upon reinforcing CNFs with CNTs for the case where no creep stress was applied, however, the electrical conductivity was reduced with introducing CNTs for the case where creep stress was applied. It was concluded that electrical transport properties are dependent mainly by the alignment of graphene planes, it may be the case that sp^2 fraction is lower, but the orientation of graphene planes appeared to be a limiting factor for the electrical transport in carbon nanofibers. Based on all this analysis, we were able to conclude that electrical transport in 1D carbon nanofibers should be defined as the cumulative effect of band-based conductivity along sp^2 units and tunneling/hopping of electrons across sp^2 to sp^3 units.

5.1 How does it serve – Future takeaway

In the present thesis work, the investigation on the carbon nanofiber structure and electrical transport has been thoroughly worked out. In my opinion, the conclusions will pave the way for future investigations in the following ways.

1) The fundamental investigations on 1D carbon nanostructures and templates should be extended to production and characterization of 2D large area graphene nanostructures by using PAN. As in the present work, detailed investigations were carried out on graphitization and stabilization of PAN. In this regard this work will serve as the basis for producing a range of carbon nanostructures for next generation application in energy and electronics. Modifications to PAN with controlled polymerization techniques and carbonization chemistry would allow to transform this unique polymer into carbon nanostructures with tailored morphology including films, nanoparticles, and porous carbon.

2) The templated graphitization and hot drawing assisted stabilization would be interesting to replicate on 2D carbon structures. In this project, we have come-up with the ideas to tailor the PAN stabilized structure using hot rolling, hence extending the uniaxial stress assisted stabilization to shear stress assisted stabilization. Since the conclusions showed that orientation of graphene nanostructures can be harnessed during application of stress in the stabilization process, it would be significant to employ hot rolling during the stabilization process on 2D thin films on PAN, to produce carbon films with tailored orientation of graphene planes. This will open further questions in carbon nanostructures using polymer routes with different types of stresses to produce different kinds of graphene structures. Especially on nanoscale, it would be interesting to investigate the effect of highly localized stresses in thin PAN films (if possible).

3) From the findings of the electrical transport properties, we were able to propose the electrical transport phenomena of carbon nanofibers which is quite different from the traditional carbon fibers. We have investigated different combinations and concluded how electrical transport possibly takes place in CNFs.

The electrical transport phenomena in commercial CF is different from CNF, due to the presence of continuous domains in CF. For CNF, there are discontinuous graphitic domains and our studies have shown that local orientation of graphene planes is very significant for dictating the electrical transport and charge transfer. In my view, this can be tailored for 2 different approaches, 1) improving the electrical transport (charge flow) for producing highly conductive carbon nanofibers and 2) improving the charge transfer for harnessing the sensor characteristics. For both these approaches, different structures are curial. This is what exactly makes CNFs unique. The in-situ structure of PAN thermodynamics during stabilization and carbonization offers range of structures to be produced from sensors to highly conductive materials by tailoring the graphene planes orientation. That's why the low temperature CNFs with turbostratic structure have excellent piezoelectric properties compared to traditional CF. The electrical conductivity of CNFs is nearly 1-2 orders higher than CFs subjected to same processing conditions. The conclusion from the last phase of the work serves as a step to the approach of using carbon nanofibers mats/yarns for electrical cables or sensor materials based on structure-property relationship.

6 Appendix

6.1 List of Publications

Journal Publications - (Included in the thesis work)

1. **Ali AB**, Slawig D, Schlosser A, Koch J, Bigall N. C, Renz F, Tegenkamp C, Sindelar R (2021). Polyacrylonitrile based Electrospun Carbon Nanofibers (E`CNFs): Probing the synergistic effects of creep assisted stabilization and CNTs addition on graphitization and low dimensional electrical transport. *Carbon* 172: 283-295. <https://doi.org/10.1016/j.carbon.2020.10.033>
2. **Ali AB**, Renz F, Koch J, Tegenkamp C, Sindelar R (2020), Graphene Nanoplatelets (GNPs) Doped Carbon Nanofiber (CNF) System: Effect of GNPs on the Graphitic Structure of Creep Stress and Non-Creep Stress Stabilized Polyacrylonitrile (PAN). *Nanomaterials* 10, 351. doi: 10.3390/nano10020351
3. **Ali AB**, Dreyer B, Renz F, Tegenkamp C, Sindelar R (2018), Electrospun Polyacrylonitrile Based Carbon Nanofibers: The Role of Creep Stress towards Cyclization and Graphitization. *Journal of Material Science & Engineering* 7: 493. doi:10.4172/2169-0022.1000493
4. **Ali AB**, Dreyer B, Renz F, Tegenkamp C, Sindelar R, Development and structural integration of electro spun carbon Nano fibers with graphene layer structure, *J Nanomater Mol Nanotechnol*, DOI: 10.4172/2324-8777-C1-020.

(Publication not Included in thesis work but derived from the thesis Project theme)

5. **Ali AB**, Pieczulewski N, Schlosser A, Bigall N. C, Renz F, Tegenkamp C, Sindelar R, Effect of ZnO nanorods on stabilization and low temperature carbonization of Polyacrylonitrile: possibility of

skipping stabilization in carbon fiber production cycle, (Under review -ACS Sustainable Chemistry & Engineering - 2021)

6. Breheme J, Ali AB, Renz F, Sindelar R, Lignin, and cellulose acetate blended polyacrylonitrile carbon nanofibers: Effect of lignin and cellulose acetate on the stabilization and carbonization of PAN nanofibers (under preparation)

(Conference talks and posters – Included/related to thesis work)

1. Oral presentation: Carbon Nanofibers – fabrication and graphitic structure investigations, Proceedings of 23rd International Conference on Nanomaterials and Nanotechnology, **March 15-16, 2018 / London, UK**.
2. Poster Presentation: Electrospun carbon nanofibers with highly anisotropic electrical conductivity: The Role of Creep Stress towards Cyclization and Graphitization. **Nanocarbon Annual conference Feb 2019, University of Wurzburg, Germany**.
3. Poster Presentation: Polyacrylonitrile Based Carbon-Nanofibers: Fabrication and structural characterization for improved functionality and electrical conductivity, **Poster presentation: Nano-Day Leibniz University Hannover**

6.2 Curriculum Vitae

Date of birth: 13.09.1990

Place of birth: Rawalpindi, Pakistan



Education and Research Experience

(May 2017 – Jan 2021)

Leibniz University Hannover, DE

Doctorate (PhD), Chemistry

Research group of Prof. Dr. Franz Renz

***Thesis theme:** Graphene based nanostructures towards application with carbon nanofibers*

(Aug 2013 – Dec 2016)

King Fahd University of Petroleum and Minerals, KSA

Masters, Materials Science and Engineering

Research group of Prof. Dr. Nescar Merah.

***Thesis theme:** Development and Characterization of Hybrid UHMWPE Polymer Nanocomposites for Bearing Applications under dry water lubricated conditions)*

(Nov 2008 – Jan 2012)

National University of Sciences and Technology, PAK

Bachelor, Materials Engineering

Research group of Prof. Dr. Ahmad Nawaz Khan

***Thesis theme:** Development, processing and testing of Acrylonitrile-Butadiene-Styrene (ABS) thermoplastic reinforced with nano-clay particles for permeability applications in seals, O-ring*